Zhang *et al. Carbon Research* (2022) 1:14
https://doi.org/10.1007/s44246-022-00009-1

Carbon Research

REVIEW Open Access

Lignin derived carbon materials: current status and future trends

Wenli Zhang[1,2,3], Xueqing Qiu[1,2*], Caiwei Wang[4], Lei Zhong[1], Fangbao Fu[4], Jiahao Zhu[1], Zejie Zhang[3], Yanlin Qin[1,2], Dongjie Yang[4] and Chunbao Charles Xu[5]

Abstract

Developing novel techniques to convert lignin into sustainable chemicals and functional materials is a critical route toward the high-value utilization of lignocellulosic biomass. Lignin-derived carbon materials hold great promise for applications in energy and chemical engineering, catalysis and environmental remediation. In this review, the state-of-art sciences and technologies for controllable synthesis of lignin-derived carbon materials are summarized, pore structure engineering, crystalline engineering, and morphology controlling methodologies are thoroughly outlined and critically discussed. Green chemical engineering with cost-effectiveness and precise carbonization tuning microstructure are future research trends of lignin-derived carbon materials. Future research directions that could be employed to advance lignin-derived carbon materials toward commercial applications are then proposed.

Highlights

✧ Recent developments in lignin-derived carbon materials for energy and environmental applications.

✧ Engineering methodologies of pore structure, crystalline, morphology, and surface chemistry are critically summarized.

✧ New opportunities for lignin-derived carbon materials in commercial applications are proposed.

Keywords: Lignin, Carbon materials, Supercapacitor, Battery, Environment, Catalysis

1 Introduction of lignin

Environmental conservation and efficient utilization of sustainable resources are two of the primary challenges for human civilization. Sustainable lignocellulosic biomasses are the most widely distributed, abundant, and renewable organic carbon resources on the earth. High-value utilization of lignocellulosic biomasses to reduce the usage of non-renewable petroleum-based chemicals is significant for the reduction and neutralization of carbon dioxide (Chen et al. 2020a; RameshKumar et al. 2020; Li et al. 2021c; Liu et al. 2021b). Therefore, it is essential and urgent to develop biomass-derived chemicals and materials for modern industry.

Cellulose, hemicellulose, and lignin are the three main organic components of plant lignocellulosic biomass. Efficient utilization of these three components in biomass is the central scientific obstacle to biomass valorization. Basically, cellulose is commercially utilized in papermaking and biorefinery industries (Fig. 1). Cellulose is usually applied in the manufacturing of papers. The cellulose components in biomass could also be hydrolyzed into glucose which afterward could be converted to fuels or chemicals such as ethanol or 2,5-furandicarboxylic acid (Takkellapati et al. 2018; Huang et al. 2022). At present, scientists have a great interest in utilizing cellulose to produce nano cellulose fibers (NCF) for functional

*Correspondence: cexqqiu@scut.edu.cn

[1] School of Chemical Engineering and Light Industry, Guangdong University of Technology (GDUT), 100 Waihuan Xi Road, Guangzhou 510006, Panyu District, China
Full list of author information is available at the end of the article

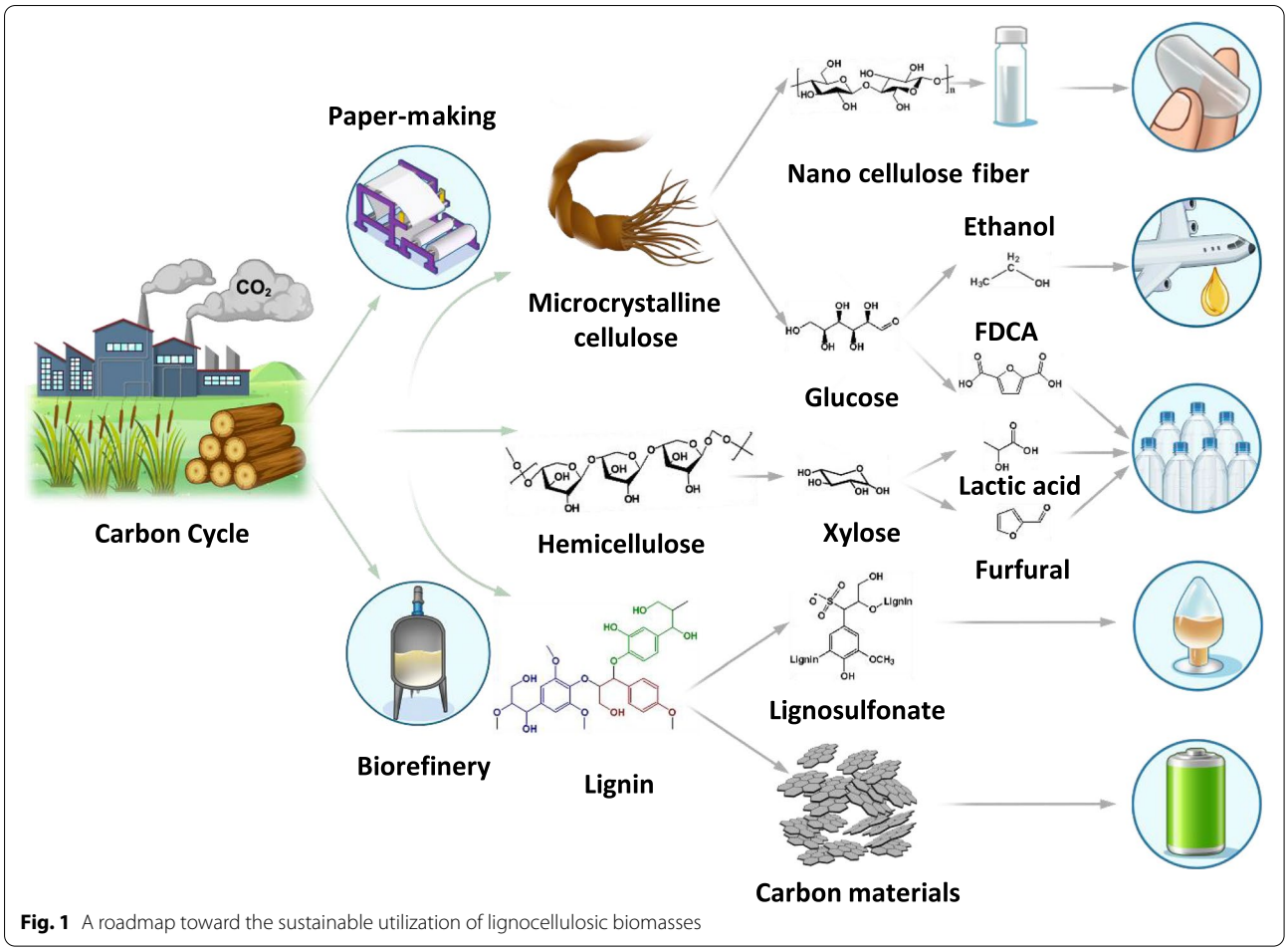

Fig. 1 A roadmap toward the sustainable utilization of lignocellulosic biomasses

materials (Hu et al. 2013b), while hemicellulose could be converted into lactic acid and furfural. Ethanol could be applied for the production of bio-jet. 2,5-furandicarboxylic acid, lactic acid, and furfural are the precursors for bio-plastics for packaging. Lignin is a by-product produced in the above paper-making and biorefinery industries. Kraft lignin (KL), alkaline lignin (AL), sodium lignosulfonate (SLS) are produced in the paper-making industry, and enzymatic hydrolysis lignin (EHL) is produced in the biorefinery industry. Currently, SLS is used as commercial dispersing agents and surfactants (Li et al. 2017, 2018; Lou et al. 2019; Zhan et al. 2019). KL, AL and EHL are mainly utilized as low-value fuels for boilers for energy recovery, although they could be valuable bio-precursors for various carbonaceous electrode materials. The origins of different lignin derivates are described in our previous review article (Zhang et al. 2021g).

Among the three main components of lignocellulosic biomass, lignin is the only aromatic polymer with benzene rings in its building block with a phenylpropane structure. Lignin has many attractive properties, e.g., low price, high carbon content (> 60%), high aromaticity, and abundant oxygen functional groups that offer good tunability in chemical structure, etc. (Isaac et al. 2019; Wang et al. 2022b). The annual production of lignin is approximately 500–3,600 million tons worldwide (Wang et al. 2021c). They are mainly produced in paper-making and biorefinery industries as by-products, as mentioned previously. The primary lignin derivatives are KL/AL and SLS. At present, only a tiny fraction (< 10%) of total lignin produced in the industry has been utilized as chemicals and materials, such as concrete additives, stabilizing agents or dispersants, and surfactants, while most of the lignin is discarded as waste or burnt as low-grade fuels.

Carbon materials have been widely used in energy and environmental applications owing to their relatively high conductivity, chemical and mechanical stability, considerable specific surface area (SSA), and tunable pore structure (Yin et al. 2020a; Zhu et al. 2020). The state-of-art commercial carbon materials are mainly produced from byproducts of petroleum refining, such as petroleum coke and pitch, and petroleum-derived polymers such as polyacrylonitrile (PAN) (Marsh and Rodríguez-Reinoso 2006). Lignocellulosic

biomasses are not often utilized for carbon materials due to their heterogeneity and hard chemical tunability. Nevertheless, lignocellulosic biomasses could be transformed into a variety of carbon materials by separation, purification, morphological control, controllable carbonization and activation processes (Liu et al. 2015a; Borghei et al. 2018; Sundriyal et al. 2021). The aromatic structure and chemical advantages of lignin resources, the motivation to reduce the contamination of lignin byproducts, and the substitute of petroleum-based chemicals by lignin have intensified the research interests in designing controllable preparation methodologies of lignin-derived carbon (LDC) materials.

In lignocellulosic biomass, lignin is present in the spaces between cellulose and hemicellulose, playing mainly as a binder in the biomass matrix (Fig. 2a) (Liu et al. 2015b). The structure of lignin is highly branched compared with cellulose and hemicellulose (Fig. 2b) (Zakzeski et al. 2010). Lignin consists of three typical hydroxycinnamyl alcohols, i.e., p-coumaryl, coniferyl, and sinapyl alcohols, corresponding to the three subunits of hydroxyphenyl (H), guaiacyl (G), and syringyl (S) in lignin (Fig. 2c) (Shen et al. 2017). There are approximately 50% aromatic compounds in lignin (Liu et al. 2015b). In a lignin molecule structure, there are various linkages of ether and C–C bonds among the three subunits, typically β-O-4, α-O-4, 4-O-5, β-1, 5–5′, β-β and β-5 bonds (Fig. 2d) (Chakar and Ragauskas 2004). The proportion of C–O–C bonds is the most abundant in lignin, generally existing as either ethers or a part of furan rings (Liu et al. 2015b). The β-O-4 linkage is dominant among these C–O–C linkages in lignin (Zakzeski et al. 2010). Besides, the presence of various oxygen-containing groups on the C_α and C_β of lignin, including methoxy, carbonyl, and hydroxyl groups, etc., further contributes to the complexity of lignin molecular structure (Zakzeski et al. 2010).

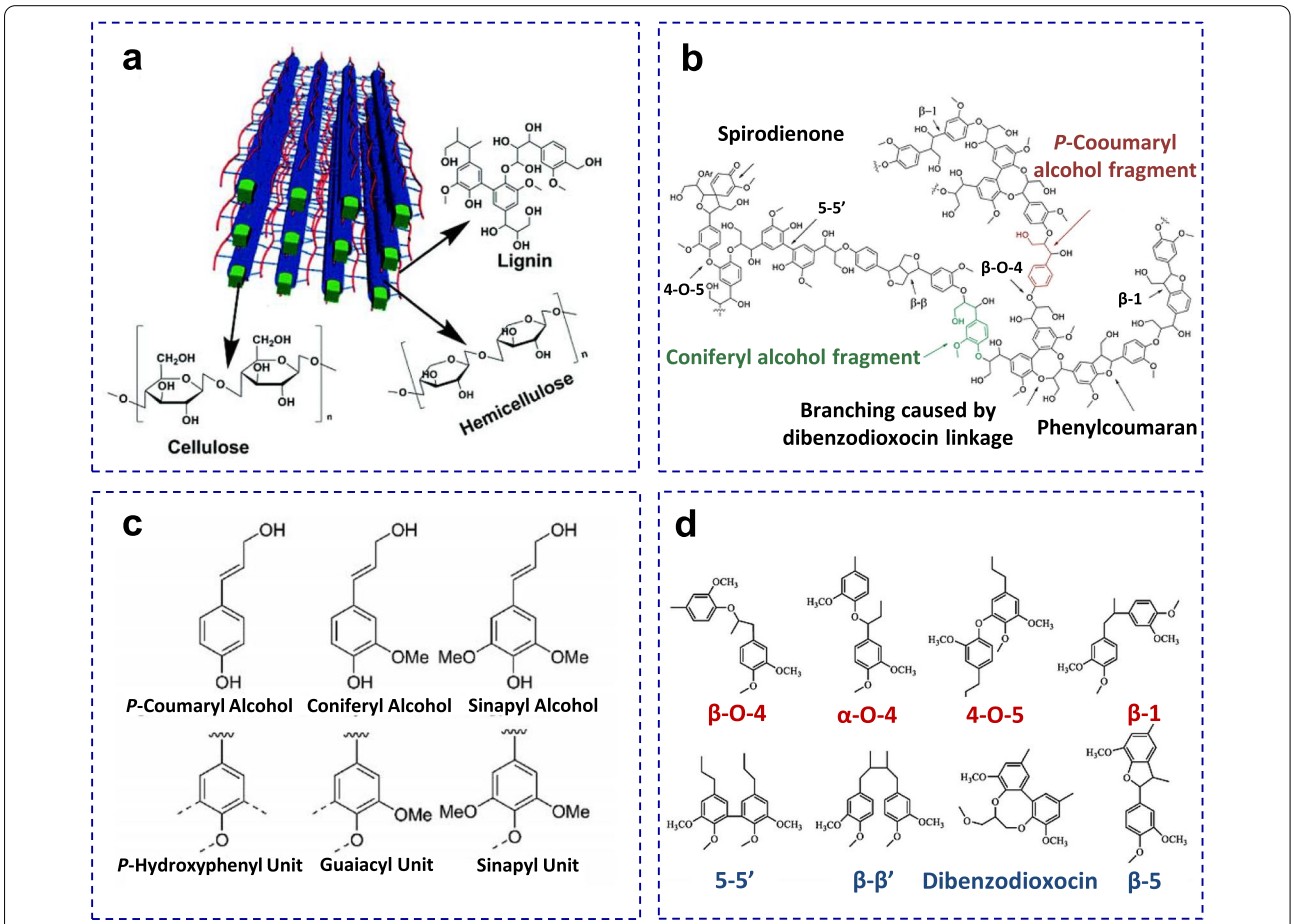

Fig. 2 **a** Structural illustration of lignin components in lignocellulosic biomass. Reproduced with permission from Ref. (Liu et al. 2015b). Copyright © 2015, Roal Society of Chemistry; **b** Typical branched structure of lignin. Reproduced with permission from Ref. (Zakzeski et al. 2010). Copyright © 2010, American Chemistry Society; **c** Basic units in lignin structure. Reproduced with permission from Ref. (Shen et al. 2017). Copyright © 2017, Progress in Chemistry; **d** Typical linkages in a lignin molecule structure. Reproduced with permission from Ref. (Chakar and Ragauskas 2004). Copyright © 2021, Elsevier

Lignin has a branched and random structure, hence is a complex, heterogeneous and three-dimensional polymer. Furthermore, the abundant aromatic sub-structure rich in β-O-4 linkage accounts for the hydrophobic properties of lignin. Therefore, natural lignin is difficult to be dissolved in water at acidic or neutral pH values, but lignin can be dissolved in some alkaline solutions (ammonium, hydroxide or carbonates) or some organic solvents (Li et al. 2017; Lou et al. 2019; Wang et al. 2021b).

Based on the chemical and physical characteristics of lignin, one can design various carbonization strategies to synthesize a variety of carbon materials with tunable morphology, crystalline structure, pores structure, and surface chemistry for various industrial applications in battery, supercapacitor, catalysis and environment (Fig. 3). There have been a couple of review papers on lignin-based electrode materials for energy storage (Espinoza-Acosta et al. 2018; Zhu et al. 2020; Liu et al. 2021b), and carbon materials from lignin precursors (Li et al. 2021b; Qu et al. 2021; Wang et al. 2021c). It is necessary for us to summarize the designing principles of carbonaceous materials from lignin and their structure-performance relationship toward energy and environmental applications.

2 Lignin-derived carbon materials (LDC)

2.1 Carbonization

A variety of carbonization techniques, such as thermal carbonization (Leng et al. 2022), hydrothermal carbonization (Hu et al. 2010; Zhou et al. 2016), flash light carbonization (Gengler et al. 2013; Choi et al. 2016; Kim et al. 2019; Song et al. 2021), and laser carbonization etc. (Wynn and Fountain 1997; Vander Wal and Choi 1999; Zhang et al. 2019d, c), have been employed for the production of carbonaceous materials from lignocellulosic biomass (Zhang et al. 2021g). In industrial practice, thermal carbonization is usually employed to obtain carbonaceous materials. In terms of the carbonization of lignin, lignin experiences solid-state carbonization, i.e., lignin does not melt during thermal treatment, resulting from the oxygen-rich backbone of the lignin molecules. As a result, LDCs are amorphous hard carbon materials rich in sp^3 hybridized C–C bonds and are hard to be graphitized at high temperatures, which is in sharp contrast to the petroleum-based precursors (petroleum coke and pitch) (Liu et al. 2020). The carbonization of lignin can be divided into three stages (Fig. 4), i.e., dehydration stage (30–200 °C), active pyrolysis stage (200–450 °C) and passive pyrolysis stage (> 450 °C) (Liang et al. 2015; Liu et al. 2016a; Ma et al. 2016; Leng et al. 2022).

Dehydration reaction occurs in the dehydration stage, generally below 200 °C. The active pyrolysis stage is the primary process of eliminating the heteroatoms in lignin. During the active pyrolysis stage in the temperature range of 200–450 °C, unstable β-O-4 linkages are broken (Liu et al. 2016a). The C–C and C-O bonds are further cleaved with increasing temperature (Li et al. 2014). Besides, the functional groups and the branches (methoxyl, methyl, and carboxyl) decompose forming the gas products (CO_2, CO, CH_4, etc.) (Fenner and Lephardt 1981; Liu et al. 2008; Hu et al. 2013a; Li et al. 2014; Zhao et al. 2014).

Due to the massive elimination of heteroatoms, extensive rearrangement reactions occur in solid products together with the release of volatile macromolecular products. The scission and rearrangement of side-chains, the removal of functional groups, and polymerization mainly occur in the passive pyrolysis stage (> 450 °C). The elimination rate of heteroatoms becomes slow, resulting in the formation of small molecule compounds (olefins, alkyl, and aromatic products) accompanied with releasing less amount of gas (CO_2, CO, CH_4, etc.). The slow decomposition and carbonization of lignin residues (Yang et al. 2007; Liang et al. 2015), and the polymerization of volatile matters occur to form coke. The coke prepared at low temperature is generally called amorphous carbon which is apparently different from hard carbon (obtained under carbonization temperature > 1000 °C). The carbon layers in amorphous carbon are randomly stacked to form a turbostratic structure, although small graphene nanodomains (GNDs) are also formed, which could enlarge with increasing temperature. However, these GNDs are highly cross-linked; therefore, lignin is difficult to be graphitized

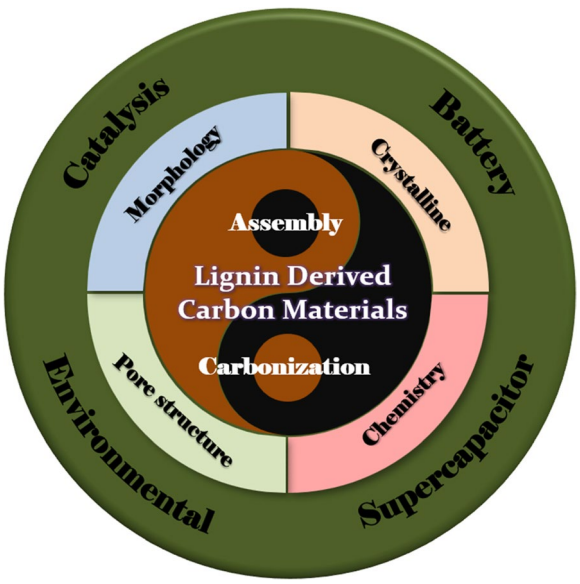

Fig. 3 Multi-dimensional strategies for the synthesis of LDC materials and their industrial applications

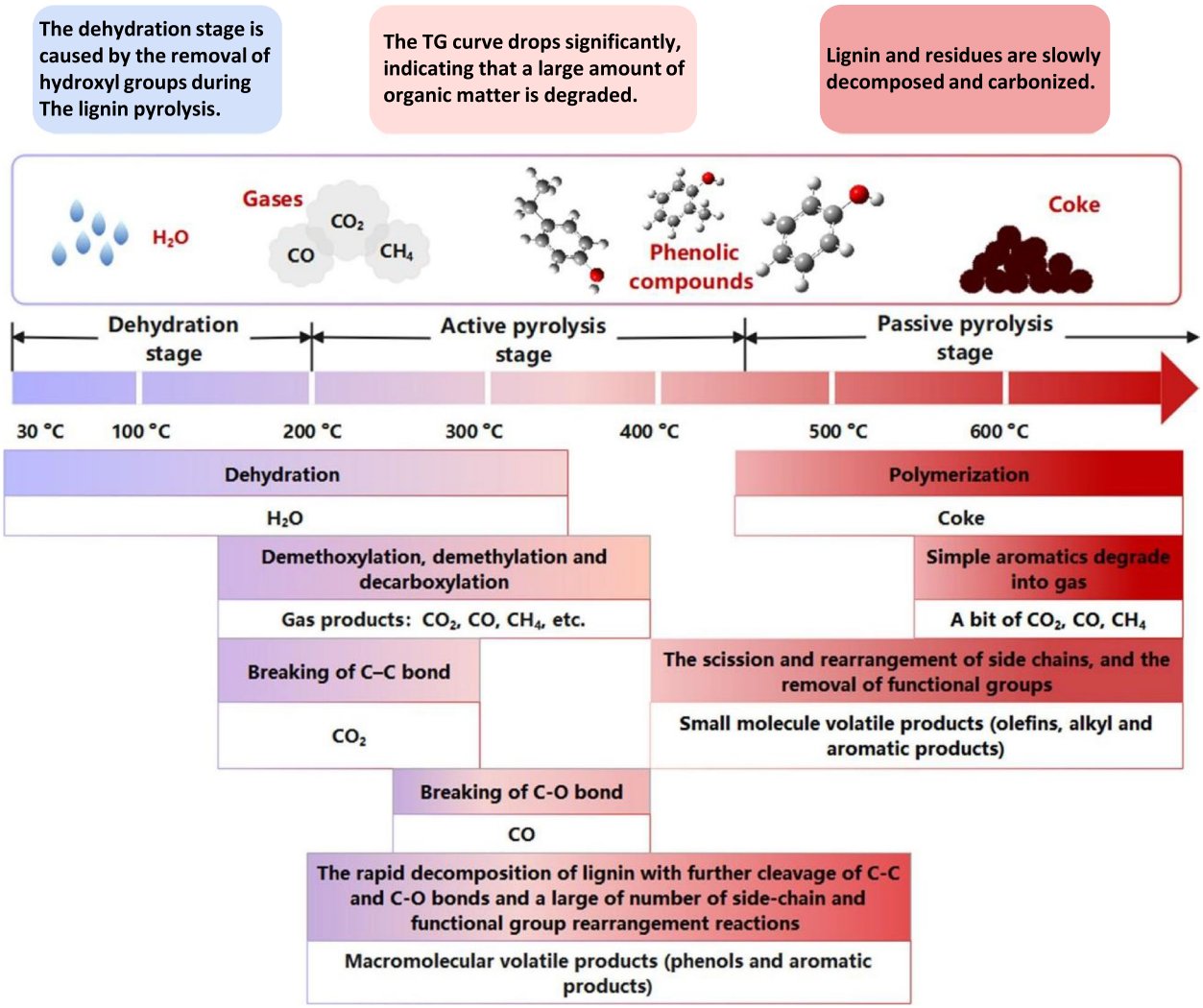

Fig. 4 A summary of pyrolytic characteristics in various pyrolysis stages of lignin molecule. Reproduced with permission from Ref. (Leng et al. 2022). Copyright © 2022, Elsevier

to form artificial graphite (Zhang et al. 2019e). In this review, LDCs refer to the carbonaceous materials derived from lignin under a carbonization temperature above 500 °C. The fewer GNDs in an LDC carbon matrix and the irregular distribution of GNDs endow its amorphous characteristics. From this perspective, LDCs are not suitable carbon sources for preparing graphite and graphene, whereas certain chemical processes could enable the production of graphene-like amorphous carbon nanosheets (Liu et al. 2017) and graphene quantum dots (Si et al. 2018; Shi et al. 2019; Zhang et al. 2019a) from lignin.

2.2 Graphitization

Graphitization produces carbon materials with a high graphitization degree and high conductivity. Graphitic carbon materials could be used as anodes of lithium-ion and potassium-ion batteries. Regardless of the recently-developed novel laser or flash carbonization techniques (Wynn and Fountain 1997; Vander Wal and Choi 1999; Gengler et al. 2013; Secor et al. 2015; Song et al. 2021), high-temperature carbonization (> 2000 °C) is a common and effective strategy to eliminate the disordered structure and improve the graphitization degree of LDCs (Kurban et al. 2010). However, as discussed above, the hyperbranched, oxygen-rich, and complex network of lignin restricts the order rearrangement of the carbon layer in the carbonization process, making it difficult for the production of highly graphitized carbon materials from lignin (Torres-Canas et al. 2020). As a result, high-temperature treatment only results in the formation

of hard carbons. The GNDs and amorphous regions are randomly cross-linked in hard carbons (Zhang et al. 2021g). The microporous structure is formed due to the disorderly stacked GNDs. With increasing temperature, the number of graphene stacking layers increases, and the interlayer spacing grows, leading to the increase in the size of the inner micropores (Kim et al. 2017; Fromm et al. 2018). Catalysts such as nickel, iron, or molybdenum catalysis proved to be effective for the graphitization of biomass or non-graphitizable precursors. Gindl-Altmutter et al. demonstrated that magnesium could play a catalytic role in improving the graphitization degree of LDC materials (Gindl-Altmutter et al. 2019). On the other hand, carbonization with some guide agents, such as graphene oxide, pitch and petroleum coke, could result in LDCs with a higher graphitization degree.

3 Morphology control of LDCs

3.1 Carbon fibers

Given the renewable characteristic of biomass, lignin is an ideal precursor for carbon fiber production. However, the spinnability of lignin is poor. Although lignin could be melt-spun in an energy-efficient way compared with wet-spinning, the spinning of various lignin is only possible in a mixed polymer solution (Kim et al. 2015; Liu et al. 2016b). In practice, melt-spinning, wet-spinning and electrospinning are usually used to prepare LDC fibers.

The preparation route for the production of LDC fibers is depicted in Fig. 5a (Fang et al. 2017). In a typical preparation process, lignin is firstly pretreated by purification, refining, additional modification, and blending. The pretreated lignin solution is spun into fibers via extrusion approaches, including melt-spinning, wet-spinning, dry-spinning, gel-spinning, or electrospinning (Lallave et al. 2007; Ruiz-Rosas et al. 2010). Then, the lignin-based fibers are oxidatively thermostabilized under an oxygen-containing atmosphere to form a cross-linked carbonaceous structure at a slow heating rate, which is one of the critical procedures in carbon fiber fabrication (Lallave et al. 2007; García-Mateos et al. 2018). After thermal stabilization, the LDC fibers further experience the carbonization process at temperatures above 600 °C, when the condensed structure is formed and the LDC fibers

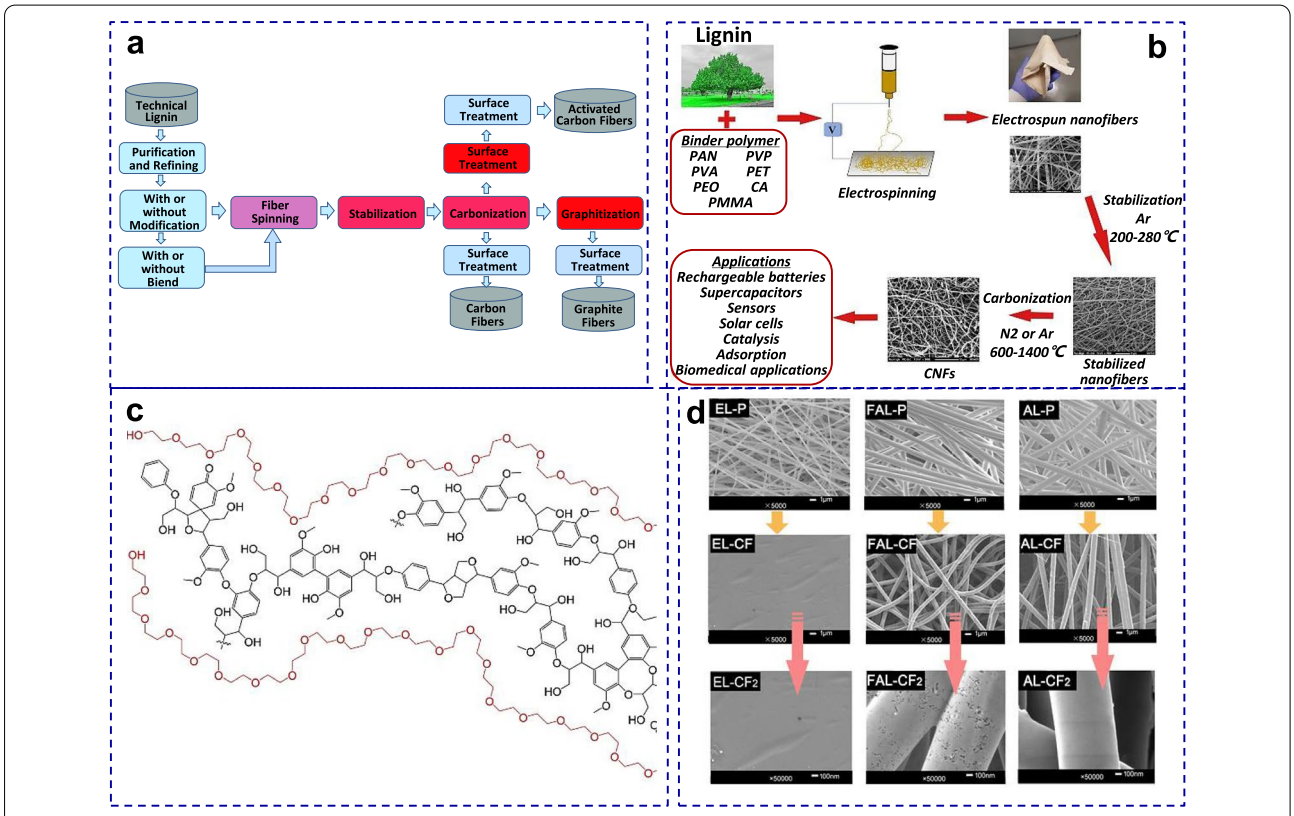

Fig. 5 **a** Typical preparation processes for LDC fibers. Reproduced with permission from Ref. (Fang et al. 2017). Copyright © 2016, Roal Society of Chemistry; **b** Methodologies of LDC fibers by electrospinning technique. Reproduced with permission from Ref. (Svinterikos et al. 2020). Copyright © 2020, American Chemistry Society; **c** A schematic showing the assembly of PEO and lignin. Reproduced with permission from Ref. (Imel et al. 2016). Copyright © 2016, American Chemistry Society; **d** Images of carbon fibers from different types of lignin. Reproduced with permission from Ref. (Shi et al. 2018). Copyright © 2020, American Chemistry Society

gain high mechanical strength. Particularly, modification treatments (e.g., activation or graphitization) could be further performed to obtain activated carbon fibers and graphitic LDC fibers with enhanced structural or functional properties (Sagues et al. 2019).

Figure 5b shows the general methodology for the production of LDC fibers using the electrospinning technique (Svinterikos et al. 2020). Generally, electrospun lignin fibers are prepared from a mixed solution of lignin and other polymers, e.g., polyacrylonitrile (PAN), polyvinyl alcohol (PVA), and polyethylene oxide (PEO), with better spinnability. Loscertales et al. prepared LDC fibers by electrospinning pure Alcell lignin without using other polymer binders (Lallave et al. 2007). Alcell lignin or called organosolv lignin is another lignin derivative from Alcell pulping process, which contains less impurities than Kraft lignin. The direct electrospinning of lignin is nevertheless rather difficult. Therefore, it is necessary to add another polymer with high molecular weight (such as PAN, PVA and PEO) into the electrospinning solution. PAN is usually chosen as a binder in the lignin solution due to its easy spinnability.

Lee et al. prepared lignin/PAN-based carbon fibers at mass ratios from 0/100 to 50/50 (lignin/PAN) (Choi et al. 2013), where the PAN used in this work had a molecule weight of 150,000. The obtained fibers were further thermostabilized, treated under 250 °C for 3 h in air and carbonized at 1000 °C for 1 h in an inert atmosphere. The carbon fibers became thinner, and the SSA decreased with increasing lignin content. Wang et al. found that increasing lignin content resulted in a decrease in average diameter and an increase of SSA (Wang et al. 2018). Ferraris et al. used Kraft lignin and PAN with mass ratios from 10/90 to 70/30 to prepare lignin/PAN-based carbon fibers (Perera Jayawickramage et al. 2019), followed by thermal stabilization, carbonization and physical activation at 1000 °C in CO_2 flow. With the highest lignin blending ratio (PAN: lignin = 70:30), the obtained carbon fiber achieved the largest SSA of 2543 $m^2\ g^{-1}$ and excellent conductivity of 530 S m^{-1}. Beck et al. prepared lignin/PVA-based carbon fibers with a lignin/PVA blend at a mass ratio of 70/30, and obtained carbon fibers with average diameters less than 200 nm, SSA of 583 $m^2\ g^{-1}$ and average pore sizes around 3.5 nm (Beck et al. 2017). The high SSA was believed to result from the phase separation process during the carbonization of the PVA/PAN blend. PEO is another choice for blending with lignin in the electrospinning process. As illustrated in Fig. 5c, PEO (1–2 wt%) can form hydrogen bonds with the hydroxyl groups of lignin macromolecules, leading to abundant chain entanglements, which would benefit electrospinning (Imel et al. 2016). Shi et al. studied the carbonization behaviors of blends of three lignins and PEO at a mass ratio of 95/5 (Fig. 5d) (Shi et al. 2018). The low-molecular-weight ethanol organosolv lignin could not be thermostabilized in the melting process. The formic acid/acetic acid organosolv lignin-derived carbon fibers showed poor mechanical properties due to the existence of many side chains. Because of the better orientation and fewer side-chains in lignin macromolecules, the alkaline LDC fibers displayed a high graphitization degree and high tensile strength of 15.58 MPa.

3.2 Carbon spheres

Carbon spheres and hollow carbon spheres are promising carbon materials for energy storage and environmental applications. The carbonization of colloidal spheres and spheres derived from spray drying are the common methods to prepare LDC spheres. The self-assembly technique for lignin nanospheres is the key to the preparation of the spherical morphology of lignin. Lignin nanospheres were prepared by solvent exchange (solvent and antisolvent) (Xiong et al. 2020) followed by spray drying or in an aerosol flow reactor (Xiong et al. 2017). Monodispersed lignin colloidal spheres can be prepared by a coupled strategy of solvent extraction, solvent/antisolvent self-assembly (Wang et al. 2022d). Solvent exchange is the most popular and efficient methodology to assemble lignin nanospheres owing to its simple and environmentally friendly advantages. The inner interaction of the lignin nanosphere is by weak intermolecular forces, generally hydrogen bonding, π-π interactions, electrostatic and hydrophobic forces (Wang et al. 2020a). The lignin nanospheres have poor solubility resistance and thermostability, and the spherical structure could hardly be maintained in organic solvents, such as tetrahydrofuran (THF), acetone, and ethanol (Xiong et al. 2017; Wang et al. 2020a).

Furthermore, lignin would undergo severe and irreversible condensation under the high-temperature carbonization process (Shuai et al. 2016). Therefore, how to prepare intact LDC spheres from the carbonization of the lignin colloidal nanosphere is another problem to be solved. Hydrothermal and thermal carbonizationa are two efficient ways for the preparation of carbon spheres. Chemical cross-linking could strengthen the three-dimensional network structure and hence improve the physical and chemical properties of the lignin spheres (Souza et al. 2019; Wang et al. 2019a).

Wu et al. prepared lignin nanospheres by solvent exchange method followed by covalent cross-linking by hydrothermal treatment, as illustrated in Fig. 6a (Wang et al. 2021a). Hydrothermal temperature played a significant role in fracturing β-O-4/C_α-C_β bonds, hydroxyl and $-OCH_3$ groups, in which free radicals form in the lignin nanospheres. The adjacent intramolecular and

intermolecular radicals could then be crosslinked via α-5, β-5 and β-β′ bonds. The higher the temperature is, the higher the crosslinking degree is; therefore, the smaller the diameter of the lignin nanosphere is. The carbon spheres prepared from the lignin nanospheres maintained perfect spherical structures and displayed a small graphitic degree and high carbon content. Qiu et al. developed a novel strategy to prepare novel uniform lignin-derived nitrogen-doped (5.73%) carbon nanospheres by direct pyrolysis of colloidal spheres of lignin-based azo polymer (AL-azo-NO_2) at 750 °C (Zhao et al. 2016). The percentage of the rigid segment around the hydrophilic segments increased after diazotization treatment. The parallel arrangement of rigid azo benzene segment drives the formation of uniform and tight colloidal spheres of a size of about 200–300 nm (Deng et al. 2016), where a large number of uniform spheres (500 nm) are also formed in the pyrolysis process.

Spray drying technique is a scalable and effective method to synthesize carbon spheres (especially hollow carbon spheres) from lignin precursor solution via a simple one-step process. Chen et al. firstly prepared a spherical lignin composite by spray drying of a mixture of lignosulfonate and KOH (Chen et al. 2018). In this synthesis strategy, KOH was used to dissolve lignin so as to form a homogeneous solution. Upon spray drying, lignin/KOH hollow structures were formed. After the simultaneous carbonization and activation at high temperatures, the porous carbon spheres showed an SSA of 1372 $m^2 g^{-1}$ and an appropriate pore structure (average pore size of 2.59 nm). Li et al. synthesized plum-like hard carbon microspheres (1–2 μm) from sodium lignosulfonate by spray drying and carbonization. The sodium SLS-derived hard carbon microspheres have enlarged interlayer spacing, fewer defects, and a small SSA of 11.89 $m^2 g^{-1}$ (Li et al. 2020a). This hard carbon anode showed superior sodium storage performance. Cao et al. used Kraft lignin as a carbon precursor and KOH as an activation agent to prepare hollow carbon spheres with high SSAs of 1536 – 2424 $m^2 g^{-1}$ and hierarchical structure (Cao et al. 2021a) (Fig. 6b). Cao et al. further precisely controlled the spherical morphologies from dense to hollow spheres by tuning the KOH concentration (Cao et al. 2021b). A high concentration of KOH resulted in the formation of hollow structures, while the highest mass ratio of KOH to lignin used was below 1.5:1. Given the low consumption of KOH for the production of activated carbon spheres with a high SSA, it is a promising method for large-scale production. Pang et al. synthesized oxygen/nitrogen co-doped hierarchical porous hollow carbon microspheres (0.2–5 μm) from sodium lignosulfonate by spray drying, thermal stabilization, carbonization, and post nitric acid modification. The as-prepared hollow carbon microspheres have an SSA of 991 $m^2 g^{-1}$, a total pore volume of 0.75 $cm^3 g^{-1}$, and abundant surface contents of oxygen (13.12 at.%) and nitrogen (0.97 at.%) (Pang et al. 2018b).

Hydrothermal technique and reverse phase polymerization coupled with a carbonization process can also be used to prepare LDC microspheres. Fan et al. synthesized nitrogen-doped lignin microspheres by lignin self-decomposition and self-polymerization via hydrothermal process at 250 °C and carbonization at 1100 °C. The nitrogen-doped LDC microspheres exhibit well-developed spherical morphology, ultramicroporous (< 0.7 nm) structure, and large interlayer spacing, which endows it with superb sodium storage performance with high specific capacity and stable cycling stability (Fan et al. 2021). Yu et al. prepared a LDC microsphere using

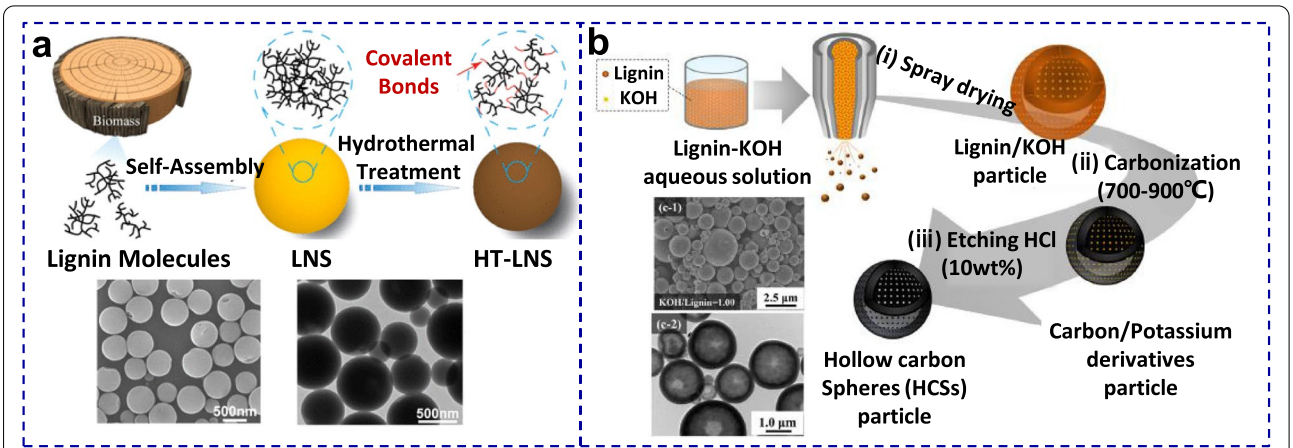

Fig. 6 **a** Schematic diagram of the preparation of lignin-derived nanosphere. Reproduced with permission from Ref. (Wang et al. 2021a). Copyright © 2021, American Chemistry Society; **b** Schematic diagram of the preparation of hollow carbon sphere from Kraft lignin. Reproduced with permission from Ref. (Cao et al. 2021a). Copyright © 2021, Elsevier

reverse-phase polymerization and direct carbonization without pre-oxidization. The morphology, size distribution and thermal stability of LDC microsphere could be controlled by coordinating the solid content and dispersed phase content of lignin emulsion (Yu et al. 2018).

3.3 Carbon foam

Carbon foam has attracted great attention due to its low density, high conductivity, high porosity, and tunable pore size. LDC foam is generally prepared by drying and carbonization of phenolic wet gel. Lignin is an appropriate candidate to replace resorcinol or other phenolic substances to prepare phenolic resin due to the similar chemical moieties of phenolic, carboxyl, carbonyl, hydroxyl groups (Vázquez et al. 1999; Jin et al. 2010). Additionally, the three-dimensional network structure and high carbon content of lignin are conducive to preparing carbon foam from a sustainability perspective.

Seo et al. synthesized LDC foams with porous structural frameworks using a thermal decomposition route at a temperature of 800 °C. The polycondensation reaction of lignin, resorcinol, and formaldehyde into crosslinked phenolic resin network was performed with colloidal poly(methyl methacrylate) microspheres as a sacrificial template. After carbonization, the carbon foam had a bulk density of 0.37–0.60 g mL^{-1} and porosity of 68.5–82.8%. The LDC foam exhibited excellent mechanical strength (Seo et al. 2014). Qu et al. used lignin to replace 25 wt.% phenol to prepare lignin-phenol–formaldehyde resole resin in an alkaline environment. Then, the carbon foams were synthesized using the resin as a carbon source and polyurethane foam as the template. The as-prepared carbon foams showed open macropores, low bulk density, and good water repellency (Qu et al. 2017). Xu et al. synthesized lignin-based carbon foams by pyrolysis and KOH activation (Xu et al. 2018a), where enzymatic hydrolysis lignin, resorcinol and formaldehyde were mixed under Na_2CO_3 catalysis to prepare lignin-based aerogels after gelation, aging and ambient drying. The as-prepared carbon foam has a high SSA of 779 $m^2\ g^{-1}$, a large total pore volume of 0.48 $cm^3\ g^{-1}$ and a large micropore volume of 0.29 $cm^3\ g^{-1}$. Furthermore, the carbon foam displayed an interconnected, hierarchical porous network structure and a high degree of graphitization (Xu et al. 2018a). The carbon foams are essential for some applications that need macropores.

4 Pore engineering of LDCs

The pore structure is an important parameter of carbon materials. Developing the pore engineering method is a long-last research theme since LDPCs with high SSA is important for many applications, such as capacitive energy storage, adsorption of inorganic or organic pollutants, and batteries. The pore engineering strategies for LDPCs can be classified into physical activation, chemical activation, template methods and direct carbonization methods (Fig. 7). There are some review papers focusing on the synthesis strategies of porous carbon materials (Borchardt et al. 2018; Jin et al. 2018; Ghosh et al. 2020; Shao et al. 2020; Yin et al. 2020a) and LDPCs (Zhu et al. 2020; Zhang et al. 2021g; Wang et al. 2022a). Herein, in this paper, we only briefly overview some general synthesis strategies, i.e., the traditional activation and template methods and novel direct carbonization strategies, for LDPCs.

4.1 Physical activation

Physical activation is also called gaseous activation. The principle of pore engineering of physical activation lies in that gaseous activation agents, such as CO_2, NH_3 and steam, gasify carbon matrix at 600–1200 °C. CO_2 activation has been used as a physical activation agent for carbon materials for a long time. CO_2 activation results in the etching of carbon matrix to form CO. Schlee et al. produced Kraft lignin-derived carbon fiber mats by carbonization at 900 °C for 30 min followed by CO_2 activation at 800 °C for 60 min. The porosity of the LDPC with CO_2 activation was more abundant than that without CO_2 activation. It was proposed that CO_2 activation expanded micropores to form mesopores and created new micropores. The carbon fiber mats with CO_2 activation showed a higher SSA of 1204 $m^2\ g^{-1}$ than that without CO_2 activation (676 $m^2\ g^{-1}$) (Schlee et al. 2019). Jayawickramage et al. prepared carbon fiber mats derived

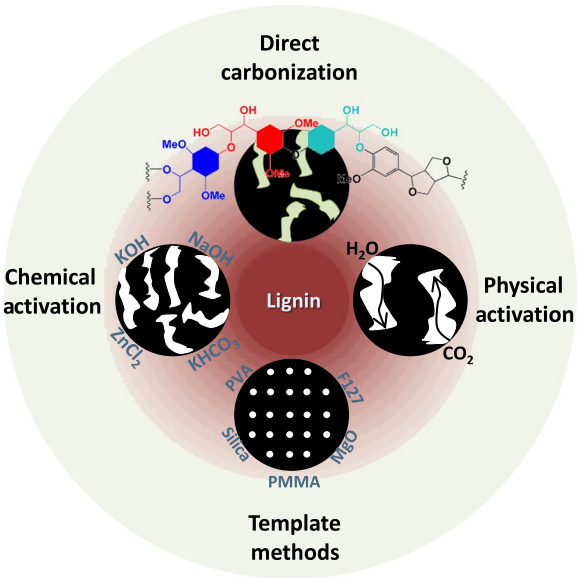

Fig. 7 A summary of strategies of pore engineering for lignin-derived porous carbons (LDPCs)

from lignin and PVA by electrospinning, and then carbonization at 1000 °C and CO_2 activation at 800 °C. With the decrease of lignin content in the lignin/PVA composite, the SSA, micropore volume and mesopore volume of LDC fiber mats firstly increased and then decreased. The LDC fiber mat derived from lignin/PVA blend of 80/20 exhibits a high SSA of 2,170 $m^2\ g^{-1}$, a mesopore volume of 0.622 $cm^3\ g^{-1}$ and a micropore volume of 0.365 $cm^3\ g^{-1}$ (Perera Jayawickramage and Ferraris 2019). Jayawickramage et al. prepared carbon fiber mats from lignin and PAN using a similar synthesis route. With the increase of lignin in lignin/PAN blend, the SSA and mesopore volume increased while the micropore volume decreased. The LDC fiber mats derived from lignin/PVA blend of 70/30 have a very high SSA of 2,543 $m^2\ g^{-1}$, a mesopore volume of 0.955 $cm^3\ g^{-1}$ and a micropore volume of 0.547 $cm^3\ g^{-1}$ (Perera Jayawickramage et al. 2019).

As a new physical activation method, NH_3 activation generates pores through the reaction between carbon and NH_3, producing N_2 and CH_4 (Luo et al. 2014). The precise reaction mechanism of NH_3 activation needs to be further explored. Zuo et al. proposed four successive stages in the process of NH_3 activation to engineer pore structure, which correspond to the temperature range lower than 800 °C (< 20% burn-off), the temperature range at 850–950 °C (20–75% burn-off), the temperature range at 950–1000 °C (75–80% burn-off) and the region higher than 1000 °C (> 80% burn-off). In the first stage, the reaction between NH_3 and carbon mainly contributed to the micropore formation with a 19.3% char burn-off. The SSA and total pore volume increased from 124 to 702 $m^2\ g^{-1}$ and 0.02 to 0.33 $cm^3\ g^{-1}$. In the second stage, the reaction between NH_3 and carbon intensified, which mainly contributed to the formation of micropores (1–2 nm) with 74.7% char burn-off. The SSA increased from 702 to 1431 $m^2\ g^{-1}$ and the total pore volume increased from 0.33 to 0.76 $cm^3\ g^{-1}$, showing a linear correlation with increasing the activation temperature. In the third stage, the porosity was remarkably developed with 5% increase in char burn-off, widening the existing micropores to form mesopores (2–4 nm), and generating new micropores (1–2 nm). The SSA increased from 1431 to 2316 $m^2\ g^{-1}$ and the total pore volume increased from 0.76 to 1.48 $cm^3\ g^{-1}$. Particularly, the mesopore volume increased from 0.05 to 0.34 $cm^3\ g^{-1}$, and micropore volume increased from 0.71 to 1.13 $cm^3\ g^{-1}$. In the fourth stage, the intensified reaction between NH_3 and carbon resulted in the decrease of SSA and pore volume due to the collapse of the pore wall with a burn-off percentage above 80% (Zuo et al. 2020). Zhang et al. prepared enzymatic hydrolysis LDPC by NH_3 activation. They explored the free radical mechanism of the NH_3 activation and the relationship between nitrogen doping configurations, doping levels, and preparation temperatures. With increasing the temperature, the SSA, total pore volume and micropore volume increased from 335.9 to 1464.0 $m^2\ g^{-1}$, 0.17 to 0.66 $cm^3\ g^{-1}$, respectively. Despite the decreased nitrogen content with increased temperature, the relative content of pyrrolic nitrogen increased. Therefore, it is demonstrated that the unsaturated electron-deficient radicals (NH_2· and NH·) reacted with electron-rich N6, leading to a larger decrease of N6 than that of N5 (Jian et al. 2022).

Water steam activation is used to generate pore structure by reacting with carbon to produce H_2 and CO. Generally, the steam activation rate is several times faster than that of CO_2 activation. Fu et al. studied the effect of preparation parameters (carbonization temperature, steam activation temperature and activation time) on the pore texture characteristics of LDPCs. With increasing the carbonization temperature from 250 °C to 450 °C, the SSA increased from 86.41 to 288.79 $m^2\ g^{-1}$ and the micropore volume increased from 30.46 to 171.04 $cm^3\ g^{-1}$. When the carbonization temperature exceeded 450 °C, the SSA remained unchanged while the average pore diameters increased. The SSA increased from 227.43 to 288.79 $m^2\ g^{-1}$ with the activation temperature rising from 700 to 725 °C, and then decreased to 193.15 $m^2\ g^{-1}$ if the activation temperature was further increased to 850 °C. An activation time of 40 min was found to be suitable for preparing LDPCs with high SSAs. When the activation time increased beyond 40 min, the SSA decreased significantly (Fu et al. 2013). Carrott et al. prepared an LDPC from enzymatic hydrolysis lignin (EHL) with a SSA of 812 $m^2\ g^{-1}$ and a micropore volume of 0.27 $cm^3\ g^{-1}$ by steam activation at 750 °C (Carrott et al. 2008). Baklanova et al. prepared an EHL-derived porous carbon with an SSA of 865 $m^2\ g^{-1}$ and a micropore volume of 0.37 $cm^3\ g^{-1}$ by steam activation at 800 °C (Baklanova et al. 2003). It needs to be noted here that air could also be used as an activation agent; however, the reaction rate of air with carbon is too fast to be controlled; therefore, air was rarely used to construct LDPCs in practice (Zhang et al. 2021g).

4.2 Chemical activation

The pore engineering by chemical activation is to use chemical activation agents, such as KOH, NaOH, H_3PO_4 and $ZnCl_2$, to etch carbon matrix at temperatures in the range of 600–900 °C. Recently, $CuCl_2$ is also employed as a chemical activation agent for LDPCs (Wen et al. 2022).

KOH has been widely used to prepare LDPC owing to its capability to promote the formation of porous carbons with high SSA and large pore volume, which is suitable for many applications (Zhang et al. 2015c, a). The activation mechanisms of NaOH, Na_2CO_3 and K_2CO_3 are

similar to that of KOH (Yin et al. 2020a). However, the SSA and pore volume of LDPCs prepared with KOH are higher than those prepared with other chemical activation agents. The KOH activation mechanisms are summarized as follows (Guo et al. 2019): (1) KOH reacts with carbon to produce K, K_2CO_3 and H_2 at 400 °C; (2) K_2CO_3 decomposes into K_2O and CO_2 above 700 °C; (3) CO_2 and H_2O react with carbon to produce CO and H_2; (4) the produced K_2CO_3 and K_2O react with carbon to produce K and CO; (5) the metallic K intercalates the carbon framework to form branch-like micropore channels.

As shown in Fig. 8a, Dai et al. used KOH as an inorganic template and chemical activation agent to prepare sodium lignosulfonate-derived LDPC with an SSA of 2,235 $m^2\ g^{-1}$ and pore volume of 1.512 $cm^3\ g^{-1}$ at a lignin/KOH mass ratio of 1/3 (Tan et al. 2021). Lee et al. investigated the difference in structural characteristics of porous carbons prepared from Kraft and alkaline lignin using KOH activation. KOH could interact with NaOH in Kraft or alkaline lignin to form NaOH/KOH eutectic mixture, which contributed to the microporous and mesoporous structure in Kraft and alkaline LDPCs. In contrast, the KOH activation of an EHL-derived carbon contributed to the microporous structure. The porous carbon materials derived from alkaline lignin and EHL with KOH activation have SSAs of 1825 and 2345 $m^2\ g^{-1}$, and pore volumes of 1.72 and 1.74 $cm^3\ g^{-1}$, respectively (Lee et al. 2018). Chen et al. prepared porous carbon spheres with a SSA of 1372.87 $m^2\ g^{-1}$ by spray drying a solution of lignosulfonate and KOH and subsequent carbonization (Chen et al. 2018). Tran et al. prepared porous graphite oxide/lignin nanocomposite films with SSA of 1744 $m^2\ g^{-1}$ using KOH activation (Tran et al. 2017). Wan et al. prepared three-dimensional hierarchical porous carbon from oxidized lignin using one-step KOH-activation and carbonization method. The lignin-derived hierarchical porous carbon shows a SSA of 3094 $m^2\ g^{-1}$ and a pore volume of 1.72 $cm^3\ g^{-1}$ under a KOH/lignin mass ratio of 3/1 (Wan et al. 2021). Wang et al. prepared N-doped porous carbon from urea-modified lignin with a high SSA of 3130 $m^2\ g^{-1}$ via carbonization and KOH activation (Wang et al. 2016b). Zhu et al. used KOH as both a lignin extraction solvent and an activation agent and melamine as a nitrogen source to prepare LDPC with a SSA of 2646 $m^2\ g^{-1}$ and a high pore volume of 1.285 $cm^3\ g^{-1}$ (Zhu et al. 2017).

Hydrothermal and microwave-assisted KOH activation has also been widely reported to prepare LDPC, as illustrated in Fig. 8b and c. Guo et al. prepared interconnected hierarchical porous nitrogen-doped carbon via hydrothermal treatment and KOH activation of EHL. The obtained LDPC has a SSA of 2218 $m^2\ g^{-1}$, high electronic conductivity of 4.8 S cm^{-1} and a nitrogen doping content of 3.4 at% (Zhang et al. 2016a). Zhang et al. used sodium lignosulfonate as a carbon precursor, 1,6-hexanediamine as a crosslinking agent and nitrogen source to prepare nitrogen-doped hierarchical porous carbon by hydrothermal crosslinking reaction and KOH activation. The as-prepared LDPC has an SSA of 1867.4 $m^2\ g^{-1}$, a moderate nitrogen-doped content of 3.6 at.% and a three-dimensional hierarchical porous structure with rich micropores, abundant mesopores and interconnected macropores (Zhang et al. 2018d). Li et al. prepared EHL-derived LDPC with a three-dimensional interconnected hierarchical structure and a SSA of 1504 $m^2\ g^{-1}$ (Li et al. 2021a). Guo et al. used KOH to activate EHL-derived hydrochar to prepare EHL-derived LDPC at 800 °C with a KOH/char mass ratio of 1–3. The obtained LDPC has a SSA of 1290–1660 $m^2\ g^{-1}$ and a three-dimensional hierarchical texture consisting of abundant micropores, as well as some mesopores and macropores, and high electronic conductivity of 4.0–5.4 S cm^{-1} (Guo et al. 2017). Microwaves could assist the activation process and shorten the reaction time. Zhou et al. explored the effects of preparation conditions on the morphology and pore structure of LDPC sphere by microwave carbonization with KOH activation. The carbon spheres with sizes of 3–6 μm were obtained by activation at 270 °C for 7 h with a KOH concentration of 0.06 g mL^{-1} (Mao et al. 2018). Zhou et al. prepared LDPC with KOH activation using a microwave heating method under humidified nitrogen atmosphere. The as-prepared LDPC exhibited a high SSA of 2866 $m^2\ g^{-1}$, hierarchical pore structure with micropores volume of 0.70 $cm^3\ g^{-1}$ and considerable meso-/macropores volume of 1.33 $cm^3\ g^{-1}$ (Chen et al. 2019b). Zhou et al. prepared LDPC using microwave heating and KOH activation in a very short duration of 10–30 min. The LDPC displayed ultra-high SSA of 3065 $m^2\ g^{-1}$, a hierarchical porous structure with a micropore volume of 0.73 $cm^3\ g^{-1}$, and a meso-/macropores ratio of 64.4% (Chen et al. 2020c). Directly mixing of KOH with lignin (Zhang et al. 2015a, 2018c), or mixing KOH with lignin-derived char (Zhang et al. 2015c) could be used to tune the micropore structure of LDPCs. Relative low SSA with micropore structure could be achieved by direct mixing, while high SSA with hierarchical micro/mesopore structure could be achieved by carbonization-activation strategy.

$ZnCl_2$ and H_3PO_4 are commonly used as low-temperature activation agents to prepare LDPCs. $ZnCl_2$ can promote gasification dehydrogenation at low temperatures and act as a supporting template (Yu et al. 2016). Phosphoric acid acts as a catalyst in the activation process to promote the fracturing of macromolecular chains and the dehydration reaction, which hence promotes the formation of pore structures in the process of

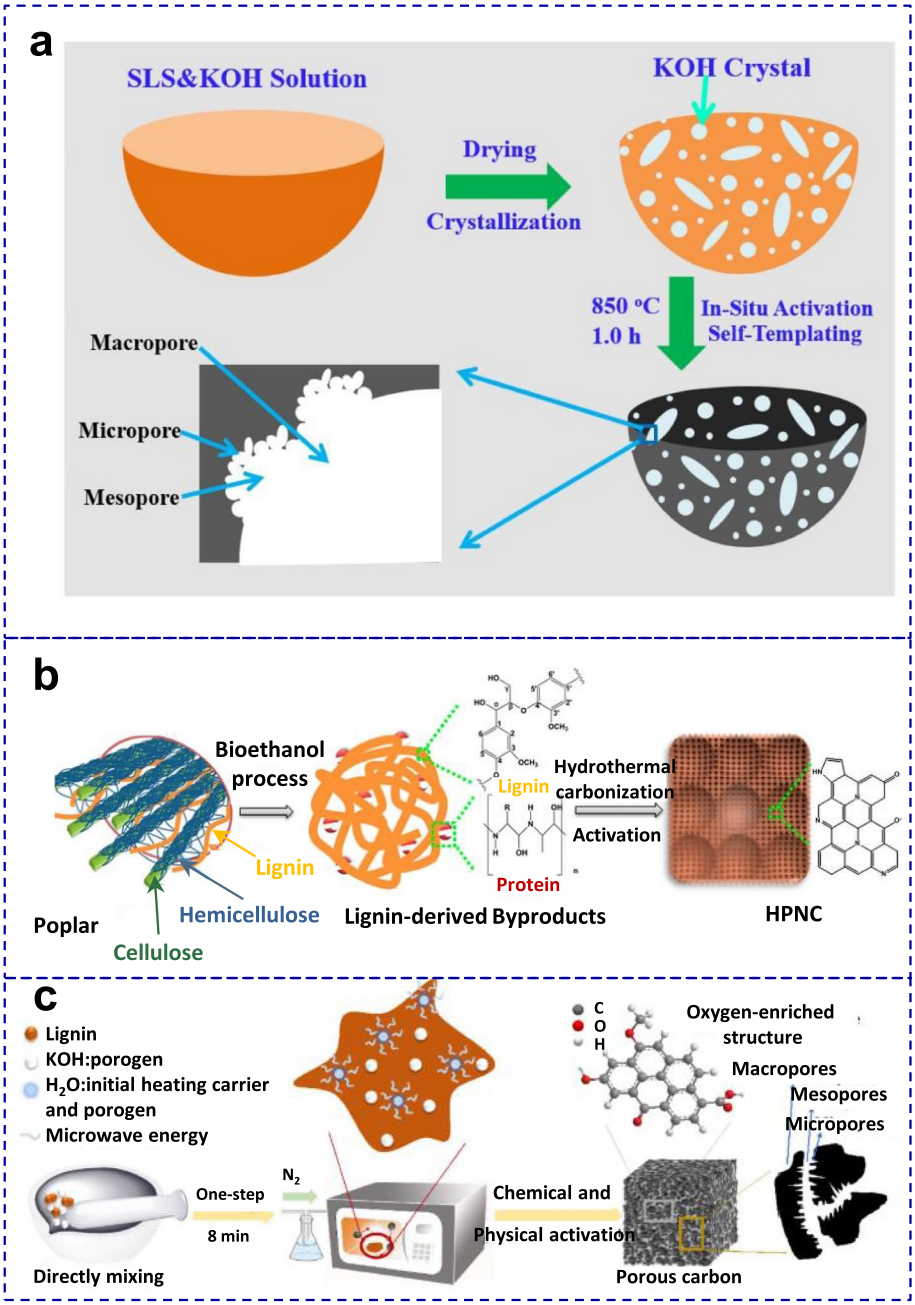

Fig. 8 Schematic diagram of the synthesis of LDPCs with hierarchical structure (**a**) using KOH activation strategy. Reproduced with permission from Ref. (Tan et al. 2021). Copyright © 2018, Elsevier; (**b**) using hydrothermal carbonization and chemical activation strategy. Reproduced with permission from Ref. (Zhang et al. 2016a). Copyright © 2016, American Chemistry Society; (**c**) using microwave and KOH activation strategy. Reproduced with permission from Ref. (Wang et al. 2019b). Copyright © 2019, Wiley

thermal polycondensation and cyclization (Yahya et al. 2015). Gonzalez-Serrano et al. prepared alkali LDPC with a H_3PO_4/char mass ratio of 1. With increasing temperature from 350 °C to 500 °C, the SSA of porous carbon increased from 534 to 1347 $m^2\ g^{-1}$. At temperatures above 500 °C, the SSA decreased to 1153 $m^2\ g^{-1}$ (Gonzalez-Serrano et al. 1997). Yang et al. prepared sulfuric acid hydrotropic LDPC with a high SSA of over 2000 $m^2\ g^{-1}$ at 450 °C using H_3PO_4 activation (Yang et al. 2020). García-Mateos et al. prepared lignin-derived microporous carbon fiber with a SSA of 2340 $m^2\ g^{-1}$ at 900 °C using H_3PO_4 activation by direct carbonization

lignin under an inert atmosphere or with diluted O_2 (García-Mateos et al. 2020). Brazil et al. investigated the effects of H_3PO_4 loading amount, time, temperature, and microwave power on the surface area of Kraft lignin-derived porous carbon prepared using conventional and microwave-assisted pyrolysis, respectively. The H_3PO_4 loading amount was an important parameter for the surface area of porous carbon. The SSA of the porous carbons obtained at lignin: H_3PO_4 ratio of 1:1 and 1:2 was 1150 and 1030 $m^2\ g^{-1}$, respectively (Brazil et al. 2020).

4.3 Template-based methods

Template methods, including soft template and hard template methods, have been widely used to synthesize lignin-derived mesoporous carbon. The pore-forming mechanism of the soft template method, in principle, is to form the composite micelles by electrostatic or hydrogen bond self-assembly of soft template and lignin. The soft template decomposes during the carbonization process to produce mesopores. The fully decomposable Pluronic P123 (poly(ethylene oxide)$_{20}$-poly(propylene oxide)$_{70}$-poly(ethylene oxide)$_{20}$), Pluronic F127 (poly(ethylene oxide)$_{106}$-poly(propylene oxide)$_{70}$-poly(ethylene oxide)$_{106}$, and partially decomposable polyvinyl chloride (PVC) or polyvinyl alcohol (PVA) are the commonly used soft templates.

As shown in Fig. 9a, Saha et al. first reported the synthesis of lignin-derived mesoporous carbon using the Pluronic F127 template. The obtained mesoporous carbon has mesopores in the range of 2.5–12.0 nm, a SSA of 418 $m^2\ g^{-1}$ and a mesopore volume of 0.34 $cm^3\ g^{-1}$ which is twice the micropore volume (Saha et al. 2013). Qin et al. investigated the effect of lignin molecular weight on the structure and morphology of mesoporous carbon. The mesoporous carbon prepared from low-molecular-weight lignin had highly ordered mesoporous channels (3.8 nm) and high SSA (466 $m^2\ g^{-1}$) (Qin et al. 2018). Herou et al. prepared lignin-derived mesoporous carbon using phloroglucinol, glyoxal, F127, and organosolv lignin. The PPO units of F127 could assemble with lignin to form micelles, and the PEO units could interact with the solvent, while phloroglucinol could surround the PEO segments through hydrogen bonds and glyoxal as a tetra-functional cross-linking precursor. The as-prepared lignin-derived mesoporous carbon with a SSA of 673 $m^2\ g^{-1}$ and a pore volume of 0.5 $cm^3\ g^{-1}$ exhibited a 2D-hexagonal pore structure (Herou et al. 2019). Similar approaches have been employed by Gan and Qi to achieve mesoporous carbon materials (Wang et al. 2020b, 2021e).

The pore-forming mechanism of the hard template method is to replicate the structure characteristics of the hard template. Therefore, the characteristics of hard templates play a key role in the formation of the porous structure. Silica-based templates and metal oxides are the common hard templates. Valero-Romero et al. used Alcell lignin as carbon precursors and different zeolite templates as hard templates to prepare lignin-derived mesoporous carbon using the liquid phase impregnation technique. Carbonization at 700 °C and a mass ratio of 1:1 were determined to be the optimal preparation conditions. The lignin-derived mesoporous caron prepared with zeolite Y, zeolite β, ZSM-5 and mordenite templates displayed high SSAs of 952, 864, 619 and 682 $m^2\ g^{-1}$, and total pore volume of 0.35, 0.32, 0.15 and 0.28 $cm^3\ g^{-1}$, respectively (Valero-Romero et al. 2014). As shown in Fig. 9b, Huang et al. used SiO_2 and cetyltrimethylammonium bromide (CTAB) dual templates to prepare lignin-derived honeycomb-like mesoporous carbon with a SSA of 1107 $m^2\ g^{-1}$, a mesopore volume of 2.06 $cm^3\ g^{-1}$ and a total pore volume of 2.35 $cm^3\ g^{-1}$ through a self-assembly strategy (Huang et al. 2021b). Li et al. found that silica nanoparticles with a size of 7 nm could lead to synthesis of a highly porous structure compared with that with sizes of 100 and 200 nm prepared using P123 and silica nanoparticles dual templates. With increasing the silica nanoparticles loading from 10 wt.% to 60 wt.%, the SSA of lignin-derived mesoporous carbon increased from 407 $m^2\ g^{-1}$ to 636 $m^2\ g^{-1}$ (Li et al. 2020c).

Although silica hard templates could be used to prepare lignin-derived mesoporous carbon with a uniform structure, the silica templates are generally removed by hydrofluoric acid, which is not environmentally friendly. Metal oxide templates have been widely used in recent years because of the green advantage. Song et al. used spherical nano MgO template to prepare alkali lignin-derived mesoporous carbon with a high mesoporous ratio of 68.93% at 1000 °C. The SSA (85 $m^2\ g^{-1}$) was four times that of the LDC without MgO template (19 $m^2\ g^{-1}$) (Song et al. 2017). Zhang et al. designed a dedicated self-assembly strategy to synthesize lignin-derived hollow carbon from EHL using a spherical MgO template. EHL coated the MgO template via hydrogen bond self-assembly. After carbonization and template removal, the EHL-derived hollow carbon was obtained (Zhang et al. 2020a). Zhang et al. further used a lamellar MgO template to prepare EHL-derived flower-like carbon by the same hydrogen bond self-assembly strategy (Zhang et al. 2020b). Combining hard templates with chemical activation is also an efficient way to engineer the porous structure of LDPC. Yin et al. prepared N/S-doped carbon from lignin amine using Fe_3O_4 as a template and KOH activation. Fe_3O_4 contributed to the formation of macropores, favoring the formation of micropores and mesoporous on the wall by the subsequent KOH activation, and the as-prepared porous carbon had a SSA of 1199 $m^2\ g^{-1}$ (Yin et al. 2020c).

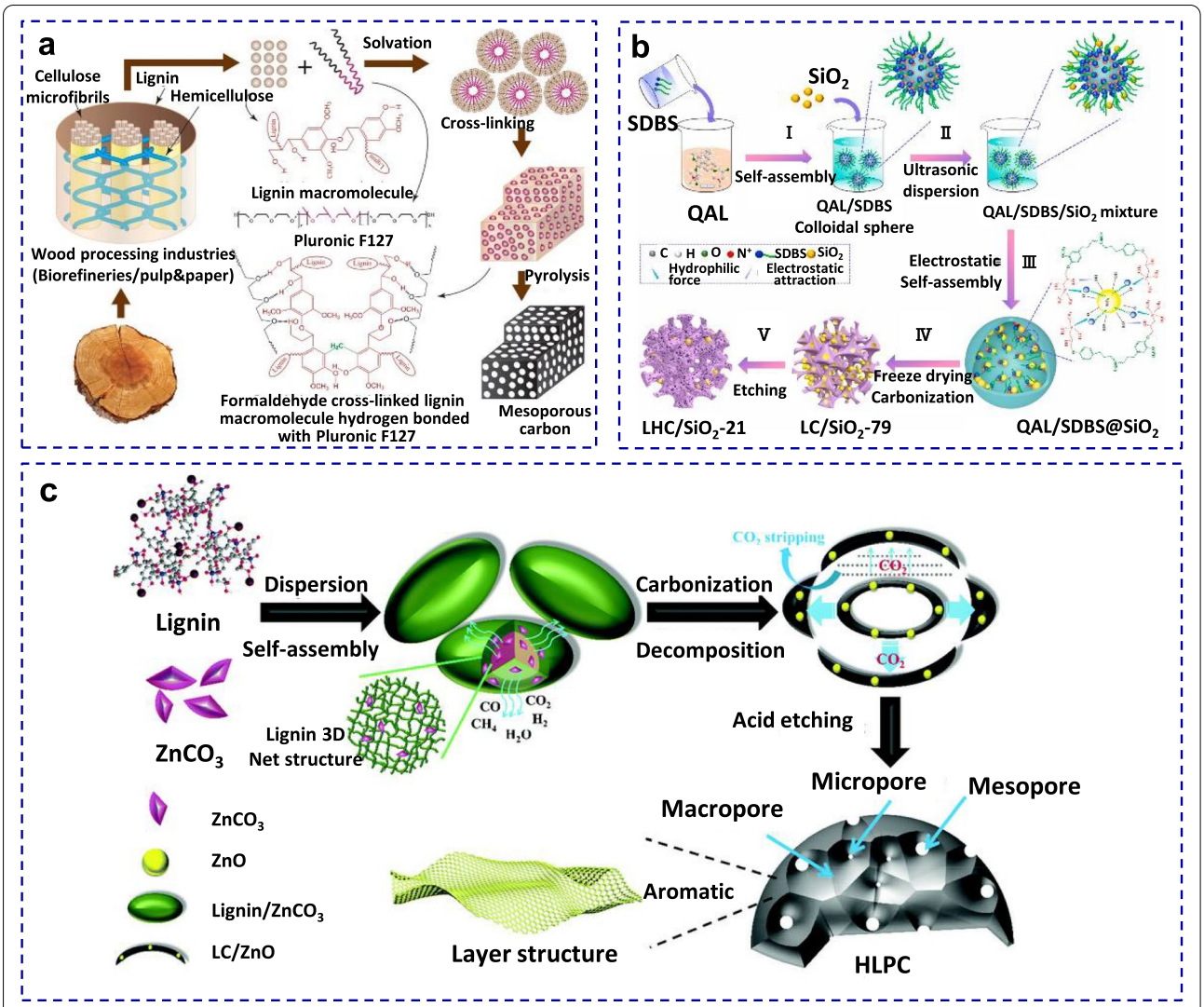

Fig. 9 **a** Schematic illustration of LDPC synthesis using a soft template. Reproduced with permission from Ref. (Saha et al. 2013). Copyright © 2013, American Chemistry Society; (b) Schematic illustrating of LDPC synthesis using soft and hard template strategy. Reproduced with permission from Ref. (Zhang et al. 2016a). Copyright © 2021, Elsevier; (c) Novel template strategy for LDPC synthesis. Reproduced with permission from Ref. (Xi et al. 2020). Copyright © 2020, Roal Society of Chemistry

The development of new templates to regulate the pore structure of LDPCs has also attracted extensive research attention. As shown in Fig. 9c, Xi et al. used $ZnCO_3$ with dual roles of gas exfoliation and an in-situ ZnO template to prepare hierarchical porous carbon from EHL. The as-prepared hierarchical porous carbon exhibited 3D porous structure and an SSA of 531 $m^2\ g^{-1}$. The SSA and pore volume increased with increasing the carbonization temperature to 600 °C (Xi et al. 2020). Fu et al. prepared lignosulfonate/ZnC_2O_4 composite using a hydrophobic bond self-assembly strategy. Owing to gas exfoliation and in-situ ZnO template roles of ZnC_2O_4 during the carbonization process, porous LDPC quasi-nanosheets with a SSA of 1069 $m^2\ g^{-1}$ and a total pore volume of 1.375 $cm^3\ g^{-1}$ were obtained (Fu et al. 2020). Furthermore, Fu et al. investigated the effects of $ZnCO_3$ and ZnC_2O_4 on the structure of LDPC, and concluded that ZnC_2O_4 had a synergistic effect with lignin, playing a key role in the preparation of hierarchical porous carbon with crumpled nanosheets (Fu et al. 2021).

4.4 Direct carbonization

The direct carbonization method is also called self-template method without additional activation agents, additives, or templates (Zhang et al. 2017; Yin et al. 2020b). A direct carbonization strategy could effectively eliminate

the usage of templates and activation agents. Therefore, direct carbonization is a facile, green-environmental, and low-cost route to engineering the pore structure of LDPCs. Direct carbonization of sodium lignosulfonate resulted in LDPCs with moderate SSAs owing to the template role of the pyrolysis product of Na_2SO_4 (Zhang et al. 2022). The pore-forming mechanism of the direct carbonization method is to use the rich inorganic minerals or metal ions in lignin to inhibit the decomposition and shrinkage of lignin or to chemically etch the carbon structure of the lignin at high temperatures. After the removal of the impurities, the developed porous structure was formed in the lignin-derived porous structure.

Liu et al. directly pyrolyzed Kraft lignin at 600–900 °C to prepare O-N-S co-doped hierarchical porous carbon with a large SSA of 338–1307 $m^2\ g^{-1}$, hierarchical porous structure and a heteroatoms co-doping level of 9.84–19.91 wt.% (Liu et al. 2019a). The Kraft lignin used contained inorganic impurities that could act as templates. Kijima et al. prepared alkaline lignin-derived microporous carbon with a SSA of 740 $m^2\ g^{-1}$ by carbonization at 900 °C. Furthermore, the SSA of alkaline lignin-derived porous carbon increased to above 1000 $m^2\ g^{-1}$ via micelle formation and polymer gelation techniques (Kijima et al. 2011). Chen et al. used calcium lignosulfonate as a carbon source to prepare porous carbon by simple carbonization at 600–800 °C. The SSA and pore volume increased from 628 to 1362 $m^2\ g^{-1}$ and 0.37 to 0.83 $cm^3\ g^{-1}$ with increasing the temperature from 600 to 800 °C (Chen and Zhou 2012). Pang et al. prepared interconnected hierarchical porous carbon from sodium lignosulfonate by direct carbonization at temperatures in the range of 600–1000 °C. The SSA and pore volume increased from 248 to 1010 $m^2\ g^{-1}$ and 0.22 to 0.56 $cm^3\ g^{-1}$, respectively, as the temperature increased from 600 °C to 800 °C. With increasing temperature from 800 °C to 1000 °C, the SSA increased to 1328 $m^2\ g^{-1}$ and pore volume further increased 1.06 $cm^3\ g^{-1}$, respectively (Pang et al. 2017). Li et al. directly carbonized the mixture of sodium lignosulfonate and melamine to prepare N–O-S doped porous carbon at 600–800 °C. With increasing temperature, the SSA of the LDPC increased from 164 to 808 $m^2\ g^{-1}$ and the micropore volume increased from 0.1 to 0.37 $cm^3\ g^{-1}$, respectively, while the nitrogen content decreased from 16.79 to 9.72 at.% (Li et al. 2021d). It needs to be noted here that the possible pore generation mechanism of lignosulfonate is that the inorganic metal species generate templates (such as Na_2SO_4). The molecular weight also influenced the pore structure of LDPCs. Jeon et al. investigated the structural properties of porous carbon derived from three types of lignin with different molecular weights. Generally, the SSA of porous carbon prepared from low-molecular-weight lignin was higher than that prepared from high-molecular-weight lignin (Jeon et al. 2015).

The developed porous structure of LDC by direct carbonization can be obtained in combination with other pretreatment techniques. Zhang et al. obtained LDPC with a large surface area of 1831 $m^2\ g^{-1}$ and abundant micropores and mesopores by a carbonization process assisted with a bacterial culture process (Zhang et al. 2019b). Liu et al. prepared LDC nanosheets by liquid nitrogen freeze-casting and direct carbonization at 900 °C (Liu et al. 2017). Demir et al. prepared sulfur self-doped porous carbon from calcium lignosulfonate by hydrothermal carbonization at 300 °C and thermal annealing at 700–1000 °C. The SSA increased from 78 to 660 $m^2\ g^{-1}$, and the pore volume increased from 0.05 to 0.25 $cm^3\ g^{-1}$ at 700–800 °C, and then decreased from 660 to 260 $m^2\ g^{-1}$, 0.25 to 0.12 $cm^3\ g^{-1}$ at 800–1000 °C (Demir et al. 2018). Liu et al. prepared nitrogen and phosphorus dual-doped LDC microspheres with a high SSA of 938.1 $m^2\ g^{-1}$ and pore volume of 0.64 $cm^3\ g^{-1}$ using pre-oxidation and carbonization of ionic liquid ([Mmim]DMP)-lignin solution (Liu et al. 2022). Pang et al. prepared sodium lignosulfonate-derived hierarchical porous carbon spheres with a high SSA of 1255–1939 $m^2\ g^{-1}$ and nitrogen content of 1.14–1.66 at.% by air thermal stabilization at 200 °C and carbonization at 700–900 °C (Pang et al. 2018a).

5 Energy storage applications of LDCs

5.1 Supercapacitors

Supercapacitors are promising candidates for energy storage devices due to their coupling merits of high power density, fast charging rate, and long cycle life (Shao et al. 2018). At present, the market share of the supercapacitor is relatively small compared with rechargeable batteries due to its low energy density and high energy storage cost (Yin et al. 2021). Supercapacitors store charge at the electrode/electrolyte interface in two ways: through fast surface ion adsorption/desorption for electrochemical double-layer capacitors (EDLCs) (Chen et al. 2017b); through fast and reversible surface or near-surface Faradic reactions for pseudocapacitors (PCs) (Yu et al. 2013). Porous carbons are commonly used as the electrode materials of EDLCs. A desirable EDLC carbon electrode should have a high SSA to build an electric double layer and a high conductivity to conduct electrons. Activated carbon, carbon nanotube, and graphene have been extensively explored for carbon electrodes, but their complex preparation procedures and high production cost hinder their commercialized applications (Peng et al. 2018). Lignin has been regarded as a promising precursor for advanced carbon materials (Espinoza-Acosta et al. 2018; Zhu et al. 2020). Over the years, diverse LDCs with

high SSA have been prepared by the chemical activation method (KOH, K_2CO_3, K_2FeO_4, $ZnCl_2$, ZnC_2O_4, etc.), template method (F127, SiO_2, MgO, Fe_3O_4, ZnO, P123, F127, etc.), or self-pyrolysis, which show good application performances when applied as the EDLCs electrodes as summarized in Table 1.

It is generally accepted that high SSA would lead to high specific capacitance (Wang et al. 2016c). As illustrated in Fig. 10, when the SSA is below 2000 $m^2 \cdot g^{-1}$, the specific capacitance of LDPC is positively correlated with the SSA. However, the specific capacitance is limited and does not continue to increase when the SSA exceeds 2000 $m^2 \cdot g^{-1}$ or even reaches 3000 $m^2 \cdot g^{-1}$. Therefore, the SSA is not the only factor that determines the specific capacitance of LDPCs. In fact, the narrow micropores (< 0.7 nm) in porous carbon are too small in size to accumulate cations, hence making a minor contribution to the capacitance (Shao et al. 2020). Therefore, pore size distribution could be another key factor affecting the capacitive performances of porous carbons.

Tremendous strategies have been proposed to improve the pore accessibility of LDPCs, including morphology structuring (Liu et al. 2017; Wang et al. 2022c), pore tailoring (Guo et al. 2017; Herou et al. 2019), and heteroatom doping (Tian et al. 2019; Liu et al. 2022). Hierarchical porous carbon materials with interconnected macro-meso-micropore structures are regarded to be desirable electrode materials. In the capacitive charge-storage process, macropore serves as a buffer site for ions, mesopore can shorten the transport distance of ions

Table 1 Representative LDPCs with their electrochemical performances

Materials	SSA ($m^2 \cdot g^{-1}$)	Capacitance ($F \cdot g^{-1}$)	Energy density ($Wh \cdot kg^{-1}$)	Refs
CNSs	854.7	281 at 0.5 $A \cdot g^{-1}$ in 1 M H_2SO_4	25.1 at 583 $W \cdot kg^{-1}$, 1 M H_2SO_4	(Liu et al. 2017)
	1660	420 at 0.1 $A \cdot g^{-1}$ in 6 M KOH	46.8, neat EMIM TFSI	(Guo et al. 2017)
MLCM	938.1	338.2 at 0.8 $A \cdot g^{-1}$ in 1 M H_2SO_4	7.81 at 62.5 $W \cdot kg^{-1}$, 1 M H_2SO_4	(Liu et al. 2022)
NS-HPC	1454.7	269 at 0.5 $A \cdot g^{-1}$ in 6 M KOH	37.4 at 62 $W \cdot kg^{-1}$, 6 M KOH	(Tian et al. 2019)
HPNC	2218	312 at 1 $A \cdot g^{-1}$ in 6 M KOH	59.8 at 875 $W \cdot kg^{-1}$, $EMIBF_4$	(Zhang et al. 2016a)
3D-7-2 K	1504	324 at 0.5 $A \cdot g^{-1}$ in 6 M KOH	17.9 at 458 $W \cdot kg^{-1}$, 6 M KOH	(Li et al. 2021a)
BALC	1831	428 at 1 $A \cdot g^{-1}$ in 6 M KOH	66.18, EMIM TFSI	(Zhang et al. 2019b)
PLC	1069	365 at 0.5 $A \cdot g^{-1}$ in 6 M KOH	13.7, PVA/KOH gel	(Fu et al. 2020)
C-LRGO	444.29	330 at 1 $A \cdot g^{-1}$ in 1 M H_2SO_4	11.3 at 254 $W \cdot kg^{-1}$, 1 M H_2SO_4	(Jiang et al. 2020)
HPCS	1255	276 at 0.1 $A \cdot g^{-1}$ in 7 M KOH	34.3, 1 M $SBPBF_4$/PC	(Pang et al. 2018a)
PCs	1372.87	340 at 0.5 $A \cdot g^{-1}$ in 3 M KOH	9.7 at 250 $W \cdot kg^{-1}$, 3 M KOH	(Chen et al. 2018)
LCNFs	1140	248 at 0.2 $A \cdot g^{-1}$ in 6 M KOH	—	(Ma et al. 2018)
PL	2265	336 at 1 $A \cdot g^{-1}$ in 6 M KOH	—	(Wang et al. 2016a)
L-U	3130	306 at 0.1 $A \cdot g^{-1}$ in 6 M KOH	15, 6 M KOH	(Wang et al. 2016b)
N-BLPC	2646	337 at 0.5 $A \cdot g^{-1}$ in 6 M KOH	9.34 at 250 $W \cdot kg^{-1}$, 6 M KOH	(Zhu et al. 2017)
NHPC	1867.4	440 at 0.5 $A \cdot g^{-1}$ in 6 M KOH	18.5 at 300 $W \cdot kg^{-1}$, 6 M KOH	(Zhang et al. 2018d)
HPCs	1269	300.5 at 0.5 $A \cdot g^{-1}$ in 6 M KOH	66.8 at 1750 $W \cdot kg^{-1}$, $EMIMBF_4$	(Liu et al. 2019a)
LHPC	2109	254 at 0.5 $A \cdot g^{-1}$ in 6 M KOH	—	(Liu et al. 2021a)
LHPC	907	165 at 0.05 $A \cdot g^{-1}$ in 1 M H_2SO_4	5.7 at 15 $W \cdot kg^{-1}$, 1 M H_2SO_4	(Zhang et al. 2015a)
HPCSLS	903	247 at 0.05 $A \cdot g^{-1}$ in 7 M KOH	8.6 at 14.3 $W \cdot kg^{-1}$, 7 M KOH	(Pang et al. 2017)
HPGCs	856.84	331 at 5 $mV \cdot s^{-1}$ in 6 M KOH	—	(Chen et al. 2017a)
LMC	712	186.3 at 0.1 $A \cdot g^{-1}$ in 1 M H_2SO_4	—	(Song et al. 2017)
PGLS	1727.1	399.2 at 0.1 $A \cdot g^{-1}$ in 6 M KOH	—	(Wang et al. 2021d)
GLB-D	2120	215 at 0.1 $A \cdot g^{-1}$ in 6 M KOH	—	(Ho et al. 2018)
HAPC	856	286 at 0.25 $A \cdot g^{-1}$ in 6 M KOH	13 at 2700 $W \cdot kg^{-1}$, 6 M KOH	(Zhao et al. 2015)
LAC	3775	286.7 at 0.2 $A \cdot g^{-1}$ in 6 M KOH	8.87 at 51.92 $W \cdot kg^{-1}$, 6 M KOH	(Zhang et al. 2015c)
SLC	635	200.2 at 0.1 $A \cdot g^{-1}$ in 6 M KOH	—	(Li et al. 2020c)
CHMSs	991	284 at 0.1 $A \cdot g^{-1}$ in 7 M KOH	7.5 at 28.7 $W \cdot kg^{-1}$, 6 M KOH	(Pang et al. 2018b)
LPC-200	3178	201.7 at 0.5 $A \cdot g^{-1}$ in 6 M KOH	—	(Wang et al. 2022e)
UreaK_2CO_3	3041	177 at 0.1 $A \cdot g^{-1}$ in 1 M Li_2SO_4	64.2, $EMIMBF_4$	(Schneidermann et al. 2017)
HMC	559	348 at 0.5 $A \cdot g^{-1}$ in 6 M KOH	7.9 at 51 $W \cdot kg^{-1}$, 6 M KOH	(Cao et al. 2021c)
LDMC	1195.4	197 at 0.2 $A \cdot g^{-1}$ in 6 M KOH	6.85 at 100 $W \cdot kg^{-1}$, 6 M KOH	(Sima et al. 2021)

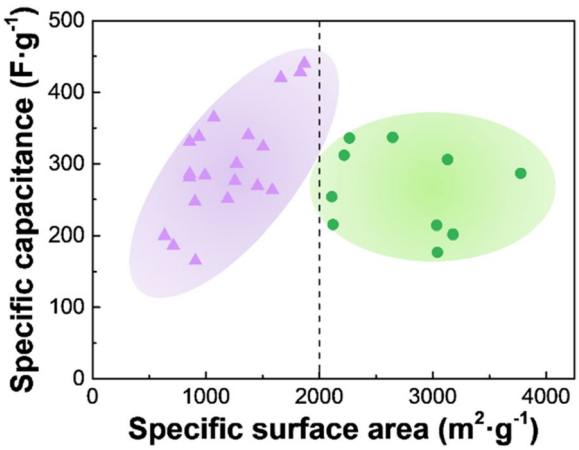

Fig. 10 A summary of the relationship between specific capacitance and SSA for the reported LDPCs. Data displayed in this figure are obtained from Table 1

in internal pores, and micropore can provide active sites for ion accumulation, which boosts the transfer kinetics of electrolyte ions to achieve high capacitance (Dutta et al. 2014). Guo et al. prepared lignin-derived hydrochar with abundant interconnected macropores by hydrothermal carbonization, and then 3D hierarchical porous carbon with honeycomb structure could be obtained through KOH activation (Fig. 11a-d) (Guo et al. 2017). The interconnect macropores, plentiful mesoporous, and rich microporous afford its excellent capacitance performance. The 3D hierarchical porous carbon showed high specific capacitance of 420 $F{\cdot}g^{-1}$ at 0.1 $A{\cdot}g^{-1}$ and 284 $F{\cdot}g^{-1}$ at 100 $A{\cdot}g^{-1}$ in 6 M KOH (Fig. 11e). Moreover, the assembled symmetric supercapacitor presented a fast frequency response in both ionic liquid and aqueous electrolytes. It delivered an outstanding energy density of 46.8 $Wh{\cdot}kg^{-1}$ and a superior power density of 25,400 $W{\cdot}kg^{-1}$ in EMIM TFSI electrolyte (Fig. 11f). Lignin-derived 3D hierarchical porous carbons were obtained through hydrothermal carbonization and activation by Xu's group (Zhang et al. 2016a) and An's group (Li et al. 2021a), where the carbon electrodes showed gravimetric specific capacitances of 312 $F{\cdot}g^{-1}$ at 1 $A{\cdot}g^{-1}$ and 324 $F{\cdot}g^{-1}$ at 0.5 $A{\cdot}g^{-1}$ in 6 M KOH, respectively. Zhang et al. proposed a novel bacterial activation method to synthesize lignin-derived hierarchical porous carbon (Zhang et al. 2019b). It was found that the bacteria cleave the stable chemical bonds (β-O-4, β-β', and β-5) of the lignin to reduce its molecular weight, resulting in the formation of interconnected hierarchical porous carbon structure during activation. The prepared porous carbon displayed a specific capacitance up to 428 $F{\cdot}g^{-1}$ at 1.0 $A{\cdot}g^{-1}$ and 355 $F{\cdot}g^{-1}$ at 30 $A{\cdot}g^{-1}$ and 82.9% capacitance retention in 6 M KOH. The carbon electrode also showed good cycling performance with a capacitance loss smaller than 3.3% after 10,000 cycles at 5 $A{\cdot}g^{-1}$. The fabricated symmetric supercapacitor using this porous carbon electrode exhibited an ultrahigh energy density of 66.18 $Wh{\cdot}kg^{-1}$ at 312 $W{\cdot}kg^{-1}$ in EMIM TFSI electrolyte.

2D carbon nanosheets can also be candidate electrode materials for supercapacitors owing to their exposed active sites, and good electronic conductivities (Peng et al. 2018). Lignin-derived 2D carbon nanosheets were prepared by freeze-casting of an aqueous lignin dispersion followed by direct carbonization (Liu et al. 2017). With the help of an ice crystal template, carbon nanosheets with a thickness of 50–150 nm were obtained, which displayed a specific capacitance of 281 $F{\cdot}g^{-1}$ at 0.5 $A{\cdot}g^{-1}$ in 1 M H_2SO_4. Unfortunately, 2D nanosheets were prone to self-stacking, reducing the effective utilization of the surface (Gao et al. 2020). To solve this issue, Fu et al. adopted self-assembly to transform sodium lignosulfonate into 3D porous carbon composed of quasi-nanosheets with the gas-exfoliation and in-situ templating of zinc oxalate (Fu et al. 2020). Benefiting from the fast ion diffusion, boosted electron conduction, and good mechanical stability, the 3D porous carbon electrode exhibited a high specific capacitance of 365 $F{\cdot}g^{-1}$ at 0.5 $A{\cdot}g^{-1}$ in 6 M KOH, as well as good durability (a 93.5% capacitance retention after 10,000 cycles at 5 $A{\cdot}g^{-1}$). The assembled solid symmetric supercapacitor using PVA/KOH gel electrolyte showed a high energy density of 9.75 $Wh{\cdot}kg^{-1}$ under a high power density of 6157.9 $W{\cdot}kg^{-1}$. Jiang et al. used reduced graphene oxide hydrogels composed of nanosheets as a template to convert lignin into 3D carbon aerogel with a lamellar interconnect structure (Jiang et al. 2020). The hierarchical porous structure and the resulted high SSA rendered the material a good capacitive performance. It showed a high specific capacitance of 330 $F{\cdot}g^{-1}$ at 1.0 $A{\cdot}g^{-1}$ in 1 M H_2SO_4 and the assembled supercapacitor showed superior cycling performance with a 100% capacitance retention over 10,000 cycles at 10 $A{\cdot}g^{-1}$.

In addition to 3D porous carbon and carbon nanosheets, LDC spheres and carbon nanofibers also have ideal performances in supercapacitor applications. Pang et al. prepared carbon spheres from sodium lignosulfonate through thermal stabilization and carbonization (Pang et al. 2018a). The carbon spheres showed a specific capacitance of 276 $F{\cdot}g^{-1}$ at 0.1 $A{\cdot}g^{-1}$ and impressive cycling stability with 99.5% capacitance retention after 10,000 cycles in 7 M KOH. Chen et al. synthesized LDPC spheres by spray drying a solution of lignosulfonate and KOH, followed by carbonization, which achieved a specific capacitance of 340 $F{\cdot}g^{-1}$ at 0.5 $A{\cdot}g^{-1}$ in 3 M KOH (Chen et al. 2018). Ma et al. used lignin as

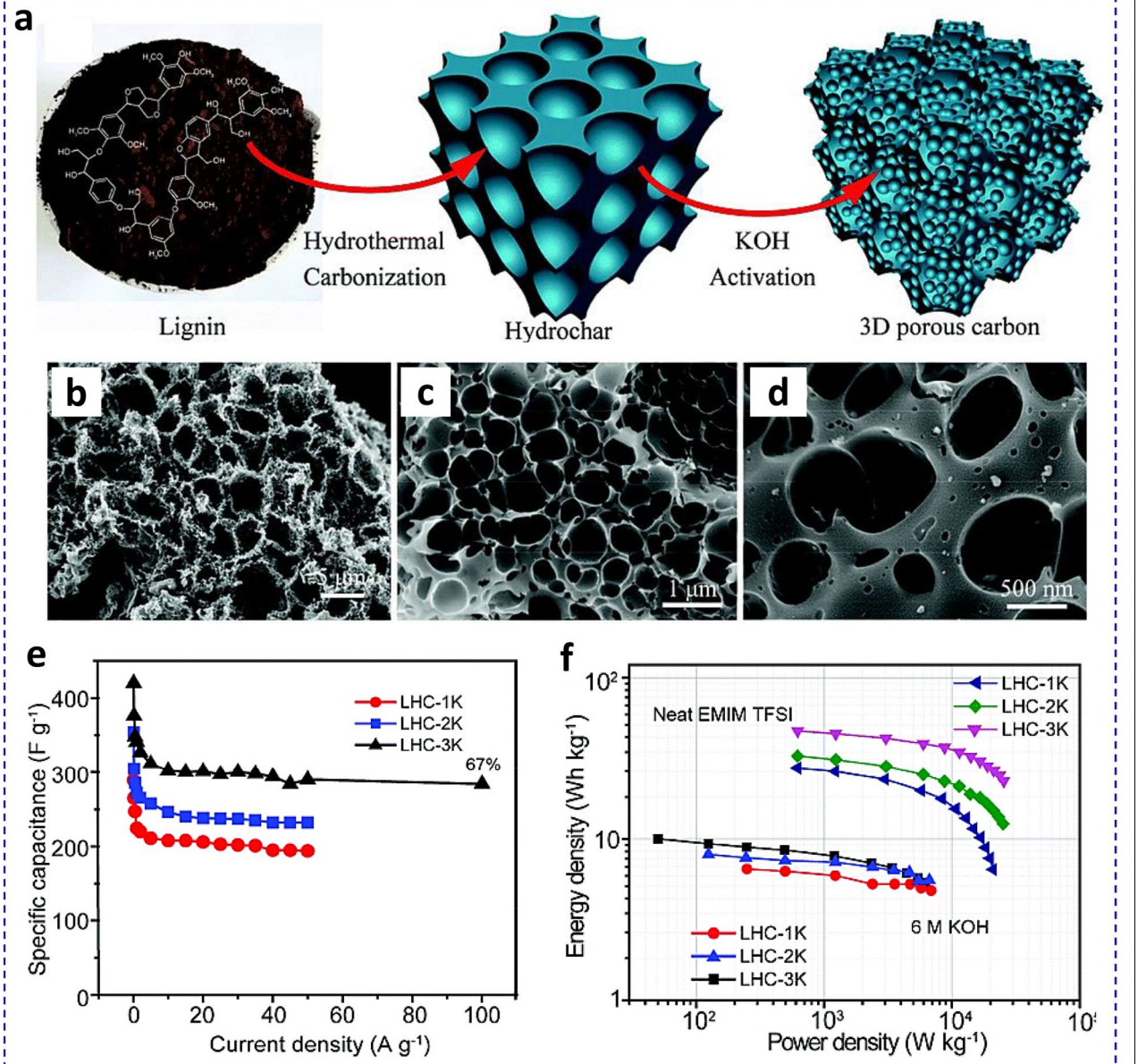

Fig. 11 **a** Schematic illustration of preparing lignin-derived 3D hierarchical porous carbons. (**b**-**d**) SEM images of the 3D hierarchical porous carbons. **e** Specific capacitance at various current densities of the 3D hierarchical porous carbons in a three-electrode system in 6 M KOH. **f** Ragone plots for the 3D hierarchical porous carbon-based supercapacitors in 6 M KOH and neat EMIM TFSI. Reproduced with permission from Ref. (Guo et al. 2017). Copyright © 2017, Roal Society of Chemistry

a carbon precursor to prepare porous carbon nanofiber by electrospinning with polyvinylpyrrolidone as a spinning agent and $Mg(NO_3)_2{\cdot}6H_2O$ as an additive (Ma et al. 2018). The obtained carbon nanofiber had a hierarchical porous structure with an SSA of 1140 $m^2{\cdot}g^{-1}$, and showed a specific capacitance of 248 $F{\cdot}g^{-1}$ at 0.2 $A{\cdot}g^{-1}$ in 6 M KOH. Titirici's group designed free-standing LDC nanofiber mats with high packing density (Hérou et al. 2021). Due to the decreased dead volume, the LDC nanofiber electrode achieved a volumetric capacitance of 130 $F{\cdot}cm^{-3}$ and an energy density of 6 $Wh{\cdot}L^{-1}$ at 0.1 $A{\cdot}g^{-1}$ with an active mass loading of 3 $mg{\cdot}cm^{-2}$, which outperforms most commercial porous carbons (volumetric capacitance: 50 ~ 100 $F{\cdot}cm^{-3}$, energy density: 1 ~ 3 $Wh{\cdot}L^{-1}$).

EDLCs store charge through ion adsorption/desorption on the electrode surface, and the surface heteroatom doping of carbon would affect the capacitive performance through specific adsorption. Impressive experimental and theoretical results have demonstrated that heteroatom doping could change the charge density distribution of carbon and induce surface polarization, thus accelerating ion adsorption (Liu et al. 2019b; Li et al. 2020b). Meanwhile, the introduction of heteroatoms can also enhance the surface wettability of carbon and increase the accessible surface area, although the wettability of porous materials can not be measured due to the capillarity effect of porous carbons. Moreover, the introduced heteroatomic functional groups can serve as redox-active sites to provide additional pseudocapacitance (Cui et al. 2020).

Pyrolyzing a mixture of lignin, additive with heteroatoms, and activation agent is the prevailing method for synthesizing heteroatom-doped LDPCs. For instance, Wang et al. prepared N-doped porous carbons via activating aniline- and urea-modified lignin with KOH, respectively, which achieved specific capacitances of 336 $F{\cdot}g^{-1}$ at 1 $A{\cdot}g^{-1}$ and 306 $F{\cdot}g^{-1}$ at 0.1 $A{\cdot}g^{-1}$ in 6 M KOH (Wang et al. 2016a). In the work done by Zhu et al., lignin-containing black liquor with KOH aqueous solution was used as a precursor and melamine was used as a nitrogen source to prepare N-doped porous carbon with high SSA (Zhu et al. 2017). The as-prepared porous carbon displayed a specific capacitance of 337 $F{\cdot}g^{-1}$ at 0.5 $A{\cdot}g^{-1}$ in 6 M KOH. Physically mixing lignin and additives is easy to cause heterogeneous doping, which limits the capacitive performance. However, lignin is rich in phenolic hydroxyl and carboxyl groups, which can be functionalized to introduce heteroatom-containing groups, thereby ensuring uniform heteroatom doping in the subsequent carbonization process. Zhang et al. fabricated 3D N-doped hierarchical porous carbons by hydrothermal crosslinking reaction and KOH activation using sodium lignosulfonate as a carbon precursor, 1,6-hexanediamine as a crosslinking agent and nitrogen source (Zhang et al. 2018d). The porous carbon possessed rich micropores, favorable mesopores and interconnected macropores with a high N content of 3.6 at.%, enabling its superior specific capacitance of 440 $F{\cdot}g^{-1}$ at 0.5 $A{\cdot}g^{-1}$ in 6 M KOH. Moreover, the as-fabricated supercapacitor delivered a high energy density of 18.5 $Wh{\cdot}kg^{-1}$ at 300 $W{\cdot}kg^{-1}$ in 6 M KOH aqueous system. The work by Liu et al. proposed a facile environmentally friendly and low-cost method to prepare porous carbon from heteroatom-doped lignin (Liu et al. 2019a). Kraft lignin was directly pyrolyzed without any additional activating agents, additives or templates to construct N, O, and S co-doped hierarchical porous carbon. The derived carbon had abundant multi-heteroatoms co-doping (up to 19.91 wt.%) and hierarchical porous structure (Fig. 12a-h), leading to its high specific capacitance of 300.5 $F{\cdot}g^{-1}$ at 0.5 $A{\cdot}g^{-1}$ in 6 M KOH (Fig. 12i) and a superior energy density of 66.8 $Wh{\cdot}kg^{-1}$ at 1750 $W{\cdot}kg^{-1}$ for the assembled supercapacitor in $EMIMBF_4$ ion liquid electrolyte (Fig. 12j).

Nowadays, with the rapid development of portable electronics and wearable devices towards lightweight and miniaturization, supercapacitors are not only required to have high gravimetric energy density, but also high areal or volume energy density (Li et al. 2019). The traditional powder carbon materials have excellent gravimetric performances, but their low densities lead to poor volume performances, which makes it difficult to be used in compact devices. Micro supercapacitors (MSCs) have attracted wide attention as a new type of capacitive energy storage device because they are easy to carry and integrate with microelectronic systems (Lin et al. 2014). Alshareef et al. developed a lignin-based laser lithography technique to convert lignin film to 3D laser-scribed graphene electrode and fabricate on-chip MSC (Zhang et al. 2018b). The electrode was hierarchically porous and electrically conductive with a conductivity up to 66.2 $S{\cdot}cm^{-1}$. The fabricated MSCs exhibited good capacitive performances with a high areal capacitance of 25.1 $mF{\cdot}cm^{-2}$, a high volumetric energy density of 1 $mWh{\cdot}cm^{-3}$, and a high volumetric power density of 2 $W{\cdot}cm^{-3}$. Sun et al. produced S-doped porous 3D graphene materials from lignin and polyethersulfone (PES) films via laser direct writing technique (Sun et al. 2021). The as-fabricated MSCs using H_2SO_4/PVA gel as electrolyte showed excellent electrochemical performances with a high areal capacitance of 22 $mF{\cdot}cm^{-2}$, and a high areal energy density of 1.53 $mWh{\cdot}cm^{-2}$ at an areal power density of 25.4 $mW{\cdot}cm^{-2}$. Yuan et al. synthesized superhydrophilic 3D porous graphene with O/S co-doping through a repeated laser scribing technique using sodium lignosulfonate slurry to coat the laser-induced graphene interdigital electrodes (Fig. 13a) (Yuan et al. 2021). The electrode possessed hierarchical porous graphene architecture, superior hydrophilicity, and O/S co-doped chemistry property, which greatly promotes the infiltration and transportation of electrolyte ions (Fig. 13b-d). Consequently, the assembled MSCs showed an outstanding areal capacitance of 53.2 $mF{\cdot}cm^{-2}$, which is 39 times larger than that of the undoped MSC (Fig. 13e). At the same time, the MSCs using PVA/H_2SO_4 gel as electrolyte supplied a high areal energy density of 4.73 $\mu Wh{\cdot}cm^{-2}$ and a high areal power density of 1.6 $mW{\cdot}cm^{-2}$ (Fig. 13f). The above findings demonstrate the good application potential of lignin in MSCs and open a new path to the application of LDC in EDLCs.

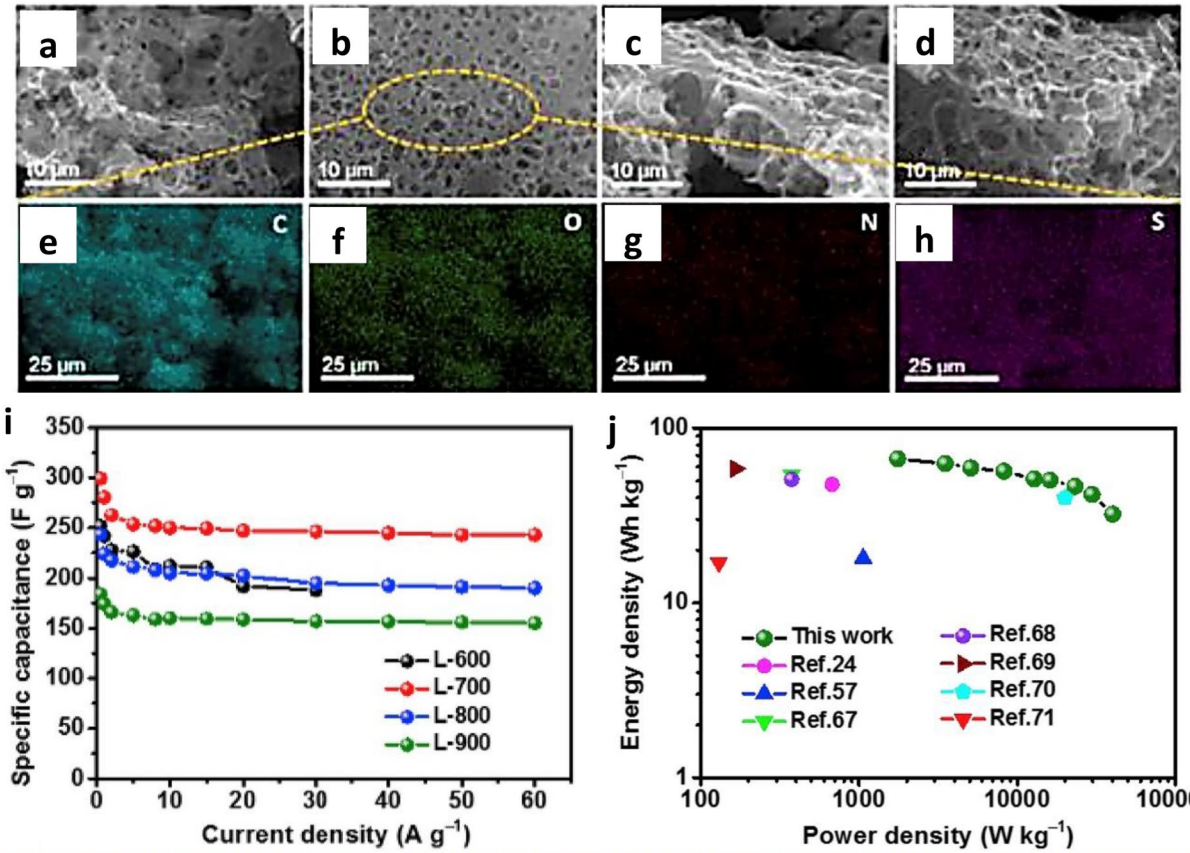

Fig. 12 **a**–**h** SEM images and EDS elemental mappings of the O-N-S co-doped hierarchical porous carbons; **i** Specific capacitance at various current densities of the O-N-S co-doped hierarchical porous carbons; **j** Ragone plot of the assembled supercapacitor in $EMIMBF_4$ system. Reproduced with permission from Ref. (Liu et al. 2019a). Copyright © 2019, Elsevier

5.2 Lithium-ion battery

Lithium-ion batteries (LIBs) have received considerable attention in consumer electronics owing to their high voltage output, good charge capability, robust stability, low self-discharge, and high power density (Lu et al. 2013). In general, a LIB is composed of a cathode, anode and organic electrolyte and stores energy physically through the intercalation reactions of Li^+ at the positive and negative carbon electrode during charge and discharge (Scrosati et al. 2011). The electrochemical performance of LIBs mainly depends on the electrode material, while the theoretical capacity of commercial graphite anode is only 372 mAh g^{-1} by LiC_6 stoichiometry, resulting in low energy density and power density of the current LIBs (Goodenough and Park 2013). Developing more lithium insertion sites in carbonaceous materials plays a positive role in improving the capacity of anode materials. Inner porosity and high crystallinity could contribute to the reversible lithiation sites (Liu et al. 2021b). LDCs can be efficiently converted into low-cost materials as anodes with highly reversible Li^+ ion-storage capacity and fast lithium-storage kinetics, providing a new promising pathway to application in batteries fields (Tenhaeff et al. 2014; Espinoza-Acosta et al. 2018; Svinterikos et al. 2020).

The mechanisms of Li^+ ions storage include pore filling, defect adsorption in the amorphous regions and the intercalation of Li^+ ions in graphitic layers (Fig. 14a) (Zhang et al. 2021a). The high SSA and hierarchical porous distribution realized by the template and activation methods can achieve effective adsorption and reversible capacity of the lithium ions, which bestows LDPC a higher capacity than carbonized lignin anode. Typically, SiO_2 as a hard template can generate porous structures. As shown in Fig. 14b, Huang et al. pioneered electrostatic self-assembly and dual-template method using cationic quaternized alkali lignin (QAL) (carbon source), sodium dodecylbenzene sulfonate (soft template) and SiO_2 nanoparticles (hard template) to prepare LDPCs possessing ordered mesoporous structure and high pore

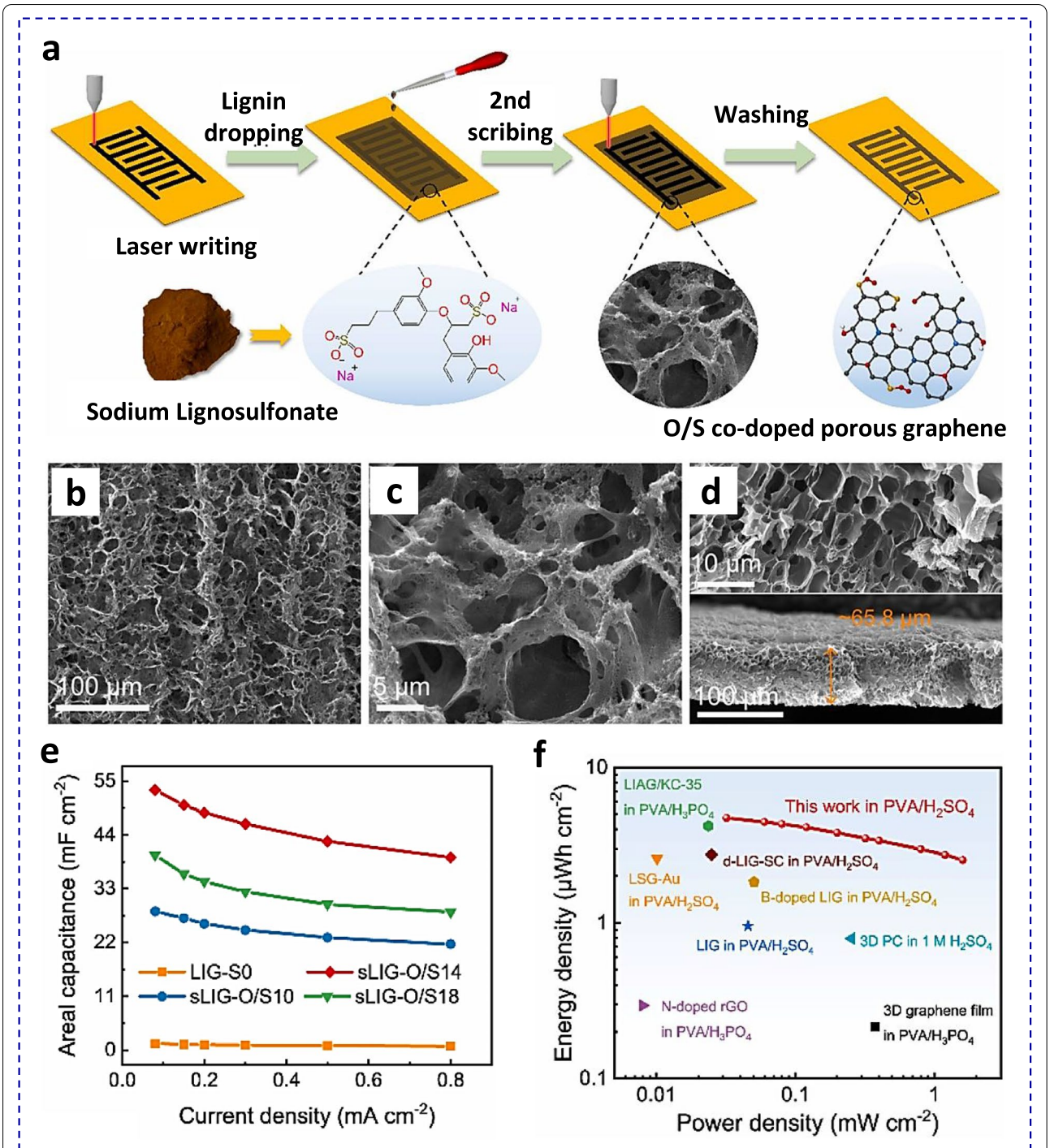

Fig. 13 **a** Schematic illustration of the fabrication of superhydrophilic O/S co-doped graphene electrodes; SEM images of the superhydrophilic O/S co-doped graphene electrode in (**b**) low-magnification, (**c**) high-resolution top-view, and (**d**) cross-sectional view; **e** Areal specific capacitance of the graphene electrodes; **f** Areal Ragone plot comparing the assembled MSC with reported graphene-based MSCs. Reproduced with permission from Ref. (Yuan et al. 2021). Copyright © 2021, Elsevier

volume (2.23 $cm^3\ g^{-1}$) (Huang et al. 2021b). The obtained carbon materials with high porosity possess fast lithium ion diffusion kinetics and more lithium-ion storage sites for LIBs, leading to LDPCs with a high reversible capacity of 1109 mA h g^{-1}. LDC could also be bonded with conversion-type anodes, e.g., lignosulphonate/

MoS_2 composite (Chen et al. 2019a), Si/C from lignin-SiO_2 composite (Du et al. 2018; Li et al. 2021e), lignin/Fe_2O_3 composite (Yi et al. 2017), and lignin/NiO composite (Zhou et al. 2018) etc. All these anode materials displayed remarkable lithium storage performance. Furthermore, Zhang et al. and Xi et al. fabricated the LDPC with KOH, K_2CO_3, $K_2C_2O_4$ and K_3PO_4, respectively, as both template and activating agents, (Zhang et al. 2015b; Xi et al. 2018, 2019). K_2CO_3 was found to be superior to other potassium compounds in the lignin activation due to the release of CO_2 gas to loosen the lignin and act as an activation agent in the high-temperature activation process (Fig. 14c). The excellent multi-stage pore structure and graphitic lamellar structure of LDPC with

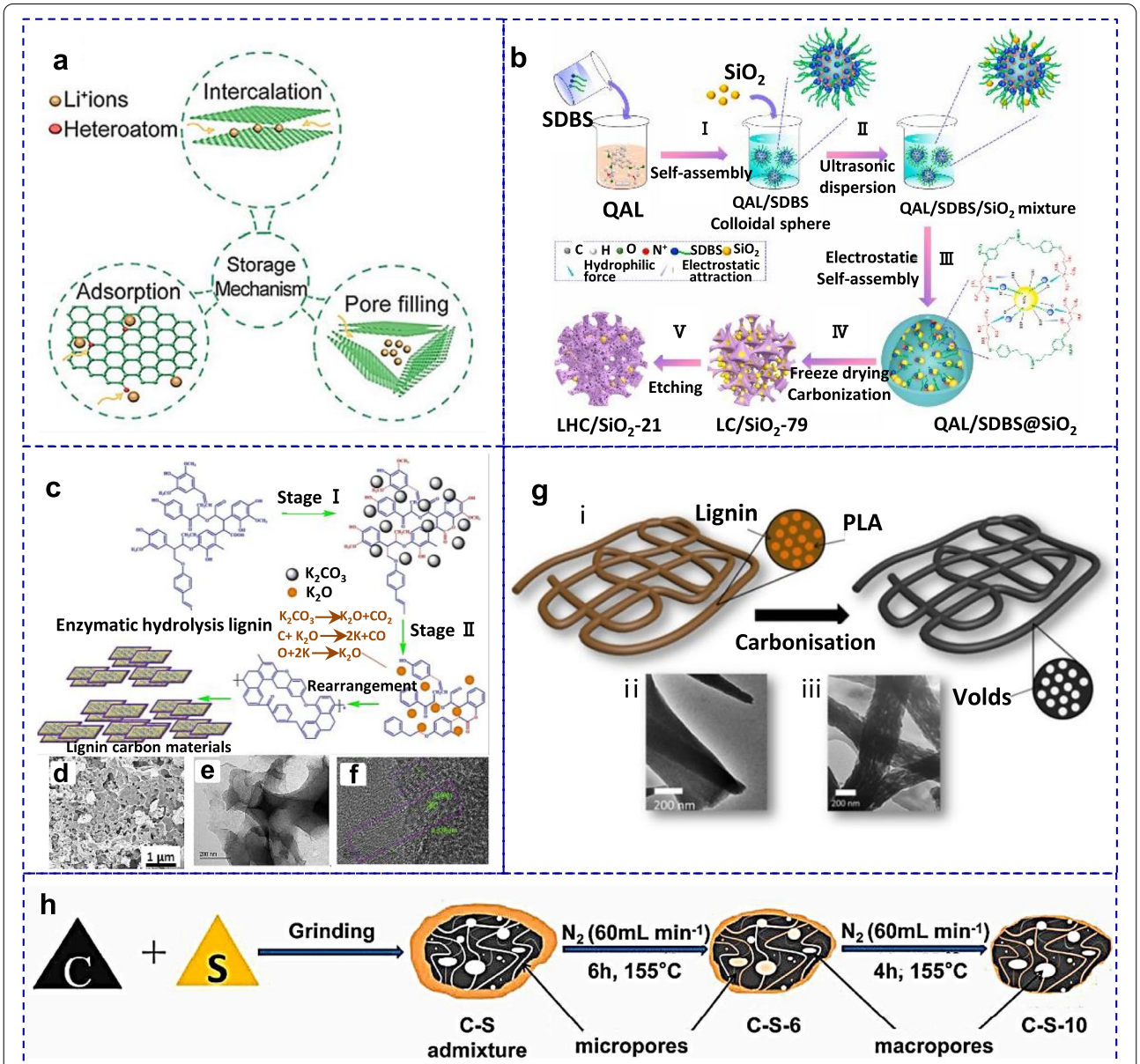

Fig. 14 **a** Available $Li.^+$ ions storage mechanism in hard carbons. Reproduced with permission from Ref. (Zhang et al. 2021a). Copyright © 2021, Wiley; **b** Schematic illustration of the fabrication process of the LHC/SiO_2. Reproduced with permission from Ref. (Huang et al. 2021b). Copyright © 2021, Elsevier; **c** The activation mechanism of K_2CO_3 to EHL; **d**-**f** SEM image, TEM and HRTEM images of LDC-K_2CO_3-900. Reproduced with permission from Ref. (Xi et al. 2018). Copyright © 2018, Elsevier; **g** Schematics of phase separation for lignin/PLA fibers (i), and TEM images of lignin/TPU-50:50 (ii) and lignin/PLA-50:50 (iii). Reproduced with permission from Ref. (Culebras et al. 2019). Copyright © 2019, Wiley; **h** Schematic illustration for the formation of C-S-6 and C-S-10 composites. Reproduced with permission from Ref. (Yu et al. 2017). Copyright © 2019, Wiley

K_2CO_3 are favorable for the (de)intercalation of lithium ions (470 mAh g^{-1} at 0.2 A g^{-1} after 400 cycles) (Fig. 14d-f). Xi and co-workers prepared LDPC using $ZnCO_3$ as an in situ templating agent (Xi et al. 2020). The decomposed $ZnCO_3$ produces gas to peel off lignin for creating micropores and mesopores and the generated ZnO could act as a hard template for generating mesopores. The resultant LDPC achieved excellent volume energy density (730 mAh·cm^{-3} after 200 cycles at 0.2 A·g^{-1}). Recently, electrospun lignin carbon fiber (LCF) also came into view, which might replace traditional carbon fiber materials (Wang et al. 2021c). Tenhaeff et al. eliminated the binder and additional additives in the LIBs anode using LCF mats produced from lignin and polyethylene (Tenhaeff et al. 2014). The LCF mats had comparable electrochemical performance to typical graphite anodes in LIBs. Similar to this work, research has been done on the preparation and application of carbon nanofibers (CNFs) from lignin and other polymers such as polyacrylonitrile (PAN) (Choi et al. 2013; Shi et al. 2017; Ma et al. 2019), polyethylene oxide (PEO) (Wang et al. 2013) and PVA (Stojanovska et al. 2019) as the anodes in LIBs. Recently, Culebras et al. reported CNFs derived from electrospun nanofibers of lignin/polylactic acid (PLA) after carbonization (Fig. 14g) (Culebras et al. 2019). The electrodes produced from 50% PLA blends exhibited a high specific capacity of 611 mAh g^{-1} after 200 cycles at 186 mAh g^{-1}, owing to the increased porosity. In addition, the surface defect site and the degree of graphitization of LDC could be enhanced through H_2 reduction (Chang et al. 2015), in which the carbonyl content and interlayer spacing of LDC were improved via pre-oxidation process (Du et al. 2021). Thus, LDC as the anode in LIBs can obtain excellent rate ability and cycling stability through ingenious microstructure design.

In addition, LDC also has found a satisfactory application in lithium-sulfur (Li–S) batteries. The poor conductivity of sulfur and the shuttling of polysulfides hinder their commercial applications, even if Li–S battery has a high theoretical energy (2600 Wh kg^{-1}). Micropores could physically hinder the diffusion of S in Li–S batteries. To address this, Yu et al. synthesized lignin-derived macro-/micro-porous carbon by carbonization/activation method and used it as a sulfur-loading matrix (Fig. 14h) (Yu et al. 2017). A porous carbon with a high SSA (1211.6 m^2 g^{-1}) and pore volume (0.59 cm^3 g^{-1}) was obtained. The research found that the sulfur loading time could affect the structure and electrochemical properties of the carbon–sulfur composites. Benefiting from the rich micropores at a long sulfur-loading time, the Li–S batteries exhibited a highly reversible capacity of 791.6 mAh g^{-1} in the 100th cycle. Subsequently, Yeon et al. grafted nitrogen heteroatoms onto LDPC via facile KOH activation, which formed N-doped honeycomb-like porous carbons (Yeon et al. 2020). The N heteroatoms could strongly interact with S by accelerating the charge-transfer kinetics, and the resulted hard carbons were used as anodes for Li–S batteries, achieving a high initial discharge capacity of up to 1295.9 mAh g^{-1} and a stable reversible capacity of 647.2 mAh g^{-1} in the subsequent 600 cycles.

5.3 Sodium-ion battery

Sodium-ion batteries (SIBs or NIBs) have recently been considered as a potential candidate for commercial applications in large-scale renewable energy storage (Zhang et al. 2019e). It is noted that Na^+ ions are incompetent to insert into graphite layers due to larger ionic radius (0.102 nm) and instability binary compounds of NaC_x, resulting in its low capacity of ~ 30 mAh g^{-1} in graphite electrode (Liu et al. 2016c; Moriwake et al. 2017). However, LDC as a hard carbon with disordered graphene nanodomain, large interlayer spacing and high electronic conductivity is expected to have a superior Na uptake performance and low-voltage plateau profile in NIBs.

The precise charge storage mechanism of Na^+ has been under debate for a long time. The storage mechanisms of Na^+ ions in hard carbon were investigated in details and summarized as follows (Qiu et al. 2017; Bai et al. 2018): "adsorption-intercalation" mechanism (Fig. 15a), "intercalation-adsorption" mechanism (Fig. 15b) and "adsorption-pore filling" mechanism (Fig. 15c). Recently, the "adsorption-pore filling" mechanism has gained more popularity as it can explain the sloping profile, mainly attributed to Na^+ adsorption at defect sites or the sites with large interlayer spacing and intercalation between layers (Zhang et al. 2021c), and for the plateau region, related to nanovoid filling. Theoretically, in order to fully exploit the sodium storage potential of hard carbon, it would be an effective method to modify its morphology, e.g., defect concentration, porosity and interlayer distance. It is critical to developing an effective design strategy for the preparation of desirable nanoscale structures according to the charge storage mechanism of Na^+ ions in LDC. For instance, CNFs fabricated from pyrolysis of polymer nano-fibers showed a greatly improved sodium storage capacity, owing to a large number of defect sites to store sodium in addition to improved electronic and ionic conductivity (Luo et al. 2013). Zhang et al. constructed a nanocarbon network as an anode material (E-KL/CA-C) for SIBs by pyrolyzing crosslinked cellulose acetate and lignin (Fig. 15d) (Jia et al. 2018), realizing a reversible capacity of 340 mAh g^{-1} after 200 cycles and a capacity of 103 mAh g^{-1} at 400 mA g^{-1}. In addition, heteroatom-doping strategies can produce defects and increase Na^+ ion-storage sites in LDC and construct

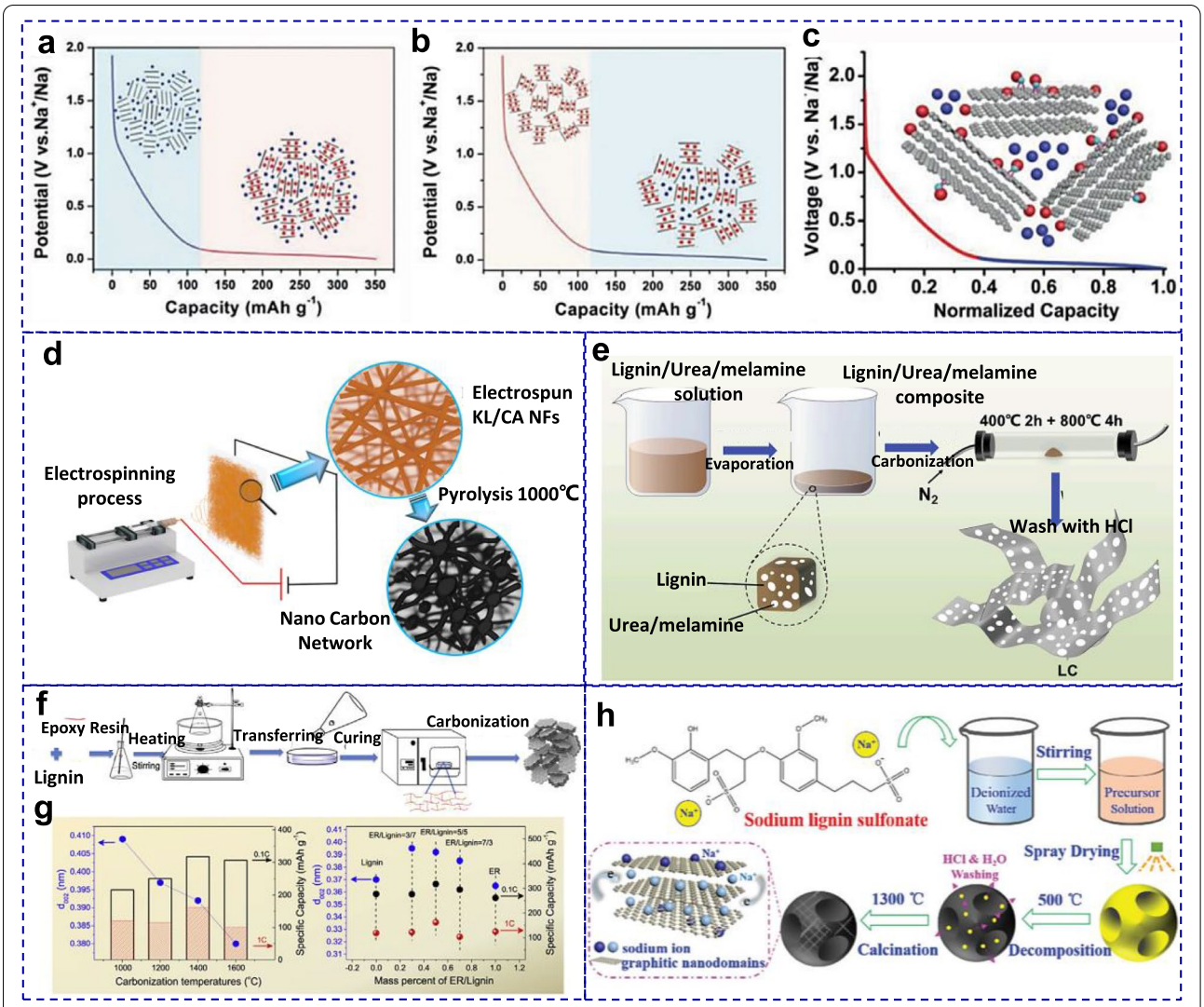

Fig. 15 Schematic illustration of the mechanisms for Na-ion storage in hard carbon: **a** "intercalation–adsorption" mechanism; **b** "adsorption–intercalation" mechanism. Reproduced with permission from Ref. (Qiu et al. 2017). Copyright © 2017, Wiley; **c** Schematic diagram of the sodium-storage mechanism in HCs. Reproduced with permission from Ref. (Bai et al. 2018). Copyright © 2017, Wiley; **d** Schematic illustration of the fabrication procedure of E-KL/CA-C. Reproduced with permission from Ref. (Jia et al. 2018). Copyright © 2018, American Chemistry Society; **e** Schematic illustration of the porous nitrogen-doped ultrathin layered carbon (LC) preparation. Reproduced with permission from Ref. (Chen et al. 2020b). Copyright © 2020, Elsevier; **f** Schematic illustration of the lignin-based interpenetrating polymer networks. **g** Relationship between carbonization temperature and the lignin/epoxy resin mass ratios to layer spacing and specific capacity. Reproduced with permission from Ref (Zhang et al. 2018a). Copyright © 2018, Elsevier; **h** Schematic illustration showing the preparation of HCM from a single sodium lignin sulfonate source and the process for Na storage. Reproduced with permission from Ref. (Li et al. 2020a). Copyright © 2020, Roal Society of Chemistry

pore structure to provide a short sodium ion diffusion path. Chen et al. employed nitrogen-doped porous ultrathin layered carbon as the anode material, prepared by annealing alkaline lignin with melamine and urea (Fig. 15e) (Chen et al. 2020b). From the discharge curves, Na^+ ions likely underwent two stages: the insertion of Na^+ ions into the defects and edges of graphite microcrystal at high potential, and into the graphitic layers-like at low potential. The N-doping mainly enhanced the capacity in the discharge voltage at high potential, delivering a high capacity of 138.7 mAh g^{-1} at 5 C and no obvious capacity decay after 4000 cycles.

But the low initial Coulombic efficiency (ICE) of the LDC reported in the above-mentioned study (26–52%) is one of the obstacles to their further commercialization. To address this issue, some research work demonstrated that the increasing SSA of LDC could improve ICE: a high SSA may increase Na^+ consumption and form an

unstable solid electrolyte interphase (SEI) layer, resulting in irreversible Na^+ insertion into the amorphous structure (Huang et al. 2014; Zhang et al. 2016b). Pure kraft lignin-derived LDPC showed poor electrochemical performances in SIBs due to its dominant microstructure (Jin et al. 2014). Similarly, electrospun lignin/PAV-derived nanofibers with high SSA (1049 $m^2 \cdot g^{-1}$) also exhibited relatively poor ICE (40%) (Stojanovska et al. 2019). In contrast, lignin/PAN-based carbon nanofibers with low SSA (approx. 27 $m^2 \cdot g^{-1}$) showed an initial Coulombic efficiency of 70.5% (Jin et al. 2014). Furthermore, Zhang and co-workers found that adjusting layer spacing can be a crucial parameter for ameliorating ICE, which could provide interconnected channels to promote the rapid transmission of ions (Fig. 15f-g) (Zhang et al. 2018a). Their work successfully synthesized a cost-effective carbon material as anodes derived from the mixture of lignin and epoxy resin via a facile pyrolyzing procedure. In their process, the structure of carbon materials was precisely controlled by altering heat-treatment temperatures and the lignin/epoxy resin mass ratios. Thanks to the enlarged interlayer spacing (0.395 nm) and lower SSA (6.5 m^2 g^{-1}), the hard carbon microsphere (HCM) possesses distinguished sodium storage behavior with a high reversible capacity of 316 mAh g^{-1}, a superior ICE of 82%, and good capacity retention of 90% after 150 cycles. The full cell with HCM versus O_3-$Na_{0.9}[Cu_{0.22}Fe_{0.30}Mn_{0.48}]O_2$ not only demonstrated a high ICE of 80%, but also presented an energy density of 247 Wh kg_{anode}^{-1} (vs. hard carbon anode). These results verified that the design strategy is feasible for the fabrication of carbon anode materials for SIBs. In addition, Li et al. obtained a practical HCM anode material using sodium lignosulfonate via facile spray drying and carbonization process (Li et al. 2020a). As displayed in Fig. 15h, the HCM has a plum-like structure with a particle size of 1 ~ 2 μm, formed from the self-assembly of the lignin functional groups and higher evaporation of spherical droplets during spray drying. The excellent sodium storage was reflected by its high reversible capacity (339 mAh g^{-1}) and outstanding ICE (88.3%), which could arise mainly from the enlarged interlayer spacing (0.396 nm), low SSA (11.89 m^2 g^{-1}) and surface defects limited SEI formation. HCM as an anode material is highly promising for sodium-ion full batteries with $Na_3V_2(PO_4)_3$ as the cathode. The $Na_3V_2(PO_4)_3$/HCM full cell can deliver a high reversible capacity (307 mAh g^{-1} at 0.1 C) and stable cycle performance (221 mAh g^{-1} up to 200 cycles at 1 C). The energy density of the full cell is up to 190 W h kg^{-1} (based on the total mass of the anode and cathode).

Importantly, the primary source and molecule structure of lignin are confirmed to have a significant impact on the structural and electrochemical properties of its derived hard carbon products. For instance, Ghimbeu found both kraft lignin- and lignosulfonate-derived carbons have different capacity stability (200 mAh g^{-1} *vs.* 120 mAh g^{-1}), attributing to different porosity (1.8 m^2 g^{-1} *vs.* 180 m^2 g^{-1}) and morphology (dense particles *vs.* spherical) (Matei Ghimbeu et al. 2019). Moreover, lignin with carboxyl group introduced by pre-oxidation can enhance its crosslinking, which in turn increases the layer distance for facilitating the Na^+ ion insertion and leads to exceptional rate capability and superb cycle life (Lin et al. 2020). The temperature regulation could precisely control the microstructure of LDC (Navarro-Suárez et al. 2018). Peuvot et al. used lignin-based carbon fiber (LCF) as free-standing anodes for SIBs, and reported that precise temperature control (800 ~ 1700 ℃) could affect SSA (4.7 ~ 355 m^2 g^{-1}), interlayer spacing (0.367 ~ 0.401 nm), and graphene nanodomain, resulting in a high specific capacity of 310 mAh g^{-1} and ICE of 89% in 1200 ℃ (Peuvot et al. 2019). Similarly, Alvin et al. combined high-temperature carbonization and low-level heteroatom doping to increase the low-voltage plateau capacity (223 mAh g^{-1}), reversible capacity (328 mAh g^{-1}) and maintain high ICE (72%). The relationship between key structural parameters and sodium storage mechanism and performance, however, needs to be investigated.

5.4 Potassium-ion battery

Recently, potassium-ion batteries (PIBs) have come under the spotlight due to their low cost, rich resources and similar working principles as those of lithium-ion batteries (LIBs) (Xu et al. 2018b). The (de)intercalation mechanism of K^+ in graphite has been confirmed and showed a low voltage plateau. But the large size of K^+ could cause the large volume expansion of graphite (KC_8, 60%) (Komaba et al. 2015; Zhang et al. 2021h), resulting in slow kinetics and rate capacity. At present, hard carbons with large interlayer spacing have been widely studied in PIBs (Wu et al. 2019). Absolutely, the charge storage mechanism of K in hard carbon is quite different compared with graphite. In addition, besides the Faradaic contribution caused by K^+ intercalation, the charge storage contribution of K^+ adsorption onto the nanovoids and surface defects/functional groups could also play an important role (Fig. 16a) (Yang et al. 2018). Based on the above mechanism, to lower the associated strain energy in hard carbon anode, efforts have been made by controlling structural engineering, including expanding interlayer space, introducing defects, and heteroatom-doping, with which significant K-storage capacity improvements have been achieved (Zhang et al. 2021a). As reported previously, the directly carbonized lignin as a hard carbon could be used as an anode material to store a high amount

of K^+ ion with impressive low voltage platform capacity (at ~ 0.25 V), and the total capacity of the K^+ ion insertion/extraction attained 246 mAh g^{-1} (Alvin et al. 2020). The research also found that tuning the carbonization temperature (1000–1500 ℃) could alter the corresponding structure and electrochemical properties of LDC. As the carbonization temperature increased, carbon was gradually arranged from short-range ordered structure to long-range ordered structure with turbostratic graphene nanodomains, leading to the increased graphitization degree and considerably collapsed micropore. Thereby the plateau capacity of KIB increased from 113 to 178 mAh g^{-1}. The adsorption-insertion mechanism of K^+ ion insertion into hard carbon was further confirmed by experimental observation and theoretical calculation. The sloping voltage capacity was attributed to the adsorption of K^+ ions on defect sites, edge sites, and micropores (Zhang et al. 2020d, c, 2021d, f), whereas the low voltage plateau capacity was caused by the intercalation of the K^+ ions into graphitic layers. Heteroatom doping also showed an effective effect on the potassium storage performance of carbon-based materials. Phosphorus-doped hard carbon (PHC) has enlarged interlayer spacing of the graphitic layer. Compared with HC, the capacity of PHC in KIB also increased from 245 to 302 mAh g^{-1} mostly owing to the increase in the plateau capacity from 153 to 192 mAh g^{-1}. In addition, pre-oxidation could cross-link the structure of lignin precursor and further promote the reaction dynamic, and as a result, the carbonized lignin has a capacity of ~ 300 mAh·g^{-1} in PIBs (Lin et al. 2020). Even though such potassium storage capacity is comparable to that of other hard carbon materials, it is still lower than the capacity of lithium storage in graphite. Jiang et al. employed a simple hydrothermal condition with graphene oxides (GO) as catalysts to reconstruct lignin (Jiang et al. 2021). Lignin, which loses the aromatic unit side chain, can be polymerized with reduced graphene oxide (rGO) foam to form a three-dimensional layered composite. Carbonized reconstructed lignin has fewer defects, fewer micropores and adjustable interlayer spacing at 750 ℃, which significantly improved the total capacity compared with directly carbonized lignin (~ 355 mA h·g^{-1} *vs* 252 mA h·g^{-1} at 50 mA g^{-1}) and the capacity (~ 200 mA h·g^{-1}) at a high current of 1 A g^{-1} for K ion storage. Note that reconstructed lignin with the graphitic nanostructures leads to lowered voltage

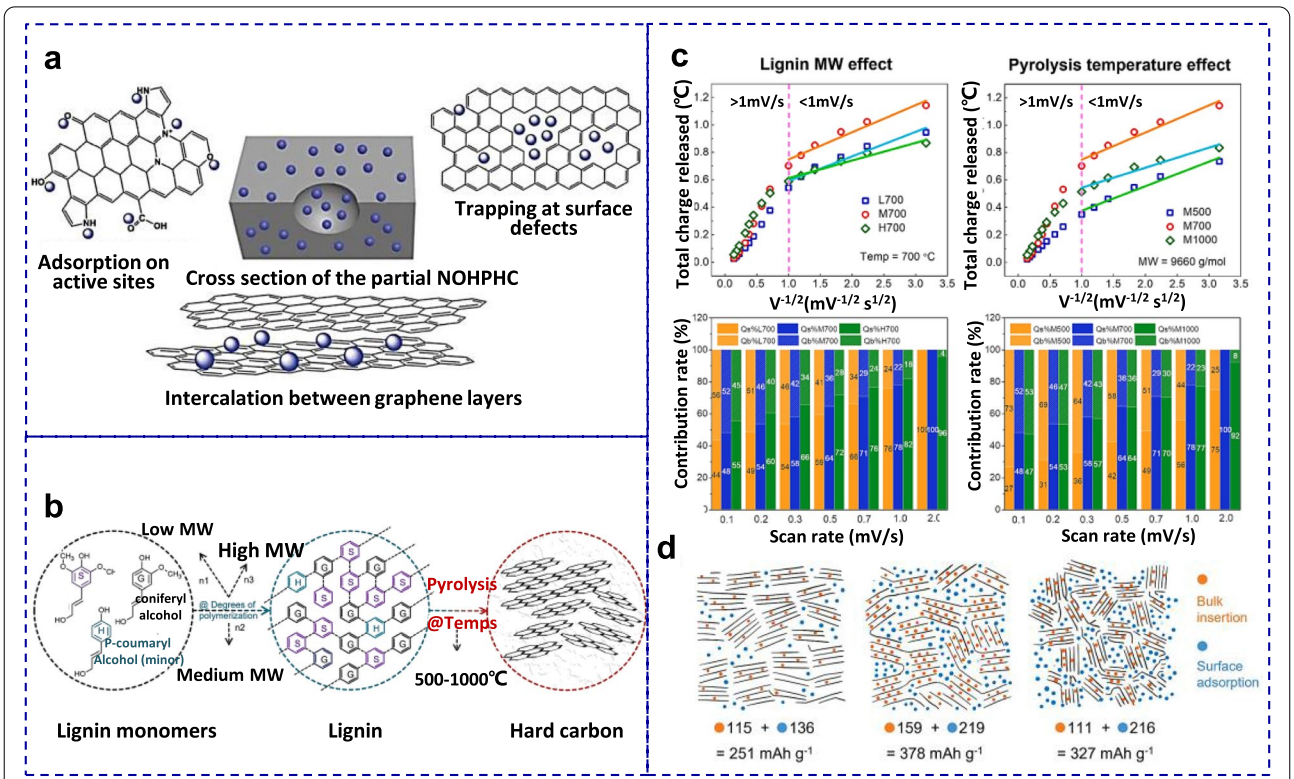

Fig. 16 **a** Schematic of the mixed mechanisms of potassium-ion storage. Reproduced with permission from Ref. (Yang et al. 2018). Copyright © 2018, Wiley; **b** Schematic of pyrolytic production of lignin-derived hard carbon; **c** The overall capacity, bulk-insertion (*Qb*) and surface-adsorption (*Qs*) contribution to the capacity of different lignin M_W and pyrolysis temperature; **d** Proposed K-ion storage mechanisms in low M_W (i), medium M_W (ii), and high M_W (iii) of lignin. Reproduced with permission from Ref. (Wu et al. 2022). Copyright © 2022, Elsevier

hysteresis between the charge and discharge process, which can be beneficial to practical application. In addition, there is still some possibility of remodeling lignin in response to potassium storage strategy, which can draw lessons from the previous relevant research work, e.g., designing high edge-nitrogen doped carbon (Zhang et al. 2020d, 2021c, e), building hierarchical porous carbon (Huang et al. 2021a), and fabricating hard/soft carbon composite (Jian et al. 2017) etc.

To better reveal the applications of LDC in potassium storage, it is important to understand the relationship between its microstructure and the charge storage mechanism. Wu et al. speculated the interplay among lignin molecular weight (MW), pyrolysis temperature, and hard carbon structure is essential in K-ion storage performance (Wu et al. 2022). In this research, lignins with M_W of 2233 (low M_W), 9660 (medium M_W), and 14,300 g mol^{-1} (high M_W) were directly pyrolyzed at 500 ~ 1000 ℃ (Fig. 16b). As shown in Fig. 16c, the lignin of a higher molecular weight is more inclined to the surface adsorption contribution (Q_b), as the high M_W lignin is difficult to get modification (depolymerized, fragmented, and graphitized). In contrast, the lignin of a lower molecular weight is more inclined to the bulk-insertion contribution (*Qs*). To be more exact, as summarized in Fig. 16d, low M_W lignin would produce more graphite-like nanocrystals, narrow interplanar distance and fewer defect sites under the modification, causing limited *Qb* (115 mAh g^{-1}) and limited *Qs* (136 mAh g^{-1}) (Fig. 16d(i)). High M_W lignin achieves massive *Qs* (216 mAh g^{-1}) and limited *Qb* (111 mAh g^{-1}) due to its amorphous dominated carbon structures, least graphite-like nanocrystals with suitable carbon interlayer distance (Fig. 16d(iii)); Medium M_W lignin would realize both high *Qs* (219 mA h g^{-1}) and high *Qb* (159 mAh g^{-1}) from their balanced disordered carbon and graphite-like nanocrystals with expanded carbon layers (Fig. 16d(ii)). Moreover, the disordered carbon rose with the pyrolysis temperature increases (500 ~ 700 ℃), resulting to the dominant mechanism of hard carbon shifted from insertion mechanism to adsorption mechanism (Fig. 16c). However, adsorption contribution was slightly attenuated at a higher pyrolysis temperature (1000 ℃) due to the reduced interlayer spacing affecting the K^+ ion bulk insertion, even with more disordered carbon. Thus, benefited from balanced disordered carbon and graphite-like nanocrystals with a considerable interlayer distance, the medium-M_W lignin at 700 ℃ achieved the best overall performance with a high reversible specific capacity (~ 300 mAh g^{-1} at 50 mA g^{-1}) and high capacity retention (80% after 100 cycles). So fine control of hard carbon structure is a key to meeting the technical requirements of the anode materials in PIBs.

6 Catalysis and environmental applications of LDCs

6.1 Electrochemical catalysis

Highly efficient catalyst for oxygen reduction reaction (ORR) has become the decisive factor for the employment of fuel cells and metal-air batteries. Currently, the scarcity of platinum (Pt)-based catalysts still can not meet the commercial requirements. In fact, Pt-based catalysts have some limitations. Metal-free or non-precious metal catalysts attract attention for the motivation of developing abundant cheap catalysts. This research topic focuses on the following issues: (i) efficient alternative carbon sources; (ii) 3D structures exposing active sites; (iii) doping heteroatom to change electron configuration, enabling the catalyst with a four-electron (4e) pathway.

N, S co-doped porous carbon enhances the ORR performance due to the synergetic effect of nitrogen and sulfur doping (Fan et al. 2019). Recently, some studies have shown that the introduction of halogen atoms in the carbon matrix could improve the ORR performance (Jeon et al. 2013). The electrochemical ORR catalytic performance of non-precious metals mainly focuses on the high catalytic performance and long-term durability. Shen et al. proposed a dual-template methodology using eutectic $NaCl/ZnCl_2$ melt to achieve a 3D mesoporous skeleton structured carbon from lignin (Shen et al. 2020). The as-prepared lignin-derived N, S and Cl-doped carbon materials have a high SSA of 1289 m^2 g^{-1}, a large pore volume of 2.80 cm^3 g^{-1} and a well-connected and stable structure. It is assumed that the excellent electrochemical activity and stability of the ORR catalyst in acidic media are attributed to the presence of C–Cl covalent bonds in the carbon material. The prepared carbon materials exhibited excellent catalytic performance and durability in the acidic electrolyte, showing an extremely high half-wave potential ($E_{1/2}$ = 0.792 V), and the electron transfer number is around 3.93, indicating an extremely low H_2O_2 yield (< 5%), the Tafel slop (43 mV dec^{-1}), with high retention of the limiting current density maintaining 89% after 5 thousand cycles. The prepared carbon material was employed in a H_2-O_2 single fuel cell which exhibited a maximum power density of 779 mW cm^{-2}.

6.2 Photocatalysis

Utilizing lignin waste to develop a value-added material has been attempted in a variety of applications. LDC can be applied as a substrate for the synthesis of a carbon-supported photocatalyst. Basically, titanium dioxide (TiO_2) is generally considered to be the most commonly used photocatalyst under UV light stimulation (Nair et al. 2016).

Carbon-based material could be coupled with photocatalyst as an electron reservoir to trap photo-generated

electrons facilitating the separation of photo-generated charge carriers. (Srisasiwimon et al. 2018). Thus, the modification of TiO_2 with lignin, as a carbon source, to form composite photocatalysts for improving their photocatalytic performance is tried in practice. As an example, TiO_2/lignin-based carbon composite photocatalyst was synthesized by a sol − gel microwave technique. Lignin as a carbon precursor for synthesizing composite photocatalysts showed improvement in the performance of TiO_2. Under UV irradiation, the conversion rate of lignin was as high as 40%, and the photocatalytic activity was enhanced. High-value chemicals such as vanillin were detected after photocatalysis by gas chromatography-mass spectrometry (Srisasiwimon et al. 2018). Structural modifications of TiO_2 with carbon have been described as a promising way to enhance the titania activity under visible radiation (Sakthivel and Kisch 2003). A. Gómez-Avilés et al. have tested the degradation of a model drug (acetaminophen) in water by C-modified TiO_2 photocatalysts under solar irradiation (Gómez-Avilés et al. 2019). The photocatalyst achieves complete conversion of acetaminophen in only 1 h under solar irradiation.

LDC could also be used to decorate ZnO photocatalyst. Zhang et al. fabricated a lignin-based hollow carbon (LHC) with a thin shell and opened structure by low-cost EHL and MgO as the template. Then ZnO nanoparticles were immobilized on the exterior and interior surface of LHC (ZnO/LHC). This two-step method avoided excessive carbon coating on the surface of ZnO (Zhang et al. 2020a).

Zhang et al. further synthesized a lignin-based flower-like carbon (LFC) using $Mg(OH)_2$ as a structural inducer (Zhang et al. 2020b). The LFC presented 3D structure, which is beneficial to anchor ZnO nanoparticles. The ZnO/LFC composite photocatalyst demonstrated extended light absorption and separation of photogenerated electron–hole pairs because of the electronic interface interaction between ZnO and LFC. Wang et al. presented a novel LC/ZnO hybrid composite synthesized through a facile yet efficient one-pot carbonization method using industrial lignin (Wang et al. 2017). The obtained LC/ZnO hybrid composite exhibited significant enhancement in photocatalytic performance compared with pure ZnO nanoparticles.

6.3 Adsorption

Carbon dioxide emissions are considered a major contributor to climate change. CO_2 adsorption by solid adsorbents, such as zeolites and metal − organic frameworks, have demonstrated to be efficient for CO_2 capture. Porous carbons remain superior CO_2 adsorbents given their stability and energy intake during regeneration (Saha and Kienbaum 2019). Bio-based resources are highly attractive as carbon precursors that can be produced sustainably in a large scale. Lignin shows promises to be a valuable source owing to its high carbon yield, but the hydrothermal treatment of lignin usually produces interconnected irregular topologies.

Zhao et al. synthesized multi-scale carbon superaparticles (SPs) by combining lignin nanoparticles and microbeads with cellulose nanofibers (CNFs) via a soft-template method (Fig. 17a) (Zhao et al. 2021). They prepared lignin SPs by evaporation induced self-assembly (EISA) of suspensions containing LPs and CNFs, and the morphology of LP-based SP and 2.5 wt% CNF-assembled carbon SP was compared at different CNF mass fractions (Fig. 17b). The CO_2 adsorption capacity was compared under conditions of SSA, carbonation temperature and nitrogen content (Fig. 17c-f). The carbon SPs formed by controlled sintering during carbonization developed high mechanical strength (58 $N{\cdot}mm^{-3}$) and surface area (1152 $m^2{\cdot}g^{-1}$). As a result, the carbon SPs offer hierarchical access to adsorption sites that are well suited for CO_2 capture (77 mg $CO_2{\cdot}g^{-1}$).

Geng et al. described a new family of carbon aerogel with a hierarchical structure from kraft lignin/TOCNF precursors and synthesized by ice-templating and further carbonization (Geng et al. 2020). This work demonstrated the suitability of using lignin and TOCNFs, which can be extracted from various renewable resources, to prepare multifunctional carbon aerogels. The best results exhibited a CO_2 adsorption capacity of 5.23 mmol g^{-1} at 273 K and 100 kPa and a gravimetric specific capacitance of 124 F g^{-1} at a current density of 0.2 A g^{-1}.

Adsorption is considered as an efficient method for capturing contaminants from waste water (Dąbrowski 2001). As discussed before, Lignin has abundant oxygen-containing groups (− C = O and − OH) in its carbon skeleton, which is beneficial for the development of functionalized lignin-derived adsorbents. Chemical activation and physical activation strategies could be used to enlarge the SSA of LDPCs to enhance the removal efficiency of dyes. Xu et al. designed and prepared a pH-responsive, easily regenerated, high-capacity, and highly selective lignin-derived sulfonated porous carbon (LSPC) by using Fe_3O_4 as a hard templating agent (Fig. 18a) (Zhu et al. 2021). The effect of pH on adsorption was explored (Fig. 18b-c), explaining the mechanism of adsorption and desorption of α-MB on LSPC (Fig. 18d). After concurrent acid etching and sulfonating process, porous structure of LSPC was obtained, and high density of negatively charged groups (including − SO_3H, − COOH, and phenolic − OH) were anchored onto the LSPC. The maximum adsorption capacity achieved was 420.40 mg/g for methylene blue (a-MB). Moreover, the a-MB adsorbed

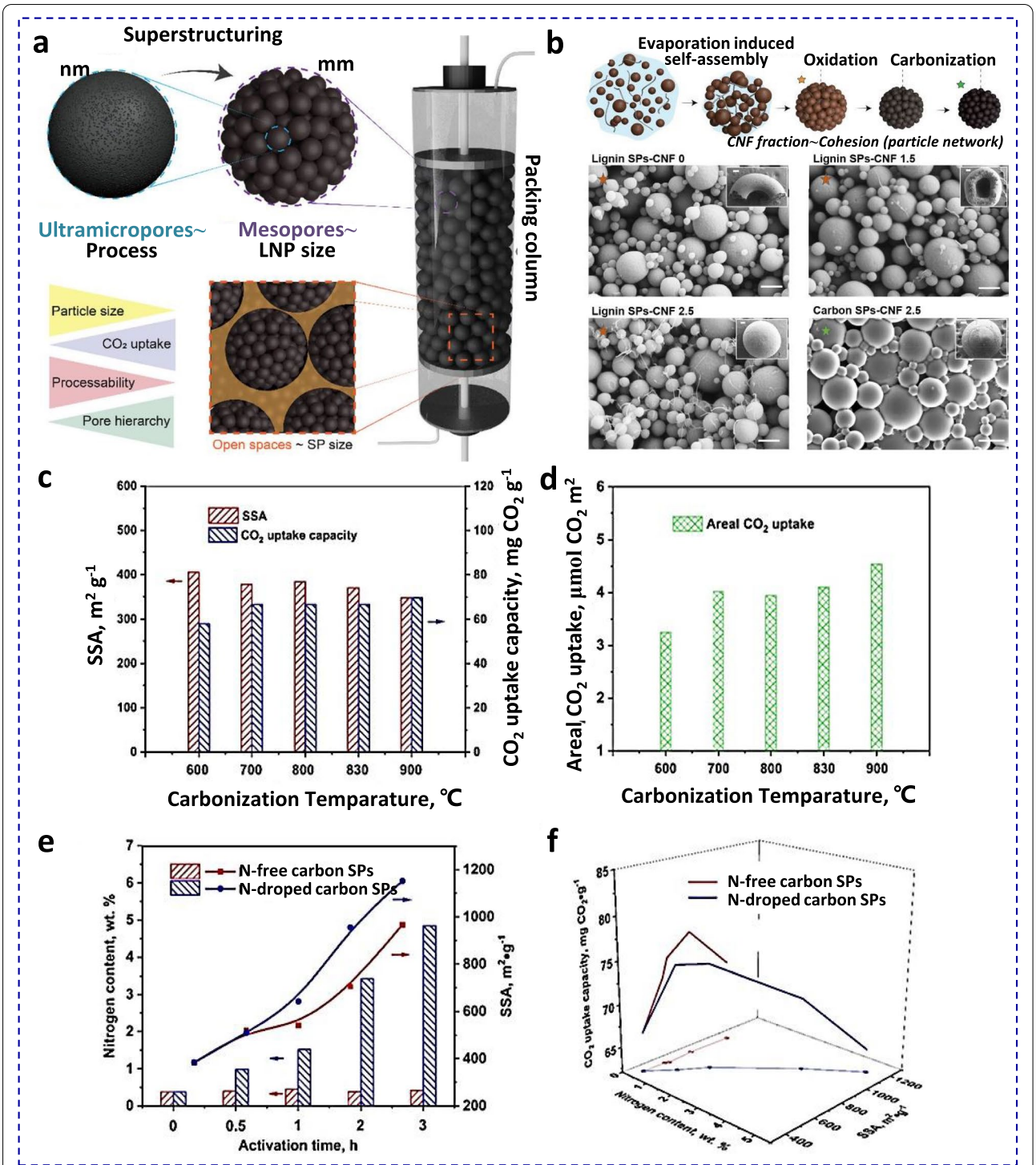

Fig. 17 **a** Superstructuring of lignin particles (nanometer-scale) into millimeter-scaled carbon supraparticles (SPs) for use in CO_2 capture. The self-assembled lignin SPs are converted into carbon-based, hierarchically structured materials following controlled carbonization and activation; **b** Schematic illustration of the preparation of lignin SPs via EISA of suspension containing LPs and CNF. SEM images show the morphology of LP-based SPs and 2.5 wt% CNF-assembled carbon SPs at different CNF mass fractions; **c** Specific surface area (SSA) and corresponding CO_2 uptake capacity as well as (**d**) areal CO_2 uptake of carbon SPs obtained at varying carbonization temperatures; **e** Nitrogen content and SSA and (f) CO_2 uptake capacity as a function of nitrogen content and SSA by carbon SPs-800 activated during given time by steam (N-free carbon SPs) and ammonia-steam (N-doped carbon SPs). Reproduced with permission from Ref. (Zhao et al. 2021). Copyright © 2021, American Chemistry Society

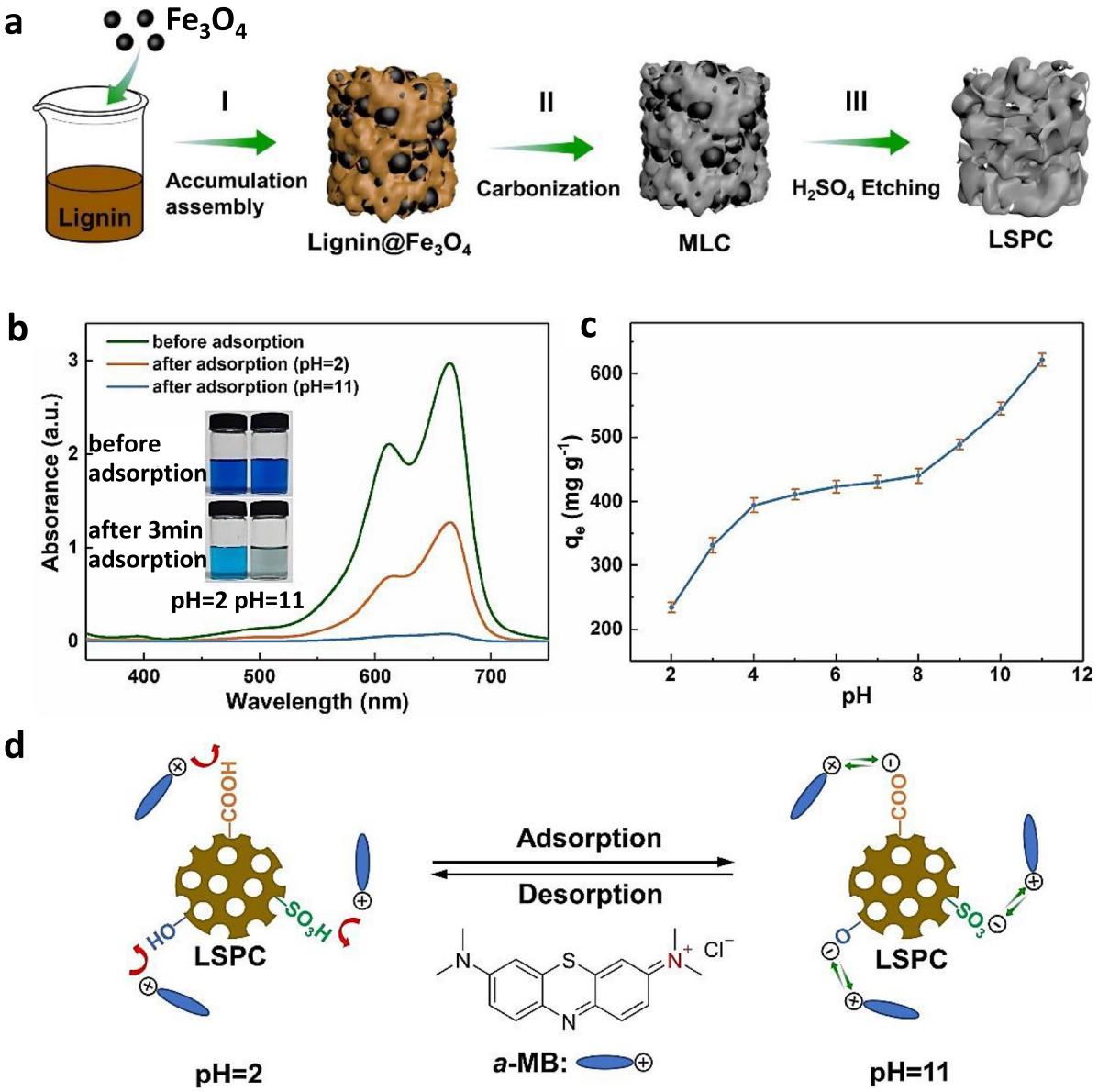

Fig. 18 **a** Schematic illustration of the preparation of LSPC; **b** UV–vis spectra of α-MB solutions (C_0 = 20 mg/L, pH = 2 and 11) before and after 3 min adsorption onto LSPC (inset: photographs of α-MB solutions before and after 3 min adsorption), **c** effect of pH values on the adsorption of α-MB onto LSPC (C_0 = 500 mg/L), and **d** the adsorption and desorption mechanism of α-MB onto LSPC. Reproduced with permission from Ref. (Zhu et al. 2021). Copyright © 2021, Elsevier

onto the LSPC could be desorbed in acidic methanol solution. The regenerated LSPC could be recycled for a-MB removal in absorption–desorption cycles.

Chromium is a representative heavy metal, and Cr(VI) is highly carcinogenic. Cr(VI) usually exists in water in the form of oxygen anions such as chromate. Because of the large hydration radius of oxygen anions, Cr(VI) is difficult to be adsorbed by adsorbents. N and S can provide electrons to reduce highly toxic Cr(VI) to nontoxic or low-toxicity Cr(III) (Saha and Orvig 2010). LDPCs could contain a large number of O groups and S groups that can effectively reduce Cr(VI) (Doherty et al. 2011). Hydrothermal-induced assembly technology can add oxygen-containing groups (-OH, etc.) on LDPCs and

thus can also be used for incorporating specific elements into the materials (Liang et al. 2021b). The generated hydrothermal carbon has a drawback of low SSA, and the structure is agglomerated, with little pore structure (Liang et al. 2021a). Alkaline activation strategies can ameliorate this defect to prepare adsorbents with more pores and a very high SSA. For instance, Liang et al. prepared lignin-based carbon spheres (L-CSs) by hydrothermally induced assembly using industrial alkali lignin as raw material (Liang et al. 2022). A novel lignin-based hierarchical porous carbon (L-HPC) with enhanced SSA showed excellent adsorption performance of Cr(VI), and the adsorption capacity reached 887.8 mg g^{-1}.

Ni(II) is one of the toxic metals present in wastewater, which poses a serious threat on the health of human beings and the local ecosystem. Activated carbon as an efficient adsorbent is widely applied to remove Ni(II) from wastewater due to its high SSA, extensive adsorption capacity and various surface functional groups. Gao et al. used papermaking black liquor lignin as raw material and prepared activated carbon with high SSA and low cost by pre-carbonized KOH activation method. The feasibility of efficient Ni(II) adsorbents was described (Gao et al. 2013).

6.4 Oil/water separation

In recent years, industrial wastewater containing oil, leaking petroleum products during extraction, storage, transport and discharge worldwide have become major environmental issues and global challenges. Cleaning of contaminants through oil–water separation is an effective method, where high efficiency and low cost adsorbents are essentially needed. There is a growing interest in the development of new materials from biomass with functional additives, such as lignin owing to its intrinsic properties.

3D porous foams or sponges are receiving increasing attention worldwide due to their lightweight, high porosity, low density, high SSA and high adsorption capacity (Priyanka and Saravanakumar 2018). Its large SSA, higher thermal stability, higher electrical conductivity, ultra-lightweight, good reusability and superhydrophobicity provide better conditions for oil–water separation. Vannarath et al. used two biopolymers, lignin (extracted from betel nut shells) and starch, to synthesize a lignin carbon foam by pyrolytic carbonization technology with zinc nitrate as an activation agent (Vannarath and Thalla 2021). The lignin and zinc oxide particles are embedded in the carbon foam, making it an ultra-light, hydrophobic and thermally stable material. The synthesized lignin-carbon foam is ultralight (density = 0.0294 g cm^{-3}), excellent hydrophobic (water contact angle was 124°), mesoporous (3D cell-like structure), fire-retardant and thermally stable. The foam showed an excellent adsorption capacity for different oils, and the highest sorption was observed for diesel oil (7842.71 mg g^{-1}).

7 A summary of current status and future trends

LDC and LDPC are promising carbon materials for next-generation commercial applications, given the controllable SSA, morphology, surface chemistry, and microcrystalline structures (Fig. 19). The overall target for LDC and LDPC development is to design green, sustainable chemical processes with low production cost (Zhang et al. 2021b), and to tune the microcrystalline structure, pore distribution, and surface chemistry (Yin et al. 2020a). LDC and LDPC can be applied in a variety of applications. Specifically, LDC and LDPC are promising in supercapacitors, batteries, energy storage, catalysts, and environmental remediation applications.

Low energy density and high energy storage cost are two obstacles impeding the development of supercapacitor commercialization. LDPCs for environmental applications are price-sensitive, in which the fabrication cost should be much lower than LDPCs for supercapacitors. In this regard, to realize the commercial application of LDPCs toward supercapacitors and environmental application, the following issues need to be addressed: (1) The uncertainty of lignin raw materials with great difference in the molecular structure of lignin results in the instability of the structure and properties of LDC products. Pre-carbonization at low temperatures could be developed to alleviate the difference between different lignin precursors; (2) Production of LDPCs mainly by carbonization and activation at high temperatures, is chemical-consuming, energy-consuming, highly corrosive, and not environmentally friendly. The development of green and efficient activation technology, such as direct pyrolysis and low-temperature activation, to replace the traditional activation of potassium salt is an urgent task for the large-scale production of LDPCs; (3) Although the rich oxygen in lignin is beneficial to improve surface wettability, oxygen functional groups tend to cause self-discharge, and excessive leakage current is not conducive to the practical application of supercapacitors, especially for organic electrolyte systems; (4) The energy density of LDPC-based supercapacitor cannot meet the requirement of practical applications, so the precise control of pore size (sub-nano pores and ordered mesopores) is needed to realize the applications of chemical adsorption and to enhance the energy density of supercapacitors.

The storage of alkaline metal ions with different charge storage mechanisms requires that LDC should have different physicochemical properties and microstructures. Generally, hard carbon for Na ion storage should have plenty of inner closed sub-nanometer-sized

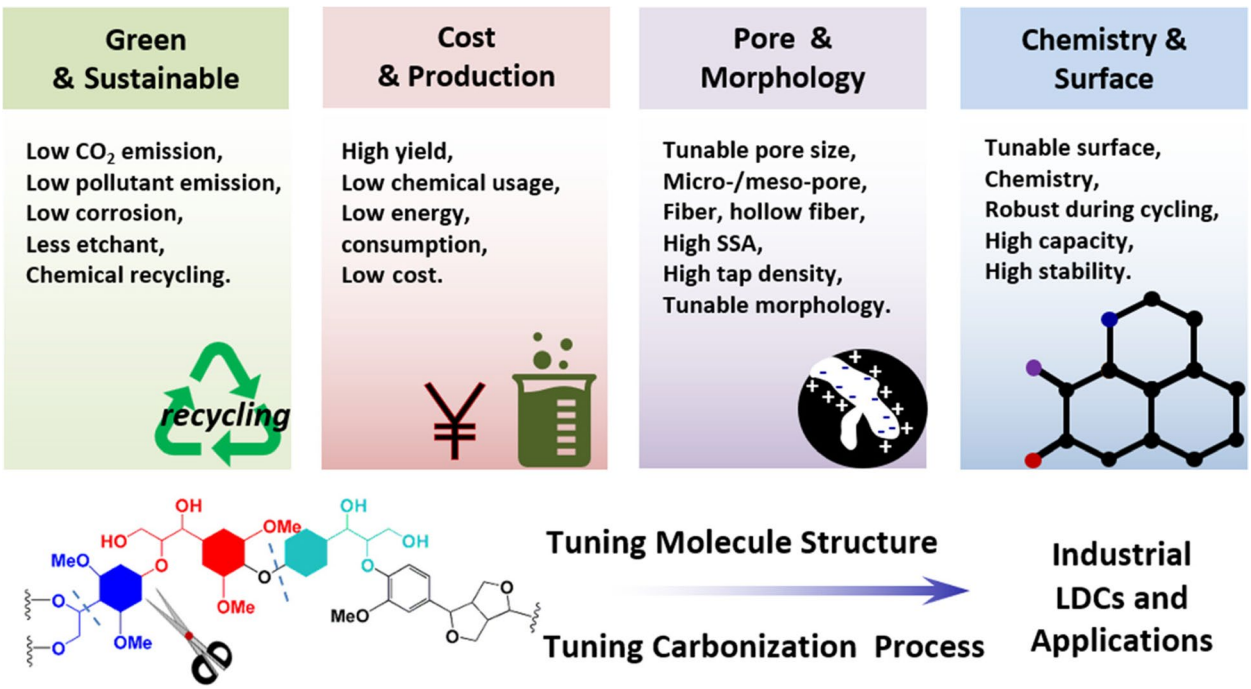

Fig. 19 A summary of the future research trends of LDC materials

pores to realize the quasi-deposition of sodium metal in these pores and large interlayer spacing to enable fast and stable intercalation/adsorption. Therefore, novel synthesis methodologies need to be developed to realize internal closed pores and high capacity. On the contrary, the storage of Li and K should fully utilize the intercalation of Li and K ions in the graphitic regions and the adsorption in defect sites.

The morphology control of LDC is limited to spheres, hollow spheres by spray drying or anti-solvent phase separation techniques and fibers by electrospinning. These methods are tedious in practice. For example, electrospinning is hard to be realized in a large-scale manner. Therefore, novel techniques that use low consumption of organic solvents and are high-throughput need to be developed for commercialization. In summary, it is significant to develop novel and facile techniques for the preparation of LDCs and LDPCs with sphere and fiber morphologies to further advance the development of lignin-derived functional carbon materials for future applications.

Developing synthesis and engineering methods for LDC and LDPCs is in the central area of LDC materials. With the pursuit of sustainable development and green preparation engineering methods, we could elaborate a novel pathway for high-value-added utilization of lignin towards commercialization.

Acknowledgements
The authors acknowledge the financial support from the National Natural Science Foundation of China (22108044), the Research and Development Program in Key Fields of Guangdong Province (2020B1111380002), the financial support from the Guangdong Provincial Key Laboratory of Plant Resources Biorefinery (2021GDKLPRB07).

Authors' contribution
Wenli Zhang: Writing-Review and Editing, Visualization, Project administration, Funding acquisition. Xueqing Qiu: Writing-Review and Editing, Supervision, Project administration, Funding acquisition. Caiwei Wang: Writing-Review and Editing. Lei Zhong: Writing-Review and Editing. Fangbao Fu: Writing-Review and Editing. Jiahao Zhu: Writing-Review and Editing. Zejie Zhang: Writing-Review and Editing. Yanlin Qin: Writing-Review and Editing. Dongjie Yang: Writing-Review and Editing. Chunbao Charles Xu: Writing-Review and Editing. The author(s) read and approved the final manuscript.

Availability of data and materials
This review artile contains no research data available.

Declarations

Competing interests
The authors declare that they have no known competing financial interests or personal relationships that influence the work reported in this paper.

Author details
[1]School of Chemical Engineering and Light Industry, Guangdong University of Technology (GDUT), 100 Waihuan Xi Road, Guangzhou 510006, Panyu District, China. [2]Guangdong Provincial Key Laboratory of Plant Resources Biorefinery, Guangdong University of Technology (GDUT), 100 Waihuan Xi Road, Guangzhou 510006, Panyu District, China. [3]School of Advanced Manufacturing, Guangdong University of Technology (GDUT), Jieyang 522000, China. [4]School of Chemistry and Chemical Engineering, South China University of Technology (SCUT), 381 Wushan Road, Guangzhou 510640, Tianhe District, China. [5]Department of Chemical and Biochemical Engineering, Western University, London, ON N6A 3K7, Canada.

Received: 18 April 2022 Accepted: 14 May 2022
Published online: 29 July 2022

References

Alvin S, Cahyadi HS, Hwang J et al (2020) Revealing the Intercalation Mechanisms of Lithium, Sodium, and Potassium in Hard Carbon. Adv Energy Mater 10:1–16. https://doi.org/10.1002/aenm.202000283

Bai P, He Y, Zou X et al (2018) Elucidation of the Sodium-Storage Mechanism in Hard Carbons. Adv Energy Mater 8:1–9. https://doi.org/10.1002/aenm.201703217

Baklanova ON, Plaksin GV, Drozdov VA et al (2003) Preparation of microporous sorbents from cedar nutshells and hydrolytic lignin. Carbon N Y 41:1793–1800. https://doi.org/10.1016/S0008-6223(03)00149-0

Beck RJ, Zhao Y, Fong H, Menkhaus TJ (2017) Electrospun lignin carbon nanofiber membranes with large pores for highly efficient adsorptive water treatment applications. J Water Process Eng 16:240–248. https://doi.org/10.1016/j.jwpe.2017.02.002

Borchardt L, Leistenschneider D, Haase J, Dvoyashkin M (2018) Revising the Concept of Pore Hierarchy for Ionic Transport in Carbon Materials for Supercapacitors. Adv Energy Mater 8:1800892. https://doi.org/10.1002/aenm.201800892

Borghei M, Lehtonen J, Liu L, Rojas OJ (2018) Advanced Biomass-Derived Electrocatalysts for the Oxygen Reduction Reaction. Adv Mater 30:1703691. https://doi.org/10.1002/adma.201703691

Brazil TR, Gonçalves M, Junior MSO, Rezende MC (2020) A statistical approach to optimize the activated carbon production from Kraft lignin based on conventional and microwave processes. Microporous Mesoporous Mater 308:110485. https://doi.org/10.1016/j.micromeso.2020.110485

Cao KLA, Kitamoto Y, Iskandar F, Ogi T (2021a) Sustainable porous hollow carbon spheres with high specific surface area derived from Kraft lignin. Adv Powder Technol 32:2064–2073. https://doi.org/10.1016/j.apt.2021.04.012

Cao KLA, Rahmatika AM, Kitamoto Y et al (2021b) Controllable synthesis of spherical carbon particles transition from dense to hollow structure derived from Kraft lignin. J Colloid Interface Sci 589:252–263. https://doi.org/10.1016/j.jcis.2020.12.077

Cao M, Wang Q, Cheng W et al (2021c) A novel strategy combining electrospraying and one-step carbonization for the preparation of ultralight honeycomb-like multilayered carbon from biomass-derived lignin. Carbon N Y 179:68–79. https://doi.org/10.1016/j.carbon.2021.03.063

Carrott PJM, Suhas RC, MML, et al (2008) Reactivity and porosity development during pyrolysis and physical activation in CO2 or steam of kraft and hydrolytic lignins. J Anal Appl Pyrolysis 82:264–271. https://doi.org/10.1016/j.jaap.2008.04.004

Chakar FS, Ragauskas AJ (2004) Review of current and future softwood kraft lignin process chemistry. Ind Crops Prod 20:131–141. https://doi.org/10.1016/j.indcrop.2004.04.016

Chang ZZ, Yu BJ, Wang CY (2015) Influence of H2 reduction on lignin-based hard carbon performance in lithium ion batteries. Electrochim Acta 176:1352–1357. https://doi.org/10.1016/j.electacta.2015.07.076

Chen XY, Zhou QQ (2012) The production of porous carbon from calcium lignosulfonate without activation process and the capacitive performance. Electrochim Acta 71:92–99. https://doi.org/10.1016/j.electacta.2012.03.166

Chen F, Zhou Z, Chang L et al (2017a) Synthesis and characterization of lignosulfonate-derived hierarchical porous graphitic carbons for electrochemical performances. Microporous Mesoporous Mater 247:184–189. https://doi.org/10.1016/j.micromeso.2017.03.010

Chen X, Paul R, Dai L (2017b) Carbon-based supercapacitors for efficient energy storage. Natl Sci Rev 4:453–489. https://doi.org/10.1093/nsr/nwx009

Chen Y, Zhang G, Zhang J et al (2018) Synthesis of porous carbon spheres derived from lignin through a facile method for high performance supercapacitors. J Mater Sci Technol 34:2189–2196. https://doi.org/10.1016/j.jmst.2018.03.010

Chen F, Wu L, Zhou Z et al (2019a) MoS2 decorated lignin-derived hierarchical mesoporous carbon hybrid nanospheres with exceptional Li-ion battery cycle stability. Chinese Chem Lett 30:197–202. https://doi.org/10.1016/j.cclet.2018.10.007

Chen W, Wang X, Feizbakhshan M et al (2019b) Preparation of lignin-based porous carbon with hierarchical oxygen-enriched structure for high-performance supercapacitors. J Colloid Interface Sci 540:524–534. https://doi.org/10.1016/j.jcis.2019.01.058

Chen C, Kuang Y, Zhu S et al (2020a) Structure–property–function relationships of natural and engineered wood. Nat Rev Mater 5:642–666. https://doi.org/10.1038/s41578-020-0195-z

Chen S, Feng F, Ma ZF (2020b) Lignin-derived nitrogen-doped porous ultrathin layered carbon as a high-rate anode material for sodium-ion batteries. Compos Commun 22:100447. https://doi.org/10.1016/j.coco.2020.100447

Chen W, Luo M, Yang K, Zhou X (2020c) Microwave-assisted KOH activation from lignin into hierarchically porous carbon with super high specific surface area by utilizing the dual roles of inorganic salts: Microwave absorber and porogen. Microporous Mesoporous Mater 300:110178. https://doi.org/10.1016/j.micromeso.2020.110178

Choi DI, Lee JN, Song J et al (2013) Fabrication of polyacrylonitrile/lignin-based carbon nanofibers for high-power lithium ion battery anodes. J Solid State Electrochem 17:2471–2475. https://doi.org/10.1007/s10008-013-2112-5

Choi SJ, Kim SJ, Kim ID (2016) Ultrafast optical reduction of graphene oxide sheets on colorless polyimide film for wearable chemical sensors. NPG Asia Mater 8:e315. https://doi.org/10.1038/am.2016.150

Cui C, Gao Y, Li J et al (2020) Origins of Boosted Charge Storage on Heteroatom-Doped Carbons. Angew Chemie - Int Ed 59:7928–7933. https://doi.org/10.1002/anie.202000319

Culebras M, Geaney H, Beaucamp A et al (2019) Bio-derived Carbon Nanofibres from Lignin as High-Performance Li-Ion Anode Materials. Chemsuschem 12:4516–4521. https://doi.org/10.1002/cssc.201901562

Dąbrowski A, (2001) Adsorption - From theory to practice. Adv Colloid Interface Sci 93:135–224. https://doi.org/10.1016/S0001-8686(00)00082-8

Demir M, Farghaly AA, Decuir MJ et al (2018) Supercapacitance and oxygen reduction characteristics of sulfur self-doped micro/mesoporous biocarbon derived from lignin. Mater Chem Phys 216:508–516. https://doi.org/10.1016/j.matchemphys.2018.06.008

Deng Y, Zhao H, Qian Y et al (2016) Hollow lignin azo colloids encapsulated avermectin with high anti-photolysis and controlled release performance. Ind Crops Prod 87:191–197. https://doi.org/10.1016/j.indcrop.2016.03.056

Doherty WOS, Mousavioun P, Fellows CM (2011) Value-adding to cellulosic ethanol: Lignin polymers. Ind Crops Prod 33:259–276. https://doi.org/10.1016/j.indcrop.2010.10.022

Du L, Wu W, Luo C et al (2018) Lignin derived Si@C composite as a high performance anode material for lithium ion batteries. Solid State Ionics 319:77–82. https://doi.org/10.1016/j.ssi.2018.01.039

Du YF, Sun GH, Li Y et al (2021) Pre-oxidation of lignin precursors for hard carbon anode with boosted lithium-ion storage capacity. Carbon N Y 178:243–255. https://doi.org/10.1016/j.carbon.2021.03.016

Dutta S, Bhaumik A, Wu KCW (2014) Hierarchically porous carbon derived from polymers and biomass: Effect of interconnected pores on energy applications. Energy Environ Sci 7:3574–3592. https://doi.org/10.1039/c4ee01075b

Espinoza-Acosta JL, Torres-Chávez PI, Olmedo-Martínez JL et al (2018) Lignin in storage and renewable energy applications: A review. J Energy Chem 27:1422–1438. https://doi.org/10.1016/j.jechem.2018.02.015

Fan H, Wang Y, Gao F et al (2019) Hierarchical sulfur and nitrogen co-doped carbon nanocages as efficient bifunctional oxygen electrocatalysts for rechargeable Zn-air battery. J Energy Chem 34:64–71. https://doi.org/10.1016/j.jechem.2018.09.003

Fan L, Shi Z, Ren Q et al (2021) Nitrogen-doped lignin based carbon microspheres as anode material for high performance sodium ion batteries. Green Energy Environ 6:220–228. https://doi.org/10.1016/j.gee.2020.06.005

Fang W, Yang S, Wang X-L et al (2017) Manufacture and application of lignin-based carbon fibers (LCFs) and lignin-based carbon nanofibers (LCNFs). Green Chem 19:1794–1827. https://doi.org/10.1039/c6gc03206k

Fenner RA, Lephardt JO (1981) Examination of the Thermal Decomposition of Kraft Pine Lignin by Fourier Transform Infrared Evolved Gas Analysis. J Agric Food Chem 29:846–849. https://doi.org/10.1021/jf00106a042

Fromm O, Heckmann A, Rodehorst UC et al (2018) Carbons from biomass precursors as anode materials for lithium ion batteries: New insights into

carbonization and graphitization behavior and into their correlation to electrochemical performance. Carbon N Y 128:147–163. https://doi.org/10.1016/j.carbon.2017.11.065
Fu K, Yue Q, Gao B et al (2013) Preparation, characterization and application of lignin-based activated carbon from black liquor lignin by steam activation. Chem Eng J 228:1074–1082. https://doi.org/10.1016/j.cej.2013.05.028
Fu F, Yang D, Zhang W et al (2020) Green self-assembly synthesis of porous lignin-derived carbon quasi-nanosheets for high-performance supercapacitors. Chem Eng J 392:123721. https://doi.org/10.1016/j.cej.2019.123721
Fu F, Zhao B, Yang D et al (2021) Insights into gas-exfoliation and the in-situ template mechanism of zinc compound for lignin-derived supercapacitive porous carbon. ACS Appl Energy Mater 4:13617–13626. https://doi.org/10.1021/acsaem.1c02283
Gao Y, Yue Q, Gao B et al (2013) Preparation of high surface area-activated carbon from lignin of papermaking black liquor by KOH activation for Ni(II) adsorption. Chem Eng J 217:345–353. https://doi.org/10.1016/j.cej.2012.09.038
Gao L, Zhang G, Cai J et al (2020) Rationally exfoliating chitin into 2D hierarchical porous carbon nanosheets for high-rate energy storage. Nano Res 13:1604–1613. https://doi.org/10.1007/s12274-020-2778-9
García-Mateos FJ, Berenguer R, Valero-Romero MJ et al (2018) Phosphorus functionalization for the rapid preparation of highly nanoporous submicron-diameter carbon fibers by electrospinning of lignin solutions. J Mater Chem A 6:1219–1233. https://doi.org/10.1039/c7ta08788h
García-Mateos FJ, Ruiz-Rosas R, María Rosas J et al (2020) Activation of electrospun lignin-based carbon fibers and their performance as self-standing supercapacitor electrodes. Sep Purif Technol 241:116724. https://doi.org/10.1016/j.seppur.2020.116724
Geng S, Wei J, Jonasson S et al (2020) Multifunctional Carbon Aerogels with Hierarchical Anisotropic Structure Derived from Lignin and Cellulose Nanofibers for CO2 Capture and Energy Storage. ACS Appl Mater Interfaces 12:7432–7441. https://doi.org/10.1021/acsami.9b19955
Gengler RYN, Badali DS, Zhang D et al (2013) Revealing the ultrafast process behind the photoreduction of graphene oxide. Nat Commun 4:2560. https://doi.org/10.1038/ncomms3560
Ghosh S, Barg S, Jeong SM, Ostrikov K (2020) Heteroatom-Doped and Oxygen-Functionalized Nanocarbons for High-Performance Supercapacitors. Adv Energy Mater 10:2001239
Gindl-Altmutter W, Köhnke J, Unterweger C et al (2019) Lignin-based multiwall carbon nanotubes. Compos Part A Appl Sci Manuf 121:175–179. https://doi.org/10.1016/j.compositesa.2019.03.026
Gómez-Avilés A, Peñas-Garzón M, Bedia J et al (2019) C-modified TiO2 using lignin as carbon precursor for the solar photocatalytic degradation of acetaminophen. Chem Eng J 358:1574–1582. https://doi.org/10.1016/j.cej.2018.10.154
Gonzalez-Serrano E, Cordero T, Rodríguez-Mirasol J, Rodríguez JJ (1997) Development of Porosity upon Chemical Activation of Kraft Lignin with ZnCl2. Ind Eng Chem Res 36:4832–4838. https://doi.org/10.1021/ie970261q
Goodenough JB, Park KS (2013) The Li-ion rechargeable battery: A perspective. J Am Chem Soc 135:1167–1176. https://doi.org/10.1021/ja3091438
Guo N, Li M, Sun X et al (2017) Enzymatic hydrolysis lignin derived hierarchical porous carbon for supercapacitors in ionic liquids with high power and energy densities. Green Chem 19:2595–2602. https://doi.org/10.1039/c7gc00506g
Guo N, Zhang S, Wang L, Jia D (2019) Application of plant-based porous carbon for supercapacitors. Acta Phys - Chim Sin 36:1903055. https://doi.org/10.3866/PKU.WHXB201903055
Herou S, Ribadeneyra MC, Madhu R et al (2019) Ordered mesoporous carbons from lignin: A new class of biobased electrodes for supercapacitors. Green Chem 21:550–559. https://doi.org/10.1039/c8gc03497d
Hérou S, Bailey JJ, Kok M, et al (2021) High-Density Lignin-Derived Carbon Nanofiber Supercapacitors with Enhanced Volumetric Energy Density. Adv Sci 2100016. https://doi.org/10.1002/advs.202100016
Ho HC, Nguyen NA, Meek KM et al (2018) A Solvent-Free Synthesis of Lignin-Derived Renewable Carbon with Tunable Porosity for Supercapacitor Electrodes. Chemsuschem 11:2953–2959. https://doi.org/10.1002/cssc.201800929
Hu B, Wang K, Wu L et al (2010) Engineering carbon materials from the hydrothermal carbonization process of biomass. Adv Mater 22:813–828. https://doi.org/10.1002/adma.200902812
Hu J, Xiao R, Shen D, Zhang H (2013a) Structural analysis of lignin residue from black liquor and its thermal performance in thermogravimetric-Fourier transform infrared spectroscopy. Bioresour Technol 128:633–639. https://doi.org/10.1016/j.biortech.2012.10.148
Hu L, Zheng G, Yao J et al (2013b) Transparent and conductive paper from nanocellulose fibers. Energy Environ Sci 6:513–518. https://doi.org/10.1039/c2ee23635d
Huang X, Yu H, Chen J et al (2014) Ultrahigh rate capabilities of lithium-ion batteries from 3D ordered hierarchically porous electrodes with entrapped active nanoparticles configuration. Adv Mater 26:1296–1303. https://doi.org/10.1002/adma.201304467
Huang S, Lv Y, Wen W et al (2021a) Three-dimensional hierarchical porous hard carbon for excellent sodium/potassium storage and mechanism investigation. Mater Today Energy 20:100673. https://doi.org/10.1016/j.mtener.2021.100673
Huang S, Yang D, Zhang W et al (2021b) Dual-templated synthesis of mesoporous lignin-derived honeycomb-like porous carbon/SiO2 composites for high-performance Li-ion battery. Microporous Mesoporous Mater 317:111004. https://doi.org/10.1016/j.micromeso.2021.111004
Huang X, Ren J, Ran JY et al (2022) Recent advances in pyrolysis of cellulose to value-added chemicals. Fuel Process Technol 229:107175. https://doi.org/10.1016/j.fuproc.2022.107175
Imel AE, Naskar AK, Dadmun MD (2016) Understanding the impact of poly(ethylene oxide) on the assembly of lignin in solution toward improved carbon fiber production. ACS Appl Mater Interfaces 8:3200–3207. https://doi.org/10.1021/acsami.5b10720
Isaac E, Samson A, Adeosun O (2019) Sustainable Lignin for Carbon Fibers Principles, Techniques, and Applications
Jeon IY, Choi HJ, Choi M et al (2013) Facile, scalable synthesis of edge-halogenated graphene nanoplatelets as efficient metal-free eletrocatalysts for oxygen reduction reaction. Sci Rep 3:1–7. https://doi.org/10.1038/srep01810
Jeon JW, Zhang L, Lutkenhaus JL et al (2015) Controlling porosity in lignin-derived nanoporous carbon for supercapacitor applications. Chemsuschem 8:428–432. https://doi.org/10.1002/cssc.201402621
Jia H, Sun N, Dirican M et al (2018) Electrospun Kraft Lignin/Cellulose Acetate-Derived Nanocarbon Network as an Anode for High-Performance Sodium-Ion Batteries. ACS Appl Mater Interfaces 10:44368–44375. https://doi.org/10.1021/acsami.8b13033
Jian Z, Hwang S, Li Z et al (2017) Hard-Soft Composite Carbon as a Long-Cycling and High-Rate Anode for Potassium-Ion Batteries. Adv Funct Mater 27:1–6. https://doi.org/10.1002/adfm.201700324
Jian W, Zhang W, Wu B et al (2022) Enzymatic Hydrolysis Lignin-Derived Porous Carbons through Ammonia Activation: Activation Mechanism and Charge Storage Mechanism. ACS Appl Mater Interfaces 14:5425–5438. https://doi.org/10.1021/acsami.1c22576
Jiang C, Wang Z, Li J et al (2020) RGO-templated lignin-derived porous carbon materials for renewable high-performance supercapacitors. Electrochim Acta 353:136482. https://doi.org/10.1016/j.electacta.2020.136482
Jiang K, Tan X, Zhai S et al (2021) Carbon nanosheets derived from reconstructed lignin for potassium and sodium storage with low voltage hysteresis. Nano Res 12:4664–4673. https://doi.org/10.1007/s12274-021-3399-7
Jin Y, Cheng X, Zheng Z (2010) Preparation and characterization of phenol-formaldehyde adhesives modified with enzymatic hydrolysis lignin. Bioresour Technol 101:2046–2048. https://doi.org/10.1016/j.biortech.2009.09.085
Jin J, Yu BJ, Shi ZQ et al (2014) Lignin-based electrospun carbon nanofibrous webs as free-standing and binder-free electrodes for sodium ion batteries. J Power Sources 272:800–807. https://doi.org/10.1016/j.jpowsour.2014.08.119
Jin H, Li J, Yuan Y et al (2018) Recent Progress in Biomass-Derived Electrode Materials for High Volumetric Performance Supercapacitors. Adv Energy Mater 8:1801007. https://doi.org/10.1002/aenm.201801007
Kijima M, Hirukawa T, Hanawa F, Hata T (2011) Thermal conversion of alkaline lignin and its structured derivatives to porous carbonized

materials. Bioresour Technol 102:6279–6285. https://doi.org/10.1016/j.biortech.2011.03.023
Kim MS, Lee DH, Kim CH et al (2015) Shell-core structured carbon fibers via melt spinning of petroleum- and wood-processing waste blends. Carbon N Y 85:194–200. https://doi.org/10.1016/j.carbon.2014.12.100
Kim DW, Kil HS, Kim J et al (2017) Highly graphitized carbon from non-graphitizable raw material and its formation mechanism based on domain theory. Carbon N Y 121:301–308. https://doi.org/10.1016/j.carbon.2017.05.086
Kim IH, Im TH, Lee HE et al (2019) Janus Graphene Liquid Crystalline Fiber with Tunable Properties Enabled by Ultrafast Flash Reduction. Small 1901529:1901529. https://doi.org/10.1002/smll.201901529
Komaba S, Hasegawa T, Dahbi M, Kubota K (2015) Potassium intercalation into graphite to realize high-voltage/high-power potassium-ion batteries and potassium-ion capacitors. Electrochem Commun 60:172–175. https://doi.org/10.1016/j.elecom.2015.09.002
Kurban Z, Lovell A, Jenkins D et al (2010) Turbostratic graphite nanofibres from electrospun solutions of PAN in dimethylsulphoxide. Eur Polym J 46:1194–1202. https://doi.org/10.1016/j.eurpolymj.2010.03.015
Lallave M, Bedia J, Ruiz-Rosas R et al (2007) Filled and hollow carbon nanofibers by coaxial electrospinning of Alcell lignin without binder polymers. Adv Mater 19:4292–4296. https://doi.org/10.1002/adma.200700963
Lee DW, Jin MH, Park JH et al (2018) Flexible Synthetic Strategies for Lignin-Derived Hierarchically Porous Carbon Materials. ACS Sustain Chem Eng 6:10454–10462. https://doi.org/10.1021/acssuschemeng.8b01811
Leng E, Guo Y, Chen J et al (2022) A comprehensive review on lignin pyrolysis: Mechanism, modeling and the effects of inherent metals in biomass. Fuel 309:122102. https://doi.org/10.1016/j.fuel.2021.122102
Li B, Lv W, Zhang Q et al (2014) Pyrolysis and catalytic pyrolysis of industrial lignins by TG-FTIR: Kinetics and products. J Anal Appl Pyrolysis 108:295–300. https://doi.org/10.1016/j.jaap.2014.04.002
Li Y, Zhou M, Pang Y, Qiu X (2017) Lignin-Based Microsphere: Preparation and Performance on Encapsulating the Pesticide Avermectin. ACS Sustain Chem Eng 5:3321–3328. https://doi.org/10.1021/acssuschemeng.6b03180
Li Y, Yang D, Lu S et al (2018) Modified Lignin with Anionic Surfactant and Its Application in Controlled Release of Avermectin. J Agric Food Chem 66:3457–3464. https://doi.org/10.1021/acs.jafc.8b00393
Li H, Qi C, Tao Y et al (2019) Quantifying the Volumetric Performance Metrics of Supercapacitors. Adv Energy Mater 9:1900079. https://doi.org/10.1002/aenm.201900079
Li C, Sun Y, Wu Q et al (2020a) A novel design strategy of a practical carbon anode material from a single lignin-based surfactant source for sodium-ion batteries. Chem Commun 56:6078–6081. https://doi.org/10.1039/d0cc01431a
Li G, Mao K, Liu M et al (2020b) Achieving Ultrahigh Volumetric Energy Storage by Compressing Nitrogen and Sulfur Dual-Doped Carbon Nanocages via Capillarity. Adv Mater 32:2004632. https://doi.org/10.1002/adma.202004632
Li H, Zhao Y, Liu S et al (2020c) Hierarchical porous carbon monolith derived from lignin for high areal capacitance supercapacitors. Microporous Mesoporous Mater 297:109960. https://doi.org/10.1016/j.micromeso.2019.109960
Li H, Shi F, An Q et al (2021a) Three-dimensional hierarchical porous carbon derived from lignin for supercapacitors: Insight into the hydrothermal carbonization and activation. Int J Biol Macromol 166:923–933. https://doi.org/10.1016/j.ijbiomac.2020.10.249
Li Q, Hu C, Li M et al (2021b) Enhancing the multi-functional properties of renewable lignin carbon fibersviadefining the structure-property relationship using different biomass feedstocks. Green Chem 23:3725–3739. https://doi.org/10.1039/d0gc03828h
Li T, Chen C, Brozena AH et al (2021c) Developing fibrillated cellulose as a sustainable technological material. Nature 590:47–56. https://doi.org/10.1038/s41586-020-03167-7
Li X, Zhang W, Wu M et al (2021d) Multiple-heteroatom doped porous carbons from self-activation of lignosulfonate with melamine for high performance supercapacitors. Int J Biol Macromol 183:950–961. https://doi.org/10.1016/j.ijbiomac.2021.05.028
Li Y, Liu L, Liu X et al (2021e) Extracting lignin-SiO2 composites from Si-rich biomass to prepare Si/C anode materials for lithium ions batteries. Mater Chem Phys 262:124331. https://doi.org/10.1016/j.matchemphys.2021.124331
Liang J, Lin Y, Wu S et al (2015) Enhancing the quality of bio-oil and selectivity of phenols compounds from pyrolysis of anaerobic digested rice straw. Bioresour Technol 181:220–223. https://doi.org/10.1016/j.biortech.2015.01.056
Liang H, Zhang H, Wang Q et al (2021a) A novel glucose-based highly selective phosphate adsorbent. Sci Total Environ 792:148452. https://doi.org/10.1016/j.scitotenv.2021.148452
Liang H, Zhang H, Zhao P et al (2021b) Synthesis of a novel three-dimensional porous carbon material and its highly selective Cr(VI) removal in wastewater. J Clean Prod 306:127204. https://doi.org/10.1016/j.jclepro.2021.127204
Liang H, Ding W, Zhang H et al (2022) A novel lignin-based hierarchical porous carbon for efficient and selective removal of Cr(VI) from wastewater. Int J Biol Macromol 204:310–320. https://doi.org/10.1016/j.ijbiomac.2022.02.014
Lin J, Peng Z, Liu Y et al (2014) Laser-induced porous graphene films from commercial polymers. Nat Commun 5:5714. https://doi.org/10.1038/ncomms6714
Lin X, Liu Y, Tan H, Zhang B (2020) Advanced lignin-derived hard carbon for Na-ion batteries and a comparison with Li and K ion storage. Carbon N Y 157:316–323. https://doi.org/10.1016/j.carbon.2019.10.045
Liu Q, Wang S, Zheng Y et al (2008) Mechanism study of wood lignin pyrolysis by using TG-FTIR analysis. J Anal Appl Pyrolysis 82:170–177. https://doi.org/10.1016/j.jaap.2008.03.007
Liu WJ, Jiang H, Yu HQ (2015a) Development of Biochar-Based Functional Materials: Toward a Sustainable Platform Carbon Material. Chem Rev 115:12251–12285. https://doi.org/10.1021/acs.chemrev.5b00195
Liu WJ, Jiang H, Yu HQ (2015b) Thermochemical conversion of lignin to functional materials: a review and future directions. Green Chem 17:4888–4907. https://doi.org/10.1039/c5gc01054c
Liu C, Hu J, Zhang H, Xiao R (2016a) Thermal conversion of lignin to phenols: Relevance between chemical structure and pyrolysis behaviors. Fuel 182:864–870. https://doi.org/10.1016/j.fuel.2016.05.104
Liu HC, Chien AT, Newcomb BA et al (2016b) Stabilization kinetics of gel spun polyacrylonitrile/lignin blend fiber. Carbon N Y 101:382–389. https://doi.org/10.1016/j.carbon.2016.01.096
Liu Y, Merinov BV, Goddard WA (2016c) Origin of low sodium capacity in graphite and generally weak substrate binding of Na and Mg among alkali and alkaline earth metals. Proc Natl Acad Sci U S A 113:3735–3739. https://doi.org/10.1073/pnas.1602473113
Liu W, Yao Y, Fu O et al (2017) Lignin-derived carbon nanosheets for high-capacitance supercapacitors. RSC Adv 7:48537–48543. https://doi.org/10.1039/c7ra08531a
Liu F, Wang Z, Zhang H et al (2019a) Nitrogen, oxygen and sulfur co-doped hierarchical porous carbons toward high-performance supercapacitors by direct pyrolysis of kraft lignin. Carbon N Y 149:105–116. https://doi.org/10.1016/j.carbon.2019.04.023
Liu J, Ji L, Wang X et al (2019b) Commercial-Level Energy Storage via Free-Standing Stacking Electrodes. Matter 1:1694–1709. https://doi.org/10.1016/j.matt.2019.07.017
Liu Y, Lu YX, Xu YS et al (2020) Pitch-Derived Soft Carbon as Stable Anode Material for Potassium Ion Batteries. Adv Mater 32:2000505. https://doi.org/10.1002/adma.202000505
Liu D, Zhang W, Liu D et al (2021a) Template-free synthesis of lignin-derived 3D hierarchical porous carbon for supercapacitors. J Mater Sci Mater Electron 32:7009–7018. https://doi.org/10.1007/s10854-021-05410-x
Liu H, Xu T, Liu K et al (2021b) Lignin-based electrodes for energy storage application. Ind Crops Prod 165:113425. https://doi.org/10.1016/j.indcrop.2021.113425
Liu C, Hou Y, Li Y, Xiao H (2022) Heteroatom-doped porous carbon microspheres derived from ionic liquid-lignin solution for high performance supercapacitors. J Colloid Interface Sci 614:566–573. https://doi.org/10.1016/j.jcis.2022.01.010
Lou H, He X, Cai C et al (2019) Enhancement and Mechanism of a Lignin Amphoteric Surfactant on the Production of Cellulosic Ethanol from a High-Solid Corncob Residue. J Agric Food Chem 67:6248–6256. https://doi.org/10.1021/acs.jafc.9b01208
Lu L, Han X, Li J et al (2013) A review on the key issues for lithium-ion battery management in electric vehicles. J Power Sources 226:272–288. https://doi.org/10.1016/j.jpowsour.2012.10.060

Luo W, Schardt J, Bommier C et al (2013) Carbon nanofibers derived from cellulose nanofibers as a long-life anode material for rechargeable sodium-ion batteries. J Mater Chem A 1:10662–10666. https://doi.org/10.1039/c3ta12389h

Luo W, Wang B, Heron CG et al (2014) Pyrolysis of cellulose under ammonia leads to nitrogen-doped nanoporous carbon generated through methane formation. Nano Lett 14:2225–2229. https://doi.org/10.1021/nl500859p

Ma Z, Sun Q, Ye J et al (2016) Study on the thermal degradation behaviors and kinetics of alkali lignin for production of phenolic-rich bio-oil using TGA-FTIR and Py-GC/MS. J Anal Appl Pyrolysis 117:116–124. https://doi.org/10.1016/j.jaap.2015.12.007

Ma C, Li Z, Li J et al (2018) Lignin-based hierarchical porous carbon nanofiber films with superior performance in supercapacitors. Appl Surf Sci 456:568–576. https://doi.org/10.1016/j.apsusc.2018.06.189

Ma X, Smirnova AL, Fong H (2019) Flexible lignin-derived carbon nanofiber substrates functionalized with iron (III) oxide nanoparticles as lithium-ion battery anodes. Mater Sci Eng B Solid-State Mater Adv Technol 241:100–104. https://doi.org/10.1016/j.mseb.2019.02.013

Mao H, Chen X, Huang R et al (2018) Fast preparation of carbon spheres from enzymatic hydrolysis lignin: Effects of hydrothermal carbonization conditions. Sci Rep 8:9501. https://doi.org/10.1038/s41598-018-27777-4

Marsh H, Rodríguez-Reinoso F (2006) Activation Processes (Thermal or Physical). Act Carbon 2:243–321. https://doi.org/10.1016/b978-008044463-5/50019-4

Matei Ghimbeu C, Zhang B, Martinez de Yuso A et al (2019) Valorizing low cost and renewable lignin as hard carbon for Na-ion batteries: Impact of lignin grade. Carbon N Y 153:634–647. https://doi.org/10.1016/j.carbon.2019.07.026

Moriwake H, Kuwabara A, Fisher CAJ, Ikuhara Y (2017) Why is sodium-intercalated graphite unstable? RSC Adv 7:36550–36554. https://doi.org/10.1039/c7ra06777a

Nair V, Dhar P, Vinu R (2016) Production of phenolics via photocatalysis of ball milled lignin-TiO2 mixtures in aqueous suspension. RSC Adv 6:18204–18216. https://doi.org/10.1039/c5ra25954a

Navarro-Suárez AM, Saurel D, Sánchez-Fontecoba P et al (2018) Temperature effect on the synthesis of lignin-derived carbons for electrochemical energy storage applications. J Power Sources 397:296–306. https://doi.org/10.1016/j.jpowsour.2018.07.023

Pang J, Zhang W, Zhang J et al (2017) Facile and sustainable synthesis of sodium lignosulfonate derived hierarchical porous carbons for supercapacitors with high volumetric energy densities. Green Chem 19:3916–3926. https://doi.org/10.1039/c7gc01434a

Pang J, Zhang W, Zhang H et al (2018a) Sustainable nitrogen-containing hierarchical porous carbon spheres derived from sodium lignosulfonate for high-performance supercapacitors. Carbon N Y 132:280–293. https://doi.org/10.1016/j.carbon.2018.02.077

Pang J, Zhang WF, Zhang JL et al (2018b) Oxygen and Nitrogen Co-enriched Sustainable Porous Carbon Hollow Microspheres from Sodium Lignosulfonate for Supercapacitors with High Volumetric Energy Densities. ChemElectroChem 5:1306–1320. https://doi.org/10.1002/celc.201701384

Peng L, Fang Z, Zhu Y et al (2018) Holey 2D Nanomaterials for Electrochemical Energy Storage. Adv Energy Mater 8:1702179. https://doi.org/10.1002/aenm.201702179

Perera Jayawickramage RA, Balkus KJ, Ferraris JP (2019) Binder free carbon nanofiber electrodes derived from polyacrylonitrile-lignin blends for high performance supercapacitors. Nanotechnology 30:355402. https://doi.org/10.1088/1361-6528/ab2274

Perera Jayawickramage RA, Ferraris JP (2019) High performance supercapacitors using lignin based electrospun carbon nanofiber electrodes in ionic liquid electrolytes. Nanotechnology 30:. https://doi.org/10.1088/1361-6528/aafe95

Peuvot K, Hosseinaei O, Tomani P et al (2019) Lignin Based Electrospun Carbon Fiber Anode for Sodium Ion Batteries. J Electrochem Soc 166:A1984–A1990. https://doi.org/10.1149/2.0711910jes

Priyanka M, Saravanakumar MP (2018) Ultrahigh adsorption capacity of starch derived zinc based carbon foam for adsorption of toxic dyes and its preliminary investigation on oil-water separation. J Clean Prod 197:511–524. https://doi.org/10.1016/j.jclepro.2018.06.197

Qin H, Jian R, Bai J et al (2018) Influence of Molecular Weight on Structure and Catalytic Characteristics of Ordered Mesoporous Carbon Derived from Lignin. ACS Omega 3:1350–1356. https://doi.org/10.1021/acsomega.7b01870

Qiu S, Xiao L, Sushko ML et al (2017) Manipulating Adsorption-Insertion Mechanisms in Nanostructured Carbon Materials for High-Efficiency Sodium Ion Storage. Adv Energy Mater 7:1–11. https://doi.org/10.1002/aenm.201700403

Qu JY, Han Q, Gao F, Qiu JS (2017) Carbon foams produced from lignin-phenol-formaldehyde resin for oil/water separation. New Carbon Mater 32:86–91. https://doi.org/10.1016/S1872-5805(17)60109-4

Qu W, Yang J, Sun X et al (2021) Towards producing high-quality lignin-based carbon fibers: A review of crucial factors affecting lignin properties and conversion techniques. Int J Biol Macromol 189:768–784. https://doi.org/10.1016/j.ijbiomac.2021.08.187

RameshKumar S, Shaiju P, O'Connor KE, P RB, (2020) Bio-based and biodegradable polymers - State-of-the-art, challenges and emerging trends. Curr Opin Green Sustain Chem 21:75–81. https://doi.org/10.1016/j.cogsc.2019.12.005

Ruiz-Rosas R, Bedia J, Lallave M et al (2010) The production of submicron diameter carbon fibers by the electrospinning of lignin. Carbon N Y 48:696–705. https://doi.org/10.1016/j.carbon.2009.10.014

Sagues WJ, Jain A, Brown D et al (2019) Are lignin-derived carbon fibers graphitic enough? Green Chem 21:4253–4265. https://doi.org/10.1039/c9gc01806a

Saha D, Kienbaum MJ (2019) Role of oxygen, nitrogen and sulfur functionalities on the surface of nanoporous carbons in CO2 adsorption: A critical review. Microporous Mesoporous Mater 287:29–55. https://doi.org/10.1016/j.micromeso.2019.05.051

Saha B, Orvig C (2010) Biosorbents for hexavalent chromium elimination from industrial and municipal effluents. Coord Chem Rev 254:2959–2972. https://doi.org/10.1016/j.ccr.2010.06.005

Saha D, Payzant EA, Kumbhar AS, Naskar AK (2013) Sustainable mesoporous carbons as storage and controlled-delivery media for functional molecules. ACS Appl Mater Interfaces 5:5868–5874. https://doi.org/10.1021/am401661f

Sakthivel S, Kisch H (2003) Daylight Photocatalysis by Carbon-Modified Titanium Dioxide. Angew Chemie - Int Ed 42:4908–4911. https://doi.org/10.1002/anie.200351577

Schlee P, Hosseinaei O, Baker D et al (2019) From Waste to Wealth: From Kraft Lignin to Free-standing Supercapacitors. Carbon N Y 145:470–480. https://doi.org/10.1016/j.carbon.2019.01.035

Schneidermann C, Jäckel N, Oswald S et al (2017) Solvent-Free Mechanochemical Synthesis of Nitrogen-Doped Nanoporous Carbon for Electrochemical Energy Storage. Chemsuschem 10:2416–2424. https://doi.org/10.1002/cssc.201700459

Scrosati B, Hassoun J, Sun YK (2011) Lithium-ion batteries. A look into the future. Energy Environ Sci 4:3287–3295. https://doi.org/10.1039/c1ee01388b

Secor EB, Ahn BY, Gao TZ et al (2015) Rapid and Versatile Photonic Annealing of Graphene Inks for Flexible Printed Electronics. Adv Mater 27:6683–6688. https://doi.org/10.1002/adma.201502866

Seo J, Park H, Shin K et al (2014) Lignin-derived macroporous carbon foams prepared by using poly(methyl methacrylate) particles as the template. Carbon N Y 76:357–367. https://doi.org/10.1016/j.carbon.2014.04.087

Shao Y, El-Kady MF, Sun J et al (2018) Design and Mechanisms of Asymmetric Supercapacitors. Chem Rev 118:9233–9280. https://doi.org/10.1021/acs.chemrev.8b00252

Shao H, Wu YC, Lin Z et al (2020) Nanoporous carbon for electrochemical capacitive energy storage. Chem Soc Rev 49:3005–3039. https://doi.org/10.1039/d0cs00059k

Shen X, Huang P, Wen J, Sun R (2017) Research status of lignin oxidative and reductive depolymerization. Prog Chem 29:162–178. https://doi.org/10.7536/PC161002

Shen Y, Li Y, Yang G et al (2020) Lignin derived multi-doped (N, S, Cl) carbon materials as excellent electrocatalyst for oxygen reduction reaction in proton exchange membrane fuel cells. J Energy Chem 44:106–114. https://doi.org/10.1016/j.jechem.2019.09.019

Shi Z, Jin G, Wang J, Zhang J (2017) Free-standing, welded mesoporous carbon nanofibers as anode for high-rate performance Li-ion batteries. J

Electroanal Chem 795:26–31. https://doi.org/10.1016/j.jelechem.2017.03.047
Shi X, Wang X, Tang B et al (2018) Impact of lignin extraction methods on microstructure and mechanical properties of lignin-based carbon fibers. J Appl Polym Sci 135:45580. https://doi.org/10.1002/app.45580
Shi Y, Liu X, Wang M et al (2019) Synthesis of N-doped carbon quantum dots from bio-waste lignin for selective irons detection and cellular imaging. Int J Biol Macromol 128:537–545. https://doi.org/10.1016/j.ijbiomac.2019.01.146
Shuai L, T A, M. Q-S, et al (2016) Formaldehyde stabilization facilitates lignin monomer production during biomass depolymerization. Science (80-) 354:329–334
Si M, Zhang J, He Y et al (2018) Synchronous and rapid preparation of lignin nanoparticles and carbon quantum dots from natural lignocellulose. Green Chem 20:3414–3419. https://doi.org/10.1039/c8gc00744f
Sima G, Gan L, Chang L et al (2021) Efficient fabrication of ordered mesoporous carbon derived from lignin via deep eutectic solvent pretreatment for supercapacitors. Microporous Mesoporous Mater 323:111192. https://doi.org/10.1016/j.micromeso.2021.111192
Song Y, Liu J, Sun K, Xu W (2017) Synthesis of sustainable lignin-derived mesoporous carbon for supercapacitors using a nano-sized MgO template coupled with Pluronic F127. RSC Adv 7:48324–48332. https://doi.org/10.1039/c7ra09464g
Song DP, Li W, Park J et al (2021) Millisecond photothermal carbonization for in-situ fabrication of mesoporous graphitic carbon nanocomposite electrode films. Carbon N Y 174:439–444. https://doi.org/10.1016/j.carbon.2020.12.036
Souza JR, Araujo JR, Archanjo BS, Simão RA (2019) Cross-linked lignin coatings produced by UV light and SF6 plasma treatments. Prog Org Coatings 128:82–89. https://doi.org/10.1016/j.porgcoat.2018.12.017
Srisasiwimon N, Chuangchote S, Laosiripojana N, Sagawa T (2018) TiO2/Lignin-Based Carbon Composited Photocatalysts for Enhanced Photocatalytic Conversion of Lignin to High Value Chemicals. ACS Sustain Chem Eng 6:13968–13976. https://doi.org/10.1021/acssuschemeng.8b02353
Stojanovska E, Pampal ES, Kilic A et al (2019) Developing and characterization of lignin-based fibrous nanocarbon electrodes for energy storage devices. Compos Part B Eng 158:239–248. https://doi.org/10.1016/j.compositesb.2018.09.072
Sun X, Liu X, Li F (2021) Sulfur-doped laser-induced graphene derived from polyethersulfone and lignin hybrid for all-solid-state supercapacitor. Appl Surf Sci 551:149438. https://doi.org/10.1016/j.apsusc.2021.149438
Sundriyal S, Shrivastav V, Pham HD et al (2021) Advances in bio-waste derived activated carbon for supercapacitors: Trends, challenges and prospective. Resour Conserv Recycl 169:105548. https://doi.org/10.1016/j.resconrec.2021.105548
Svinterikos E, Zuburtikudis I, Al-Marzouqi M (2020) Electrospun Lignin-Derived Carbon Micro- And Nanofibers: A Review on Precursors, Properties, and Applications. ACS Sustain Chem Eng 8:13868–13893. https://doi.org/10.1021/acssuschemeng.0c03246
Takkellapati S, Li T, Gonzalez MA (2018) An overview of biorefinery-derived platform chemicals from a cellulose and hemicellulose biorefinery. Clean Technol Environ Policy 20:1615–1630. https://doi.org/10.1007/s10098-018-1568-5
Tan Y, Wang X, Xiong F et al (2021) Preparation of lignin-based porous carbon as an efficient absorbent for the removal of methylene blue. Ind Crops Prod 171:113980. https://doi.org/10.1016/j.indcrop.2021.113980
Tenhaeff WE, Rios O, More K, McGuire MA (2014) Highly robust lithium ion battery anodes from lignin: An abundant, renewable, and low-cost material. Adv Funct Mater 24:86–94. https://doi.org/10.1002/adfm.201301420
Tian J, Liu C, Lin C, Ma M (2019) Constructed nitrogen and sulfur codoped multilevel porous carbon from lignin for high-performance supercapacitors. J Alloys Compd 789:435–442. https://doi.org/10.1016/j.jallcom.2019.03.070
Torres-Canas F, Bentaleb A, Föllmer M et al (2020) Improved structure and highly conductive lignin-carbon fibers through graphene oxide liquid crystal. Carbon N Y 163:120–127. https://doi.org/10.1016/j.carbon.2020.02.077
Tran CD, Ho HC, Keum JK et al (2017) Sustainable Energy-Storage Materials from Lignin-Graphene Nanocomposite-Derived Porous Carbon Film. Energy Technol 5:1927–1935. https://doi.org/10.1002/ente.201700090
Valero-Romero MJ, Márquez-Franco EM, Bedia J et al (2014) Hierarchical porous carbons by liquid phase impregnation of zeolite templates with lignin solution. Microporous Mesoporous Mater 196:68–78. https://doi.org/10.1016/j.micromeso.2014.04.055
Vander Wal RL, Choi MY (1999) Pulsed laser heating of soot: Morphological changes. Carbon N Y 37:231–239. https://doi.org/10.1016/S0008-6223(98)00169-9
Vannarath A, Thalla AK (2021) Synthesis and characterisation of an ultra-light, hydrophobic and flame-retardant robust lignin-carbon foam for oil-water separation. J Clean Prod 325:129263. https://doi.org/10.1016/j.jclepro.2021.129263
Vázquez G, Rodríguez-Bona C, Freire S et al (1999) Acetosolv pine lignin as copolymer in resins for manufacture of exterior grade plywoods. Bioresour Technol 70:209–214. https://doi.org/10.1016/S0960-8524(99)00020-6
Wan X, Shen F, Hu J et al (2021) 3-D hierarchical porous carbon from oxidized lignin by one-step activation for high-performance supercapacitor. Int J Biol Macromol 180:51–60. https://doi.org/10.1016/j.ijbiomac.2021.03.048
Wang SX, Yang L, Stubbs LP et al (2013) Lignin-derived fused electrospun carbon fibrous mats as high performance anode materials for lithium ion batteries. ACS Appl Mater Interfaces 5:12275–12282. https://doi.org/10.1021/am4043867
Wang K, Cao Y, Wang X et al (2016a) Rod-shape porous carbon derived from aniline modified lignin for symmetric supercapacitors. J Power Sources 307:462–467. https://doi.org/10.1016/j.jpowsour.2016.01.008
Wang K, Xu M, Gu Y et al (2016b) Symmetric supercapacitors using urea-modified lignin derived N-doped porous carbon as electrode materials in liquid and solid electrolytes. J Power Sources 332:180–186. https://doi.org/10.1016/j.jpowsour.2016.09.115
Wang Y, Song Y, Xia Y (2016c) Electrochemical capacitors: Mechanism, materials, systems, characterization and applications. Chem Soc Rev 45:5925–5950. https://doi.org/10.1039/c5cs00580a
Wang H, Qiu X, Liu W, Yang D (2017) Facile preparation of well-combined lignin-based carbon/ZnO hybrid composite with excellent photocatalytic activity. Appl Surf Sci 426:206–216. https://doi.org/10.1016/j.apsusc.2017.07.112
Wang L, Liu Z, Liu Y, Wang L (2019a) Crosslinked polybenzimidazole containing branching structure with no sacrifice of effective N-H sites: Towards high-performance high-temperature proton exchange membranes for fuel cells. J Memb Sci 583:110–117. https://doi.org/10.1016/j.memsci.2019.04.030
Wang X, Liu Y, Chen M et al (2019b) Direct Microwave Conversion from Lignin to Micro/Meso/Macroporous Carbon for High-Performance Symmetric Supercapacitors. ChemElectroChem 6:4789–4800. https://doi.org/10.1002/celc.201901315
Wang J, Qian Y, Li L, Qiu X (2020a) Atomic Force Microscopy and Molecular Dynamics Simulations for Study of Lignin Solution Self-Assembly Mechanisms in Organic-Aqueous Solvent Mixtures. Chemsuschem 13:4420–4427. https://doi.org/10.1002/cssc.201903132
Wang S, Sima G, Cui Y et al (2020b) Preparations of lignin-derived ordered mesoporous carbon by self-assembly in organic solvent and aqueous solution: Comparison in textural property. Mater Lett 264:127318. https://doi.org/10.1016/j.matlet.2020.127318
Wang H, Xiong F, Tan Y et al (2021a) Preparation and Formation Mechanism of Covalent-Noncovalent Forces Stabilizing Lignin Nanospheres and Their Application in Superhydrophobic and Carbon Materials. ACS Sustain Chem Eng 9:3811–3820. https://doi.org/10.1021/acssuschemeng.0c08780
Wang J, Qian Y, Zhou Y et al (2021b) Atomic Force Microscopy Measurement in the Lignosulfonate/Inorganic Silica System: From Dispersion Mechanism Study to Product Design. Engineering 7:1140–1148. https://doi.org/10.1016/j.eng.2021.07.004
Wang S, Bai J, Innocent MT et al (2021c) Lignin-based carbon fibers: Formation, modification and potential applications. Green Energy Environ. https://doi.org/10.1016/j.gee.2021.04.006
Wang T, Hu S, Wu D et al (2021d) Boosting the capacity of biomass-based supercapacitors using carbon materials of wood derivatives and redox molecules from plants. J Mater Chem A 9:11839–11852. https://doi.org/10.1039/d1ta01542g

Wang X, Liu X, Smith RL et al (2021e) Direct one-pot synthesis of ordered mesoporous carbons from lignin with metal coordinated self-assembly. Green Chem 23:8632–8642. https://doi.org/10.1039/d1gc03030b
Wang C, Yang D, Qiu X, Zhang W (2022a) Applications of Lignin-Derived Porous Carbons for Electrochemical Energy Storage. Prog Chem 34:285–300
Wang H, Fu F, Huang M et al (2022b) Lignin-based materials for electrochemical energy storage devices. Nano Mater Sci. https://doi.org/10.1016/j.nanoms.2022.01.002.10.1016/j.nanoms.2022.01.002
Wang H, Xiong F, Yang J et al (2022c) Preparation of size-controlled all-lignin based carbon nanospheres and their electrochemical performance in supercapacitor. Ind Crops Prod 179:114689. https://doi.org/10.1016/j.indcrop.2022.114689
Wang L, Feng X, Li X et al (2022e) Hydrothermal, KOH-assisted synthesis of lignin-derived porous carbon for supercapacitors: value-added of lignin and constructing texture properties/specific capacitance relationships. J Mater Res Technol 16:570–580. https://doi.org/10.1016/j.jmrt.2021.12.040
Wang X, Zhang W, Chen M, Zhou X (2018) Electrospun enzymatic hydrolysis lignin-based carbon nanofibers as binder-free supercapacitor electrodes with high performance. Polymers (Basel) 10:. https://doi.org/10.3390/polym10121306
Wang J, Chen W, Yang D, et al (2022d) Monodispersed Lignin Colloidal Spheres with Tailorable Sizes for Bio-Photonic Materials. Small 2200671. https://doi.org/10.1002/smll.2022d00671
Wen F, Zhang W, Jian W et al (2022) Sustainable production of lignin-derived porous carbons for high-voltage electrochemical capacitors. Chem Eng Sci 255:117672. https://doi.org/10.1016/j.ces.2022.117672
Wu X, Chen Y, Xing Z et al (2019) Advanced Carbon-Based Anodes for Potassium-Ion Batteries. Adv Energy Mater 9:1900343. https://doi.org/10.1002/aenm.201900343
Wu Z, Zou J, Zhang Y et al (2022) Lignin-derived hard carbon anode for potassium-ion batteries: Interplay among lignin molecular weight, material structures, and storage mechanisms. Chem Eng J 427:131547. https://doi.org/10.1016/j.cej.2021.131547
Wynn GH, Fountain AW (1997) Development and characterization of electrochemical devices using ultraviolet laser induced carbonization of polyimide films. J Electrochem Soc 144:3769–3772. https://doi.org/10.1149/1.1838089
Xi Y, Yang D, Qiu X et al (2018) Renewable lignin-based carbon with a remarkable electrochemical performance from potassium compound activation. Ind Crops Prod 124:747–754. https://doi.org/10.1016/j.indcrop.2018.08.018
Xi Y, Wang Y, Yang D et al (2019) K2CO3 activation enhancing the graphitization of porous lignin carbon derived from enzymatic hydrolysis lignin for high performance lithium-ion storage. J Alloys Compd 785:706–714. https://doi.org/10.1016/j.jallcom.2019.01.039
Xi Y, Huang S, Yang D et al (2020) Hierarchical porous carbon derived from the gas-exfoliation activation of lignin for high-energy lithium-ion batteries. Green Chem 22:4321–4330. https://doi.org/10.1039/d0gc00945h
Xiong F, Han Y, Wang S et al (2017) Preparation and formation mechanism of size-controlled lignin nanospheres by self-assembly. Ind Crops Prod 100:146–152. https://doi.org/10.1016/j.indcrop.2017.02.025
Xiong F, Wang H, Xu H et al (2020) Self-assembled lignin nanospheres with solid and hollow tunable structures. Ind Crops Prod 144:112063. https://doi.org/10.1016/j.indcrop.2019.112063
Xu J, Zhou X, Chen M et al (2018a) Preparing hierarchical porous carbon aerogels based on enzymatic hydrolysis lignin through ambient drying for supercapacitor electrodes. Microporous Mesoporous Mater 265:258–265. https://doi.org/10.1016/j.micromeso.2018.02.024
Xu Y, Zhang C, Zhou M et al (2018b) Highly nitrogen-doped carbon nanofibers as potassium-ion battery anodes with superior rate capability and cyclability. Nat Commun 9:1720. https://doi.org/10.1038/s41467-018-04190-z
Yahya MA, Al-Qodah Z, Ngah CWZ (2015) Agricultural bio-waste materials as potential sustainable precursors used for activated carbon production: A review. Renew Sustain Energy Rev 46:218–235. https://doi.org/10.1016/j.rser.2015.02.051
Yang H, Yan R, Chen H et al (2007) Characteristics of hemicellulose, cellulose and lignin pyrolysis. Fuel 86:1781–1788. https://doi.org/10.1016/j.fuel.2006.12.013
Yang J, Ju Z, Jiang Y et al (2018) Enhanced Capacity and Rate Capability of Nitrogen/Oxygen Dual-Doped Hard Carbon in Capacitive Potassium-Ion Storage. Adv Mater 30:1–11. https://doi.org/10.1002/adma.201700104
Yang Z, Gleisner R, Mann DH et al (2020) Lignin based activated carbon using H3PO4 activation. Polymers (basel) 12:2829. https://doi.org/10.3390/polym12122829
Yeon JS, Park SH, Suk J et al (2020) Confinement of sulfur in the micropores of honeycomb-like carbon derived from lignin for lithium-sulfur battery cathode. Chem Eng J 382:122946. https://doi.org/10.1016/j.cej.2019.122946
Yi X, He W, Zhang X et al (2017) Graphene-like carbon sheet/Fe3O4 nanocomposites derived from soda papermaking black liquor for high performance lithium ion batteries. Electrochim Acta 232:550–560. https://doi.org/10.1016/j.electacta.2017.02.130
Yin J, Zhang W, Alhebshi NA et al (2020a) Synthesis Strategies of Porous Carbon for Supercapacitor Applications. Small Methods 4:1900853. https://doi.org/10.1002/smtd.201900853
Yin J, Zhang W, Wang W et al (2020b) Electrochemical Zinc Ion Capacitors Enhanced by Redox Reactions of Porous Carbon Cathodes. Adv Energy Mater 10:2001705. https://doi.org/10.1002/aenm.202001705
Yin WM, Tian LF, Pang B et al (2020c) Fabrication of dually N/S-doped carbon from biomass lignin: Porous architecture and high-rate performance as supercapacitor. Int J Biol Macromol 156:988–996. https://doi.org/10.1016/j.ijbiomac.2020.04.102
Yin J, Zhang W, Alhebshi NA et al (2021) Electrochemical Zinc Ion Capacitors: Fundamentals, Materials, and Systems. Adv Energy Mater 11:2100201. https://doi.org/10.1002/aenm.202100201
Yu G, Xie X, Pan L et al (2013) Hybrid nanostructured materials for high-performance electrochemical capacitors. Nano Energy 2:213–234. https://doi.org/10.1016/j.nanoen.2012.10.006
Yu Z-L, Li G-C, Fechler N et al (2016) Polymerization under Hypersaline Conditions: A Robust Route to Phenolic Polymer-Derived Carbon Aerogels. Angew Chemie 128:14843–14847. https://doi.org/10.1002/ange.201605510
Yu F, Li Y, Jia M et al (2017) Elaborate construction and electrochemical properties of lignin-derived macro-/micro-porous carbon-sulfur composites for rechargeable lithium-sulfur batteries: The effect of sulfur-loading time. J Alloys Compd 709:677–685. https://doi.org/10.1016/j.jallcom.2017.03.204
Yu B, Chang Z, Zhang Y, Wang C (2018) Preparation and formation mechanism of size-controlled lignin based microsphere by reverse phase polymerization. Mater Chem Phys 203:97–105. https://doi.org/10.1016/j.matchemphys.2017.08.039
Yuan M, Luo F, Rao Y et al (2021) Laser synthesis of superhydrophilic O/S co-doped porous graphene derived from sodium lignosulfonate for enhanced microsupercapacitors. J Power Sources 513:230558. https://doi.org/10.1016/j.jpowsour.2021.230558
Zakzeski J, Bruijnincx PCA, Jongerius AL, Weckhuysen BM (2010) The catalytic valorization of lignin for the production of renewable chemicals. Chem Rev 110:3552–3599. https://doi.org/10.1021/cr900354u
Zhan X, Cai C, Pang Y et al (2019) Effect of the isoelectric point of pH-responsive lignin-based amphoteric surfactant on the enzymatic hydrolysis of lignocellulose. Bioresour Technol 283:112–119. https://doi.org/10.1016/j.biortech.2019.03.026
Zhang W, Lin H, Lin Z et al (2015a) 3D Hierarchical Porous Carbon for Supercapacitors Prepared from Lignin through a Facile Template-Free Method. Chemsuschem 8:2114–2122. https://doi.org/10.1002/cssc.201403486
Zhang W, Yin J, Lin Z et al (2015b) Facile preparation of 3D hierarchical porous carbon from lignin for the anode material in lithium ion battery with high rate performance. Electrochim Acta 176:1136–1142. https://doi.org/10.1016/j.electacta.2015.08.001
Zhang W, Zhao M, Liu R et al (2015c) Hierarchical porous carbon derived from lignin for high performance supercapacitor. Colloids Surfaces A Physicochem Eng Asp 484:518–527. https://doi.org/10.1016/j.colsurfa.2015.08.030
Zhang L, You T, Zhou T et al (2016a) Interconnected Hierarchical Porous Carbon from Lignin-Derived Byproducts of Bioethanol Production for Ultra-High Performance Supercapacitors. ACS Appl Mater Interfaces 8:13918–13925. https://doi.org/10.1021/acsami.6b02774

Zhang X, Zhou J, Liu C et al (2016b) A universal strategy to prepare porous graphene films: Binder-free anodes for high-rate lithium-ion and sodium-ion batteries. J Mater Chem A 4:8837–8843. https://doi.org/10.1039/c6ta01907b
Zhang W, Lin N, Liu D et al (2017) Direct carbonization of rice husk to prepare porous carbon for supercapacitor applications. Energy 128:618–625. https://doi.org/10.1016/j.energy.2017.04.065
Zhang H, Zhang W, Ming H et al (2018a) Design advanced carbon materials from lignin-based interpenetrating polymer networks for high performance sodium-ion batteries. Chem Eng J 341:280–288. https://doi.org/10.1016/j.cej.2018.02.016
Zhang W, Lei Y, Ming F et al (2018b) Lignin Laser Lithography: A Direct-Write Method for Fabricating 3D Graphene Electrodes for Microsupercapacitors. Adv Energy Mater 8:1801840. https://doi.org/10.1002/aenm.201801840
Zhang W, Xu J, Hou D et al (2018c) Hierarchical porous carbon prepared from biomass through a facile method for supercapacitor applications. J Colloid Interface Sci 530:338–344. https://doi.org/10.1016/j.jcis.2018.06.076
Zhang W, Yu C, Chang L et al (2018d) Three-dimensional nitrogen-doped hierarchical porous carbon derived from cross-linked lignin derivatives for high performance supercapacitors. Electrochim Acta 282:642–652. https://doi.org/10.1016/j.electacta.2018.06.100
Zhang B, Liu Y, Ren M et al (2019a) Sustainable Synthesis of Bright Green Fluorescent Nitrogen-Doped Carbon Quantum Dots from Alkali Lignin. Chemsuschem 12:4202–4210. https://doi.org/10.1002/cssc.201901693
Zhang K, Liu M, Zhang T et al (2019b) High-performance supercapacitor energy storage using a carbon material derived from lignin by bacterial activation before carbonization. J Mater Chem A 7:26838–26848. https://doi.org/10.1039/c9ta04369a
Zhang W, Jiang Q, Lei Y, Alshareef HN (2019c) Wettability-Driven Assembly of Electrochemical Microsupercapacitors. ACS Appl Mater Interfaces 11:20905–20914. https://doi.org/10.1021/acsami.9b05635
Zhang W, Lei Y, Jiang Q et al (2019d) 3D Laser Scribed Graphene Derived from Carbon Nanospheres : An Ultrahigh-Power Electrode for Supercapacitors. Small Methods 3:1900005. https://doi.org/10.1002/smtd.201900005
Zhang W, Zhang F, Ming F, Alshareef HN (2019e) Sodium-Ion Battery Anodes: Status and Future Trends. EnergyChem 1:100012. https://doi.org/10.1016/j.enchem.2019.100012
Zhang B, Yang D, Qian Y et al (2020a) Engineering a lignin-based hollow carbon with opening structure for highly improving the photocatalytic activity and recyclability of ZnO. Ind Crops Prod 155:112773. https://doi.org/10.1016/j.indcrop.2020.112773
Zhang B, Yang D, Qiu X et al (2020b) Fabricating ZnO/lignin-derived flower-like carbon composite with excellent photocatalytic activity and recyclability. Carbon N Y 162:256–266. https://doi.org/10.1016/j.carbon.2020.02.038
Zhang W, Cao Z, Wang W et al (2020c) A Site-Selective Doping Strategy of Carbon Anodes with Remarkable K-Ion Storage Capacity. Angew Chemie - Int Ed 59:4448–4455. https://doi.org/10.1002/anie.201913368
Zhang W, Yin J, Sun M et al (2020d) Direct Pyrolysis of Supermolecules: An Ultrahigh Edge-Nitrogen Doping Strategy of Carbon Anodes for Potassium-Ion Batteries. Adv Mater 32:2000732. https://doi.org/10.1002/adma.202000732
Zhang L, Wang W, Lu S, Xiang Y (2021a) Carbon Anode Materials: A Detailed Comparison between Na-ion and K-ion Batteries. Adv Energy Mater 11:2003640. https://doi.org/10.1002/aenm.202003640
Zhang W, Jian W, Yin J et al (2021b) A comprehensive green utilization strategy of lignocellulose from rice husk for the fabrication of high-rate electrochemical zinc ion capacitors. J Clean Prod 327:129522. https://doi.org/10.1016/j.jclepro.2021.129522
Zhang W, Sun M, Yin J et al (2021c) Rational design of carbon anodes by catalytic pyrolysis of graphitic carbon nitride for efficient storage of Na and K mobile ions. Nano Energy 87:106184. https://doi.org/10.1016/j.nanoen.2021.106184
Zhang W, Sun M, Yin J et al (2021d) A Cyclized Polyacrylonitrile Anode for Alkali Metal Ion Batteries. AngewChem Int Ed 60:1355–1363. https://doi.org/10.1002/anie.202011484
Zhang W, Sun M, Yin J et al (2021e) Accordion-Like Carbon with High Nitrogen Doping for Fast and Stable K Ion Storage. Adv Energy Mater 11:2101928. https://doi.org/10.1002/aenm.202101928
Zhang W, Yin J, Chen C, Qiu X (2021f) Carbon nitride derived nitrogen-doped carbon nanosheets for high-rate lithium-ion storage. Chem Eng Sci 241:116709. https://doi.org/10.1016/j.ces.2021.116709
Zhang W, Yin J, Wang C et al (2021g) Lignin Derived Porous Carbons: Synthesis Methods and Supercapacitor Applications. Small Methods 15:2100896. https://doi.org/10.1002/smtd.202100896
Zhang W, Yin J, Wang W et al (2021h) Status of Rechargeable Potassium Batteries. Nano Energy 83:105792. https://doi.org/10.1016/j.nanoen.2021.105792
Zhang X, Jian W, Zhao L et al (2022) Direct carbonization of sodium lignosulfonate through self-template strategies for the synthesis of porous carbons toward supercapacitor applications. Colloids Surfaces A Physicochem Eng Asp 636:128191. https://doi.org/10.1016/j.colsurfa.2021.128191
Zhao J, Xiuwen W, Hu J et al (2014) Thermal degradation of softwood lignin and hardwood lignin by TG-FTIR and Py-GC/MS. Polym Degrad Stab 108:133–138. https://doi.org/10.1016/j.polymdegradstab.2014.06.006
Zhao Z, Hao S, Hao P et al (2015) Lignosulphonate-cellulose derived porous activated carbon for supercapacitor electrode. J Mater Chem A 3:15049–15056. https://doi.org/10.1039/c5ta02770e
Zhao H, Wang Q, Deng Y et al (2016) Preparation of renewable lignin-derived nitrogen-doped carbon nanospheres as anodes for lithium-ion batteries. RSC Adv 6:77143–77150. https://doi.org/10.1039/c6ra17793j
Zhao B, Borghei M, Zou T et al (2021) Lignin-Based Porous Supraparticles for Carbon Capture. ACS Nano 15:6774–6786. https://doi.org/10.1021/acsnano.0c10307
Zhou J, Li Z, Xing W et al (2016) A New Approach to Tuning Carbon Ultramicropore Size at Sub-Angstrom Level for Maximizing Specific Capacitance and CO2 Uptake. Adv Funct Mater 26:7955–7964. https://doi.org/10.1002/adfm.201601904
Zhou Z, Chen F, Kuang T et al (2018) Lignin-derived hierarchical mesoporous carbon and NiO hybrid nanospheres with exceptional Li-ion battery and pseudocapacitive properties. Electrochim Acta 274:288–297. https://doi.org/10.1016/j.electacta.2018.04.111
Zhu L, Shen F, Smith RL et al (2017) Black liquor-derived porous carbons from rice straw for high-performance supercapacitors. Chem Eng J 316:770–777. https://doi.org/10.1016/j.cej.2017.02.034
Zhu J, Yan C, Zhang X et al (2020) A sustainable platform of lignin: From bioresources to materials and their applications in rechargeable batteries and supercapacitors. Prog Energy Combust Sci 76:100788. https://doi.org/10.1016/j.pecs.2019.100788
Zhu S, Xu J, Kuang Y et al (2021) Lignin-derived sulfonated porous carbon from cornstalk for efficient and selective removal of cationic dyes. Ind Crops Prod 159:113071. https://doi.org/10.1016/j.indcrop.2020.113071
Zuo S, Zhang W, Wang Y, Xia H (2020) Low-Cost Preparation of High-Surface-Area Nitrogen-Containing Activated Carbons from Biomass-Based Chars by Ammonia Activation. Ind Eng Chem Res 59:7527–7537. https://doi.org/10.1021/acs.iecr.9b06836